The Behavior of Spokes in Saturn's B Ring

C.J. Mitchell[a,*], C.C. Porco[a], H.L. Dones[b], J.N. Spitale[c]

[a] *Cassini Imaging Central Laboratory for Operations, 4750 Walnut Street Suite 205, Boulder, CO 80301, USA*
[b] *Southwest Research Institute, 1050 Walnut Street, Boulder, CO 80302, USA*
[c] *Planetary Science Institute, 1700 E. Ft. Lowell, Suite 106, Tucson, AZ 85719, USA*

Abstract

We present the first results from Cassini ISS observations aimed at determining both the short-term and long-term behavior of the spokes in Saturn's B ring. We have observed multiple spokes which appear between images where there was not a spoke before. The radial termini of these new spokes expand radially at ~ 0.5 km/s in both the inward and outward directions and both towards and away from corotation. Defining a spoke's activity as the area-integrated optical depth over the region of the ring it covers, we find that the majority of spokes which are found in multiple images are either increasing or decreasing in activity. In addition, in analyzing the shapes and motions of spokes, we find the azimuthal profiles to be well-fitted by Gaussians for the majority of spokes. We have found that several of the imaged spokes were undergoing an "active" phase during which the spoke's optical depth increases and the spoke grows both azimuthally and radially. We interpret these motions to be either due to the Lorentz force acting on dust grains charged by a very high temperature plasma or the group velocity of an advancing spoke-forming front. The spokes' light scattering behavior suggests that the particles comprising them are not spherical but instead are irregularly shaped.

We search for periodicities in the longer-term temporal variability of spoke

*Corresponding author
Email addresses: colin@ciclops.org (C.J. Mitchell), carolyn@ciclops.org (C.C. Porco), luke@boulder.swri.edu (H.L. Dones), spitale@pirl.lpl.Arizona.EDU (J.N. Spitale)

activity, and for correlations between spoke activity and other processes ongoing in Saturn's magnetosphere and atmosphere. Using the latest results on the periods and locations of the sources of Saturn's Kilometric Radiation (SKR) obtained by the Cassini Radio and Plasma Wave experiment (RPWS) (Gurnett et al., 2011), we find that spoke activity observed on both sides of Saturn's rings occurs with a period equal to, within all uncertainties, the period of the SKR emissions arising from the northern SKR source, though a period equal to that of the southern SKR source seems also to be present. The period for of the Saturn Electrostatic Discharges (SED) falls within the uncertainty of the spoke activity on the northern side of the rings. However, spokes have been observed during SED-quiescent periods, which strongly suggests that there is no connection between the two phenomena (Fischer et al., 2011).

Finally, we use the latest SLS4 coordinate systems and locate the peak spoke activity on both sides of the rings at $\approx 200^\circ$ in both the northern and southern SLS4 coordinate systems on both sides of the rings. This peak is $\approx 100^\circ$ away from the locations expected from Voyager observations in both coordinate systems.

---

1. Introduction

Spokes are narrow, quasi-radial features composed of icy micron-sized grains which were first discovered on the northern side of Saturn's rings in the outer portion of the B ring during the Voyager 1 spacecraft's encounter with Saturn during 1980 and subsequently studied by Voyager 2 in 1981 (Smith et al., 1981). At low phase angles, the spokes were observed as dark features located near the synchronous orbital radius, where the orbital periods of the ring particles match the rotational period of Saturn's magnetic field. Additional Voyager observations at high phase angles showed that while both the spokes and the spoke free regions of the ring had darkened, the spokes had reversed contrast, becoming bright features on the ring. This indicated that the spokes were composed of forward-scattering, micron-sized particles (Smith et al., 1981; Doyle

et al., 1989; Doyle and Grün, 1990). A later analysis of data taken by the Hubble Space Telescope (McGhee et al., 2005) modeled the spoke particle size distribution and determined the effective size of a spoke particle to be $r_{\rm eff} = 0.57 \pm 0.05$ μm with an effective variance of $b = 0.09 \pm 0.03$ (see Doyle and Grün (1990), Eq. 10, et seq.). However, this size distribution was based on data limited to wavelengths less than 900 nm. More recent work based on observations of the Cassini Visual and Infrared Mapping Spectrometer, which measured the spectrum of a spoke out to 5.1 μm, indicate that average particle sizes may be larger - ≈ 3.5 μm - with a considerably larger variance (D'Aversa et al., 2010).

Spokes were observed by the Voyagers to exhibit a range of morphologies (Smith et al., 1981; Grün et al., 1983), but most commonly a wedge shape, extending more radially than azimuthally, with the narrow part of the spoke closest to the synchronous radius and dimensions typically $10,000$ km long and ~ 2000 km wide. It was found that these wedge shaped spokes usually orbit Saturn at the Keplerian rate and exhibit Kepler shear with the part of the spoke closer to Saturn outpacing the outer part as it orbits the planet. However, the edges of some spokes showed substantial deviations from Keplerian motion for short periods, strong evidence that the dust grains comprising the spokes are charged. Such spokes broaden as one edge orbits at speeds intermediate between Keplerian and corotating with the magnetic field, while the other exhibits Keplerian motion (Grün et al., 1983). A few spoke edges were even observed to switch from corotating to Keplerian motion (Eplee and Smith, 1984).

Voyager observed spokes to be most common on the B ring's morning (west, or astronomical east) ansa and due to their rather short lifespan, on the order of half an orbital period, they are presumably formed preferentially in this region or near midnight (Smith et al., 1981; Porco and Danielson, 1982). If one assumes that a spoke has radial edges when it forms and that the edges shear at the normal Keplerian rate, an apparent age can be calculated for both edges of the spoke. Combining these ages with the location of the spoke shows that most spokes are radial (and hence presumably formed) somewhere on the

morning ansa (Grün et al., 1983). Voyager observed some spokes to be composed of multiple components, one laid on top of the other, with each component exhibiting different degrees of shear (Porco and Danielson, 1982), as if the spoke formation event occurred twice at the same location on the rings, but at different times. The number of spokes present has also shown a correlation with the optical depth of the background rings (Grün et al., 1992), with more spokes at the highest optical depth part of the rings.

Spoke activity, defined loosely by Porco and Danielson (1982) as the area-integrated *contrast* of all spokes within a specified section of the rings, was observed by the Voyagers during their flybys to be greatest on the morning ansa of the rings and periodic in time. On long timescales, the level of activity exhibited a period equal to that of the Saturn Kilometric Radiation (SKR) (Porco and Danielson, 1982), radio emissions from high latitude regions of Saturn, which had a period during the Voyager flybys of ~ 639.4 minutes. There was also a suggestion (Porco and Danielson, 1984) of a period equal to that of the Voyager-era Saturn Electrostatic Discharges (SED), ~ 610 minutes, radio emissions associated with lightning in Saturn's atmosphere. Spoke activity was examined as a function of location in the Saturn Longitude System (SLS), a rotating coordinate system based on the northern SKR and presumed at the time to rotate with Saturn's internal rotation rate. The magnetic field geometry at the peak of spoke activity had the northern SKR active region (the magnetic field region which, when pointing at the Sun, produces the largest northern SKR emissions) coincident with the morning ansa of the rings. Spokes were observed by Voyager to be both more common and to have higher contrast during this geometry. This behavior indicated a possible link between spokes and magnetospheric processes, and suggested that passage of the northern SKR-active sector through Saturn's shadow may play a significant role in the creation and/or rejuvenation of spokes (Porco and Danielson, 1982).

The actual formation of a spoke in Voyager images was rarely observed. One spoke was seen to appear in a Voyager image taken a mere 5 minutes after an image in which it was not present (Smith et al., 1982). Such a short timescale

for formation puts serious restrictions on the origin of the spokes. Some spokes, presumably newly formed, have been observed to spread out and increase in contrast. These spokes have one edge (leading (trailing) for spokes outside (inside) the corotation radius, approximately 112,200 km) which orbits at a rate between Keplerian and corotation with the magnetic field. This "active" period can last for > 4000 seconds and depends on the spoke morphology (Grün et al., 1983).

Many ideas have been proposed to account for spoke formation. Of these, the best developed invoked meteoroid impacts onto the B ring (Goertz and Morfill, 1983). In this model, the impact forms an expanding cloud of neutrals which is then ionized by solar ultraviolet radiation. The resulting plasma negatively charges both the large ring particles and the small dust grains on their surfaces. The resulting repulsive electrostatic force levitates the dust grains off the larger ring bodies. Finally, the plasma is then transported radially by an $\vec{E} \times \vec{B}$ force, where the azimuthally-directed electric field is generated by the charge separation caused by the dust grains leaving the plasma. As it moves, the plasma cloud continuously charges and levitates more dust grains. The resulting radially-extended line of levitated dust comprises the newly formed spoke. According to the authors, the rate at which the plasma moves across the rings is sufficient to form a spoke rapidly. However a recent paper has challenged this hypothesis (Farmer and Goldreich, 2005), claiming that the plasma would move considerably slower than originally predicted. Additionally, an $\vec{E} \times \vec{B}$ drift can only push the plasma in one direction, away from the corotation radius in the impact model, so the radial growth of a spoke will be solely away from corotation.

A more recent suggestion invokes lightning-induced electron beams originating from thunderstorms on Saturn (Jones et al., 2006). In this model, a discharge produces a quasi-static electric field which accelerates the electrons to high energies. These electrons follow the magnetic field lines passing through the storm until they impact the ring. This electron beam charges the ring particles and any loose regolith particles on their surfaces, and levitates the latter, forming

a spoke (Horányi et al., 2010). Such a model can be readily tested by comparing the rotational periods, magnetic field locations and temporal variability of Saturn's electrical storms with those of the spokes.

As observed by HST over the course of 9 years, spokes were seen to gradually become less common as the ring opening angle to the Sun increased and disappeared entirely at tilt angles above 15° (McGhee et al., 2005). This was originally believed to be a photometric effect due to the reduced path length through the optically thin spokes as the ring opening angle increased. Based on this idea, it was expected that Cassini would observe spokes soon after entering orbit since the spacecraft would be imaging the rings at low elevation angles, geometries that would enhance spoke visibility.

Despite this prediction, no spokes were observed in any Cassini images until September of 2005, over a year after orbit insertion. This indicates that, instead of being solely a photometric effect, the appearance of spokes has a seasonality which has yet to be well-understood. One possibility is that the formation mechanism had simply stopped or become much less active during this time, such as the proposal by Farrell et al. (2006) where spokes only form when both sides of the rings are negatively charged. Another possibility is that the formation of spokes is continuous, but the charging environment above the ring can under certain circumstances rapidly destroy them. In this model (Mitchell et al., 2006), the spoke particles and the underlying ring both initially get charged in the same sense, then develop opposite charges, so that the spoke particles are pulled back down to the ring. If the spoke particles and large ring particles are normally positively charged, and suddenly both are charged negatively by a dense plasma cloud to form a spoke, then once the plasma dissipates, the large particles will revert back to a positive charge very rapidly due to the photoelectric effect, while the small spoke particles will take much longer to become positive due to their smaller cross section. Examination of the detailed behavior of spokes will shed light on which possibility is correct and constrain models explaining the spokes' variability.

While some early Cassini imaging sequences did contain spokes, the majority

were not designed to determine the spoke periodicity and would typically image only a few spokes for a short period of time. Due to the paucity of spokes in these earlier observations, this paper will concentrate on more recent observations which were specifically designed to look for periodicities in the spoke activity and were taken during Cassini's extended mission.

In this paper, we analyze the data from two distinct sets of observations. The first is composed of 6 spoke movies from early in Cassini's extended mission which were distantly separated in time and taken on the morning portion of the southern side of the rings in 2008, prior to northern vernal equinox in August 2009. The second is a series of 13 closely spaced spoke movies taken of the northern side of the rings near local noon over a period of approximately two weeks shortly after equinox. Both are of the lit side of the rings.

We use the first southern set of observations to measure the activity levels of individual spokes as a function of time as they orbit Saturn and calculate the rate at which spoke particles are being levitated or settling back onto the large ring bodies. We measure the positions and motions of the most prominent spokes' edges in an effort to understand their short-term dynamics.

We further examine the southern observations for spokes which appear new on the rings between images or which come out of Saturn's shadow not fully grown. We measure the radial growth of these spokes and, where possible, the shearing of the leading and trailing edges.

Finally, we analyze both data sets for the presence of any periodic variation in the appearance of spokes, which may exhibit correlations with other Saturn-system phenomena, of which Cassini has significantly enriched our understanding. First, the Cassini RPWS instrument detected SEDs and found them to repeat with a period closer to 640 min (Fischer et al., 2007). Second, comparison of the period and phasing of the SEDs with ISS images of Saturn's southern hemisphere has shown that (i) the SEDs originate within 'storm alley', a narrow latitude band within the southern hemisphere of the planet in which storms, large and small, regularly appear, and (ii) the SED period corresponds to the rotational period of the individual storms (Dyudina et al., 2007). Second,

Cassini's long-term monitoring of the SKR has revealed two SKR sources – one in the southern auroral region and one in the north - each with different periods and temporal behavior in their emissions (Gurnett et al., 2011). For example, the SKR period of the southern source (which has been observed the longest by Cassini) has slipped by $\approx$ 5 minutes over a 4-year timespan. Cassini imaging observations of spokes on both sides of the rings (north and south), both prior to and just after northern vernal equinox in August 2009, now make it possible to search for the influence of both SKR sources on the spokes' behavior on either side of the rings. We search for correlations between spoke activity and these phenomena.

2. Observations and Data Reduction

All of the observations discussed in this paper consist of "point and stare" movies where the spacecraft points the Imaging Science Subsystem (ISS) at one of the B ring ansae and images at regular intervals for approximately one Saturn rotation period. For the early observations, only the Wide Angle Camera was used, while for the later observations, either the Wide Angle Camera (WAC) or the Narrow Angle Camera (NAC) were used, depending on the range to the rings. To maximize longitudinal coverage of the rings, the NAC was used only when the range exceeded 2.8×10^6 km, or about 47 Saturn radii (R_S). These observations were taken exclusively of the lit side of the rings, with the spokes directly illuminated by the Sun. We do not consider any unlit observations in this paper.

The first set of observations, consistint of the six spoke movies taken prior to equinox, were all taken at low phase on the southern (lit) side of the rings. This set spans a 147 day period between July 2nd and November 25th of 2008. The interval between images for these observations varied between 752 seconds and 1042 seconds. (The exposure times for these images is always considerably shorter, on the order of 10 ms.) As these movies were taken at low phase, the spokes appear dark against the background B ring. These observations are summarized in Table 1. Figure 1 shows typical images from both the beginning

and end of a southern observation (the August observation in this case) which have been contrast enhanced to bring out the spokes. The ring opening angle always decreases from the start of the observation to the end, as does the phase angle. These observations were at a high enough spatial resolution and imaged frequently enough to allow for the tracking of individual spokes in multiple images and we use them here to study the kinematics of individual spokes' edges and activity levels in addition to the overall spoke activity.

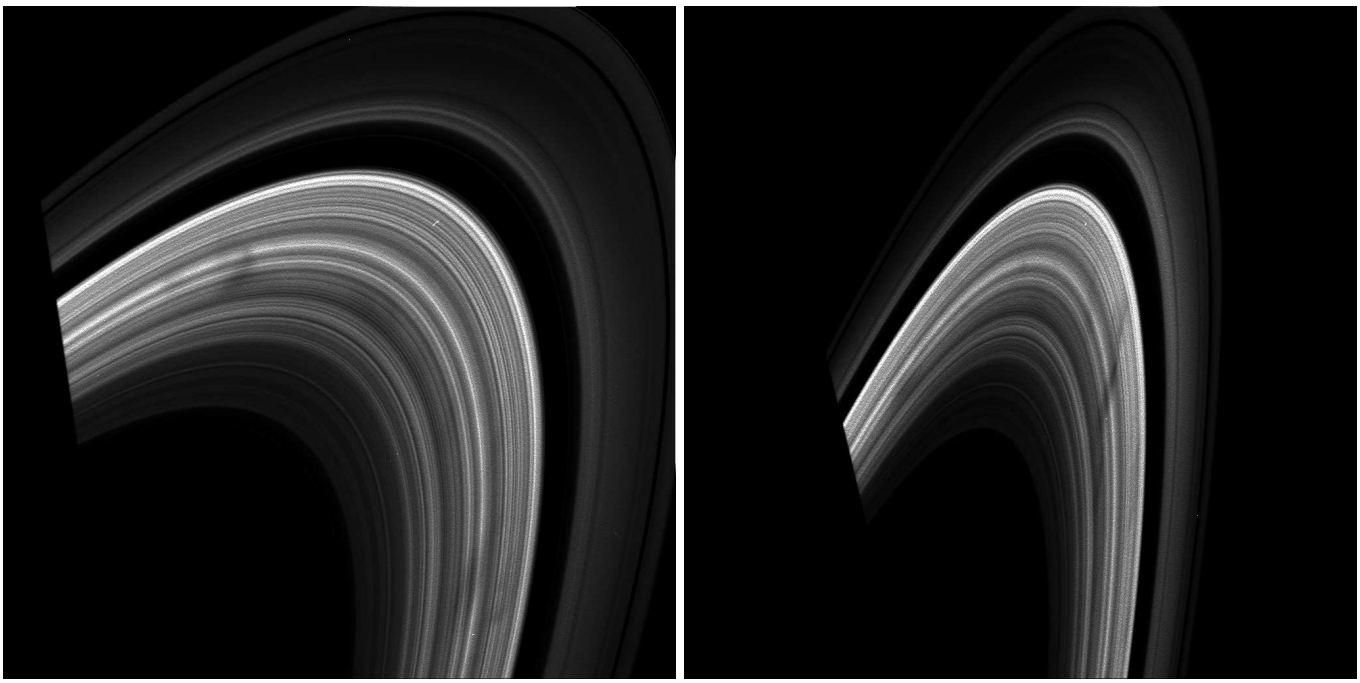

Figure 1: A pair of images of the morning ansa of Saturn's B ring taken during the August, 2008 observation from approximately 17 R_S with the Wide Angle Camera. (Left) Start of the observation (W1597971520), where the opening angle to the rings is 19.1 degrees and the resolution is 57.7 km per pixel. (Right) End of the observation (W1598009545), with an opening angle of 11.4 degrees and the resolution is 64.0 km per pixel. In both of these images, north is to the lower right and orbital motion is clockwise. Both images have been stretched to bring out the spokes, which have contrasts of $< 10\%$.

The second set of observations was taken of the northern (lit) side of the rings shortly after the solar ring plane crossing, which occurred on August 11, 2009. Between August 30 and September 13, 2009, 13 observations were taken at modest phase ($80^\circ \leq \alpha \leq 120^\circ$), during a single long orbit of modest inclination

(12°) and high apoapse ($49R_s$). WAC movies were taken of the rings until the range increased to $\approx$ 47 R_S, after which NAC movies were taken, for a total of 6 WAC movies and 7 NAC movies. Table 2 summarizes these observations while Fig. 2 shows two images from two separate observations, one from a WAC movie and the other from a NAC movie. Though these observations are not as suitable as the earlier ones for tracking individual spokes due to a combination of low spatial resolution for the WACs and low imaging rate for the NACs, the excellent coverage of the ring they provide during this time, and the long temporal duration, make them ideal for determining periodicities in the spoke activity.

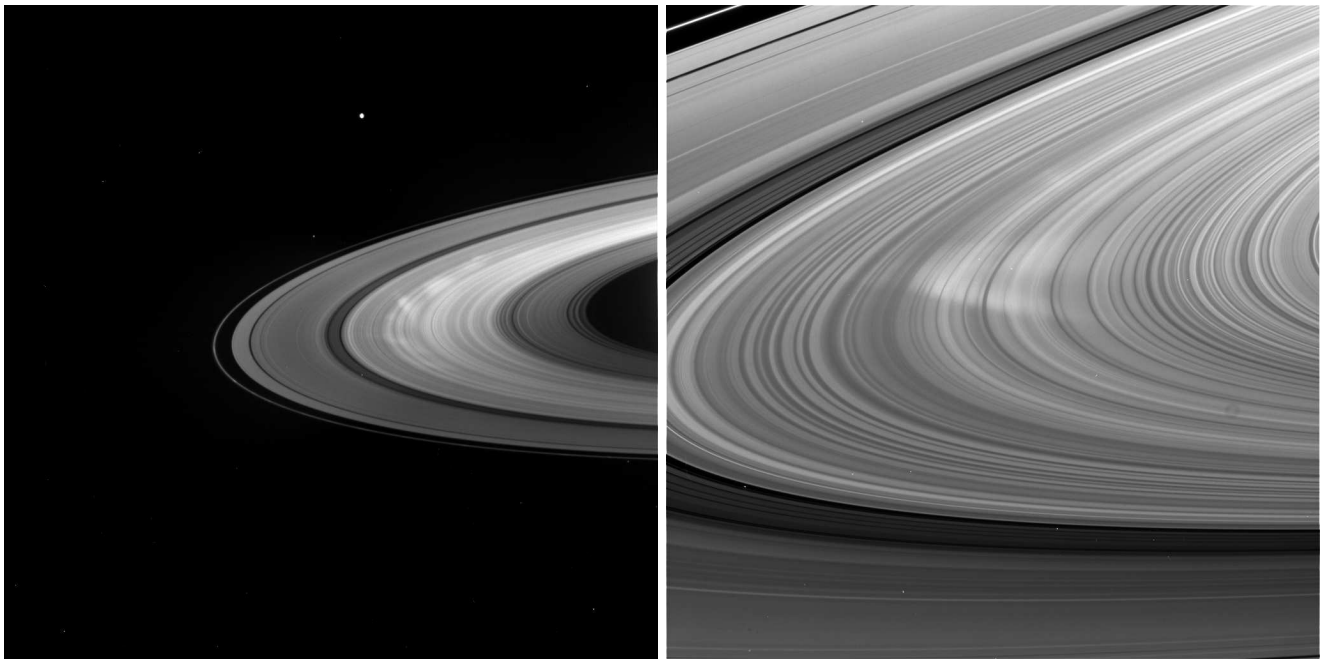

Figure 2: Typical images of the north side of the rings from a WAC movie (W1630376554, left) and NAC movie (N1631517179, right), with prominent spokes on the ansa. Variation in the background B ring I/F due to Saturn shine is visible in the images as a brightening of the upper portion of the rings compared to the lower portion. Resolutions for these images are (left) 112 km per pixel and (right) 15.6 km per pixel.

For all of our observations, the images were first calibrated using the latest version of the Cassini ISS Calibration (CISSCAL) software package archived

with the NASA Planetary Data System to convert the raw data numbers (DN) for the pixels into I/Fs (Porco et al., 2004; West et al., 2010). All the images in these observations were taken using the clear filters for the WAC or NAC.

For accurate radial and longitudinal measurements, it is necessary to determine the absolute pointing of the image by navigation on features of known absolute radius. Accurate pointing of the images is achieved by fitting to the outer A ring edge in all the images it appears, which includes all the southern observations except the November, 2008 observation as well as all the WAC movies in the northern observations. At the distance at which these images were taken ($\approx 10^6$ km for the southern observations and between 1.7×10^6 and 2.9×10^6 km for the northern observations), sky plane pixel scales are approximately 60 km for the southern observations, while the northern observations have a minimum of 100 km for the WAC movies. The $m = 7$ pattern of the outer edge of the A ring can introduce an error as high as 50 km, less than one pixel (Spitale and Porco, 2009). For the November observation and the northern NAC movies, where not enough of the outer A ring edge was visible and only the B ring edge is present in the images, respectively, we fit to the outer edge of the B ring instead. The $m = 2$ pattern of this edge introduces an error as high as 85 km for these observations (Spitale and Porco, 2010).

Since the observed spokes always appear against the B ring, all images containing spokes have a spatially varying background which varies slowly in the azimuthal direction but changes rapidly as a function of radius due to the individual ring features. We therefore scanned in azimuth across very limited radial regions for the entire radial extent of the spoke in order to determine its 2D radial profile. These scans were obtained using a well-tested image navigation and analysis software package developed within CICLOPS known as the Modular Image Navigation and Analysis Software or MINAS. The individual scans taken from the southern observations are all 200 km in radial extent while the northern observations are 1000 km in extent. All the radial locations are chosen so that there are no gaps or overlap in the radial coverage of the spoke. We perform the scans between a radial range of $97,000$ and $117,000$ km for

all but the northern NAC movies, where the scans ranged from 103,000 and 113,000 km due to the more narrow view. These ranges cover the region of the B ring in which the spokes appear and are most prominent, respectively. The azimuthal extent of the scans varies depending on the exact viewing geometry, but is always in excess of 60° for WAC images (of either set) and 40° for NAC images.

In order to search for correlations between spoke activity on the rings and the SKR sources, as was previously found for Voyager era spokes, we calculate the location of the spokes using a rotating coordinate system which maintains the SKR source at a fixed longitude. Such a calculation is complicated by the fact that the SKR does not have a fixed period as was previously thought. Additionally, recent observations have determined that the SKR emanating from the two different poles have different periods.

The southern spoke observations occurred from July to November of 2008, while the northern ones were from August to September of 2009. During these two periods of time, the relevant coordinates based on the SKR are SLS4-N and SLS4-S, which depend on the northern and southern SKR sources, respectively (Gurnett et al., 2011). Analyses have shown that the shorter period emissions arose from the northern hemisphere source during the time of our observations, while the longer period emissions (the ones originally presented in Kurth et al. (2007)) arose from a source in the southern hemisphere (Gurnett et al., 2009a; Kurth et al., 2008). The shorter northern period is close to that believed, by some, to match the internal rotation of the planet (Anderson and Schubert, 2007), though this inference has been questioned (Gombosi and Ingersoll, 2010).

To determine a spoke's magnetic longitude, we first determine the position of the spoke - taken to be the centroid of the spoke weighted by its optical depth – in an inertial coordinate system. To convert this into a magnetic longitude, we use the position of the Sun in our inertial coordinate system and calculate its position in the chosen magnetic longitude. These three quantities are then used

to calculate the spoke's magnetic coordinates by the simple transformation:

$$\lambda_{Mag}^{spoke} = \lambda_{Mag}^{Sun} + \lambda_{inertial}^{Sun} - \lambda_{inertial}^{spoke} \quad (1)$$

which converts the spoke longitude in our inertial right handed coordinate system into the non-inertial left handed magnetic coordinates.

2.1. Measuring Spoke I/F

To analyze an individual spoke in an image from our early southern-side observations, we take each of the ring profiles in which it appears and perform a separate linear fit of the background I/F of the B ring near the spoke for each azimuthal profile. This background is then subtracted out and the remaining I/F is fit to a Gaussian, representing the spoke at the specific profile's radius. This method has the advantage of providing a functional form for the spoke profile, allowing spokes which appear in multiple images to be tracked. We find that for the majority of spokes, Gaussians produce good fits, regardless of whether or not the spoke is active. Figure 3 shows two examples of typical spoke profiles. The upper profile is from a spoke with an I/F which is increasing with time, while the I/F of the spoke in the lower profile is decreasing.

Spokes which are not well fit by a Gaussian can often be shown to consist of two or more overlapping spokes by examining the profiles as a function of radius. As spokes are narrower near the corotation radius and will typically have different degrees of shear, the overlapping spokes will often separate azimuthally for some range of radii. Figure 4 shows a series of scans for two different spoke clusters. The individual scans have been placed at the appropriate radii to allow a better visualization of the spokes. Both clusters consist of three spokes. In the first of these clusters, the spokes become distinct as the radius increases, with the spokes separating near the corotation radius. (The corotation radius is at $\approx 112.3 \times 10^3$ km for a rotation period of 637 minutes.) In the second cluster, the spokes are overlapping near corotation, but exhibit different degrees of shear, and become distinct as the radius decreases.

To fit spoke clusters such as these, the background I/F is first fit in the usual way, ignoring any spokes in the region of interest. Portions of the cluster

which appear to be just a single spoke are then selected for fitting. These fits are then subtracted from the profile and the remaining spokes are fit. This process will not provide an accurate enough fit for the tracking of the edges of such complex spokes (section 3.3), but does provide a measure of spoke activity for the cluster as a whole.

Observation	Date 2008	Start Time UT	Duration (min)	Phase Angle (°)	Sub-Spacecraft Latitude (°)	Sub-Solar Latitude (°)	Pixel Scale (km)	Images	Interval (min)
ISS_074RI_SPKLFMOV001_PRIME	Jul 2	07:10	544	14.41 – 13.82	-8.0 – -3.1	-6.2	63.5 – 68.1	17	33.98
ISS_081RI_SPKMVLFLP001_PRIME	Aug 21	00:20	634	23.15 – 18.45	-19.1 – -11.3	-5.5	57.7 – 64.	40	16.25
ISS_085RI_SPKMVLFLP001_PRIME	Sep 19	19:22	590	21.49 – 18.55	-13.8 – -7.4	-5.0	60.0 – 62.1	35	17.37
ISS_086RI_SPKMVLFLP002_PRIME	Sep 26	22:12	596	24.58 – 20.40	-18.3 – -11.2	-4.9	57.2 – 61.4	36	17.03
ISS_088RI_SPKMVLFLP001_PRIME	Oct 11	22:30	708	21.94 – 18.85	-13.0 – -5.5	-4.7	60.5 – 61.7	50	14.45
ISS_094RI_SPKMVLFLP001_PRIME	Nov 25	21:55	602	38.78 – 30.68	-32.6 – -22.6	-4.0	50.8 – 57.9	49	12.53

Table 1: The date, start time, duration, range of phase angle, range of sub-spacecraft latitude, sub-solar latitude, skyplane pixel scale, number of images, and imaging interval for the early southern-side observations. Negative values denote southern latitudes. Ranges for angles are given from the start of the observation until the end. All observations were taken in 2008 using the Wide Angle Camera.

Observation	Date 2009	Start Time UT	Duration (min)	Phase Angle Range (°)	Sub-Spacecraft Latitude (°)	Sub-Solar Latitude (°)	Pixel Scale (km)	Camera	Images	Interval (min)
ISS_117RI_SPKMVLFHP001_PRIME	Aug 30	16:53	905	81.5	11.7	0.30	101.5 – 111.5	WAC	78	10.8
ISS_117RI_SPKMVLFHP003_PRIME	Sep 1	20:33	1054	84.5	11.2	0.32	121.1 – 131.3	WAC	110	9.7
ISS_117RI_SPKMVLFHP004_PRIME	Sep 2	00:03	845	89.2	10.9	0.34	136.5 – 143.1	WAC	90	9.5
ISS_117RI_SPKMVLFHP005_PRIME	Sep 3	00:03	813	92.5	10.3	0.35	147.3 – 152.5	WAC	85	10.0
ISS_117RI_SPKMVLFHP006_PRIME	Sep 4	02:03	1085	95.7	9.9	0.37	156.6 – 161.7	WAC	119	9.1
ISS_117RI_SPKMVLFHP007_PRIME	Sep 5	06:33	759	98.9	9.5	0.39	164.2 – 170.6	WAC	85	9.0
ISS_117RI_SPKMVLFHP008_PRIME	Sep 6	06:33	782	100.5	9.1	0.40	17.2 – 17.4	NAC	62	12.8
ISS_117RI_SPKMVLFHP009_PRIME	Sep 7	07:27	419	103.0	8.7	0.42	17.5 – 17.5	NAC	23	19.0
ISS_117RI_SPKMVLFHP010_PRIME	Sep 8	05:57	865	105.2	8.4	0.43	17.6 – 17.6	NAC	45	19.7
ISS_118RI_SPKMVLFHP001_PRIME	Sep 9	08:12	715	107.8	8.0	0.45	17.5 – 17.4	NAC	36	20.4
ISS_118RI_SPKMVLFHP002_PRIME	Sep 11	05:48	321	112.5	7.2	0.48	16.9 – 16.8	NAC	27	12.3
ISS_118RI_SPKMVLFHP003_PRIME	Sep 12	01:02	748	114.7	6.8	0.49	16.5 – 16.1	NAC	36	21.4
ISS_118RI_SPKMVLFHP004_PRIME	Sep 13	01:02	591	117.6	6.3	0.51	15.8 – 15.4	NAC	28	21.9

Table 2: The date, start time, duration, range of phase angle, sub-spacecraft latitude, sub-solar latitude, skyplane pixel scale, camera used, number of images and imaging interval for the later northern observations. All observations were taken in 2009.

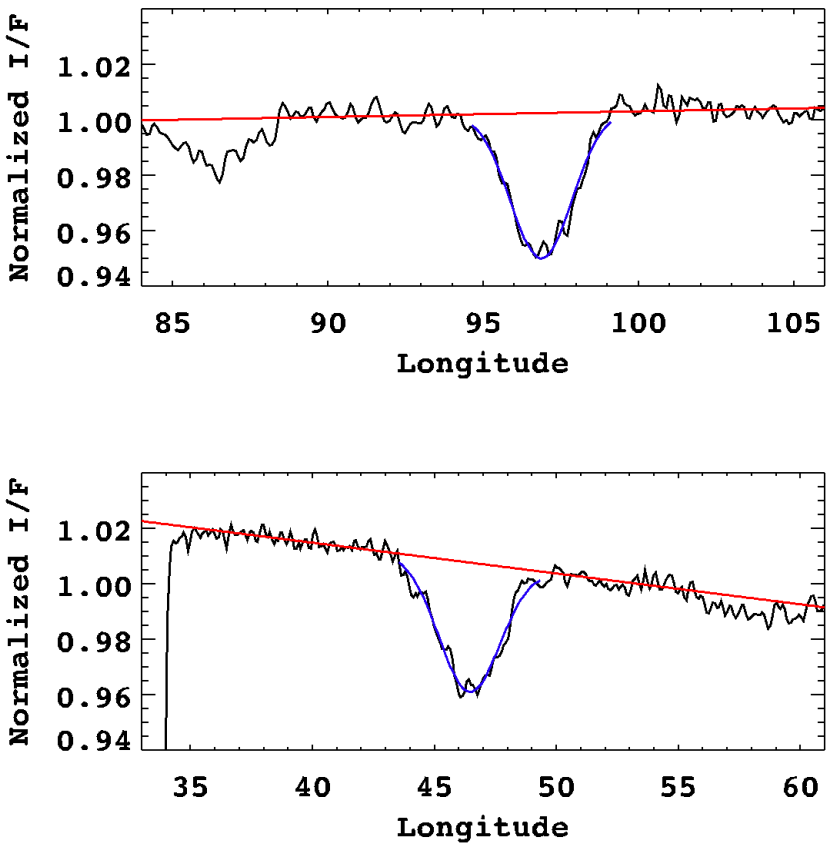

Figure 3: Azimuthal I/F profiles for two spokes in the August, 2008 observation, a WAC movie of the southern side of the rings. The red curves are the local linear fits to the background while the blue curves are Gaussian fits for the spoke profile added to the background. I/F has been normalized to the median value in each scan. Longitudes are right-handed with the Sun located at 180°. Resolutions for the images were (top) 64.0 km per pixel and (bottom) 60.2 km per pixel.

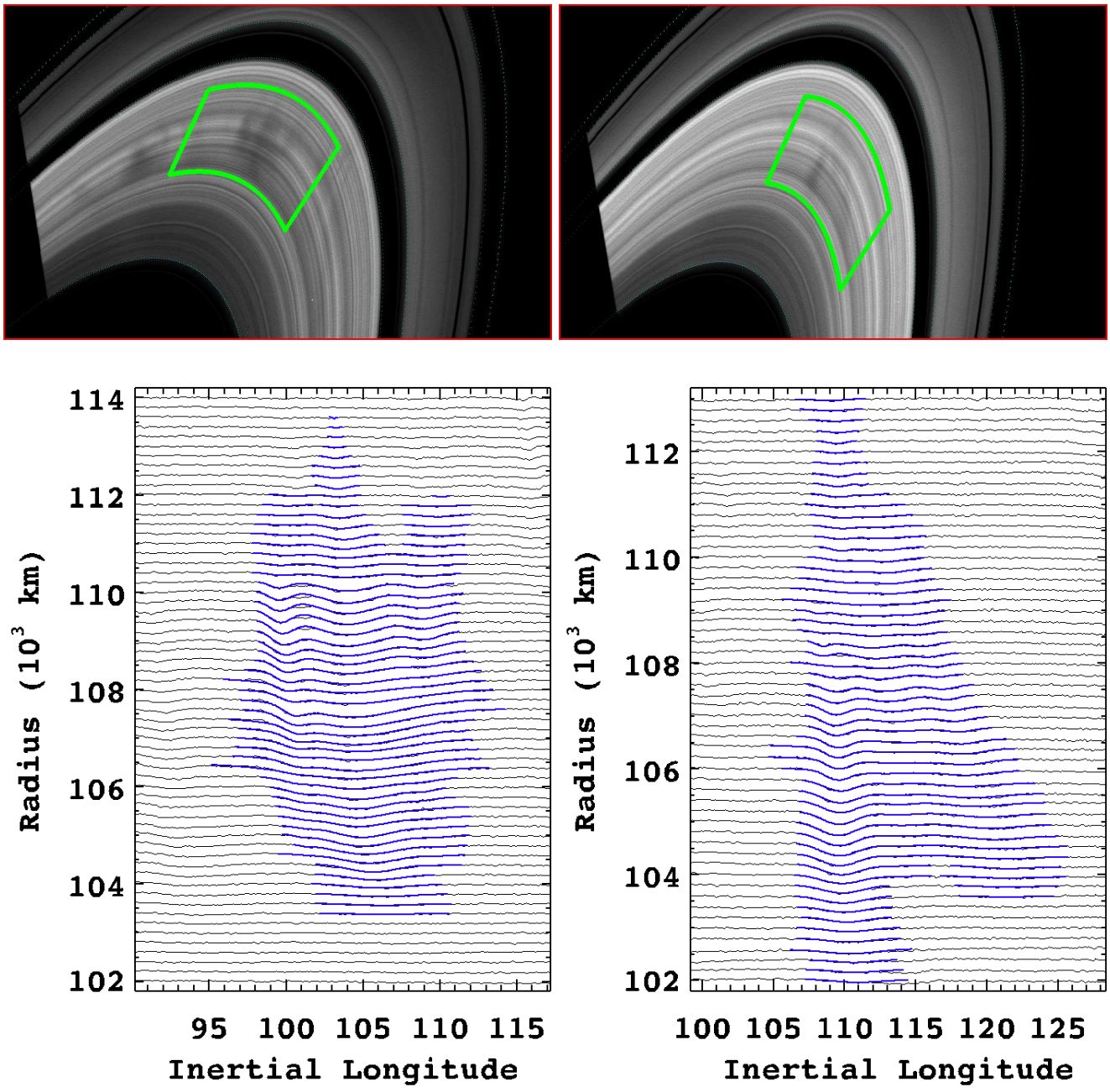

Figure 4: Azimuthal profiles over a range of sequential radii for two overlaying spoke clusters in the second September, 2008 observation. The vertical axes of the scans are normalized to the background ring I/F and then plotted at the appropriate radius. The blue curve is the sum of the spokes' Gaussian fits, while the horizontal dashed line at 112.3×10^3 km marks the approximate location of the corotation radius. The longitudinal scale is approximately 1960 km per degree at this radius. Resolutions for the images were (left) 58.0 km per pixel and (right) 59.2 km per pixel.

For the later northern-side observations, we do not fit the individual spokes, but instead perform a global fit to the entire B ring I/F, excluding the spokes where possible. This fit is then subtracted from the scans to get the spoke I/F as a function of longitude. We find that in this geometry, the spoke-free B ring I/F is well approximated by a constant, plus a long wavelength sinusoid due to reflected Saturn-shine which is a major contributor to the illumination for these observations taken soon after equinox. We exclude the spoke-filled regions of the B ring by first performing the fit to the entire scan, excluding the edges. We then calculate the standard deviation of the data from the fit and then refit after removing from consideration all of the data that falls more than one standard deviation above the previous fit to remove the spokes, which are bright in this geometry. Iterating this process produced a converging fit in all cases. Figure 5 shows the calculated background overlaid on a scan.

2.2. Conversion to Optical Depth

Because the microscopic spoke particles occupy an optically thin layer of forward-scattering particles, their contrast with the surrounding B ring depends strongly on the observing geometry. Thus, once the change in I/F due to a spoke has been determined, the next step is to use a photometric model to convert the $\Delta I/F$ into an optical depth of dust particles. Since the optical depth in spoke particles is very small ($\approx 1\%$ (McGhee et al., 2005)) the optical depth is proportional to the number of particles in the spoke. So once the conversion has been achieved, the optical depth can be integrated to yield the activity level for the spoke.

We treat the spoke as a haze layer above the ring (McGhee et al., 2005) and use a modified version of a plane-parallel polarized radiative transfer code, `rt3`, originally designed to model planetary atmospheres (Evans and Stephens, 1991) (also see `http://nit.colorado.edu/polrad.html`). We use a haze layer as previous attempts to model the spoke particles as intermixed with the larger B ring bodies produced unphysically high optical depths for the dust. Additionally, previous simulations of the spoke particle trajectories indicate the particles can

achieve heights above the rings of tens of kilometers (Mitchell et al., 2006).

The size distribution for the spoke particles was chosen to be a gamma (Hansen-Hovenier) distribution with an effective radius of $r_{\rm eff} = 0.57$ μm and a variance of $b = 0.09$, as measured by Hubble (McGhee et al., 2005).

To perform the conversion, we use `rt3` to calculate $\Delta I/F$, i.e., the I/F for a spoke minus the I/F of the background B ring, for an assumed normal optical depth of spoke particles $\tau = \tau_0 = 0.01$. We then scale, assuming that $\Delta I/F$ is proportional to τ, so that the optical depth of the spoke is given by

$$\tau_{\rm spoke} = \tau_0 \frac{\Delta I/F_{spoke}}{\Delta I/F_0} \tag{2}$$

where $\tau_0 = 0.01$ and $\Delta I/F_0$ is the change in I/F calculated for a spoke with an optical depth of τ_0.

We calculate the conversion factor for each individual spoke. In any case, as there is little change in the geometry of the observation during the short time that a spoke passes through the field of view (typically < 2 hours), the conversion from I/F to optical depth is nearly constant for an individual spoke. More important is the change in the viewing geometry over the entire observation. The phase angle in all the early observations decreases with time, as does the ring opening angle to Cassini. These changes in geometry would cause a spoke with a given optical depth to appear darker at the end of the observation than at the beginning. While this works well for the early observations, the late ones are at an extreme geometry which precludes us from using this technique. For those we use a different technique, as explained in section 5.

An error estimate for this conversion process was determined by choosing an optical depth and calculating the $\Delta I/F$ of the spoke after changing the size distribution to reflect the quoted 1σ error in the Hubble model estimates. (i.e., $\sigma_{r_{\rm eff}} = 0.05$ μm and $\sigma_b = 0.03$). Specifically, reducing the effective particle size $r_{\rm eff}$ to 0.52 μm while keeping the variance b at its nominal value of 0.09 changed the conversion factor by no more than 5%, while assuming the nominal $r_{\rm eff} =$ 0.57 μm and reducing b to 0.06 changed the conversion factor by less than 2%.

Finally, to check the assumption of linearity in Eq. 2, we calculated $\Delta I/F$

for spokes with varying τ. We found that $\Delta I/F$ was approximately linear, with some deviation for high optical depth spokes. For $\tau = 0.05$, a very active spoke, the deviation is approximately 20%. The effect of this deviation is to slightly underestimate the optical depth of the spokes with the highest optical depths.

3. Individual Spoke Analysis

3.1. Individual Activity as a Function of Time

We first examine the activity levels of individual spokes, defined as the area-integrated optical depth of the dust grains comprising it, for the spokes observed in the southern movies. Using the $\Delta I/F$ fitting procedure for individual spokes and the optical depth conversion technique described previously, we determine the optical depth of the spokes as a function of longitude and radius. We then perform an integration of this optical depth over the area of the ring containing the spoke, yielding the spoke's activity. Using these techniques, we have performed measurements on a total of 118 of the darkest spokes appearing in multiple images in the southern observations as well as 7 spokes seen in single images.

A typical image covers a range of longitude in the B ring on the order of 60° or more and contains perhaps 5 to 10 measurable spokes. As the slowest imaging rate for these movies was one image per 34 minutes in the July, 2008 observation and did not drop below one per 17 minutes for the other southern movies, the majority of spokes were imaged multiple times, as a Keplerian spoke at a typical radius travels between 32° and 42° in longitude per hour. While we have not imaged rapidly enough in these observations to confirm spoke formation on the timescale seen by Voyager (Smith et al., 1981, 1982), the multiple detections allow us to track the activity of individual spokes as a function of time.

We find that the activity level for a typical spoke is usually changing as a function of time. This includes spokes which are growing in optical depth, the "active" spokes first reported by Grün et al. (1992), as well as spokes which are fading out at the end of their lives. To illustrate the details of how a spoke's activity changes, we follow a single active spoke over the portion of its lifetime

which was captured, calculating its activity as a function of time and location. We do not have any examples of spokes where we have observed for its entire lifetime due to the relatively small portion of the ring which was imaged.

Figure 6 shows a series of azimuthal I/F scans over a fixed range of radii and corotating longitude for a solitary active spoke. Each panel is taken from a different image in which it appears, with the earliest image on the left and the image immediately before the spoke leaves the field of view on the right. The spoke grows both radially and azimuthally and increases in peak contrast over the 5850 seconds it is visible before it leaves the field of view.

To further investigate this spoke's activity, we calculate the area under the Gaussian fits using the Gaussian's amplitude and width as a function of radius This quantity is effectively an activity per unit length of the spoke. Figure 7 shows the results for this active spoke. As the spoke expands, the central portion continues to increase its $\Delta I/F$ during the entire time. The shape of this radial profile, being slightly asymmetrical, is typical of a lone spoke. It is difficult to reconcile this behavior with spoke formation models which rely on drifting plasma clouds as not only is the optical depth of the entire spoke growing for the entire time, but the spoke expands both away from and towards the corotation radius, while a plasma moving along the ring due to $\vec{E} \times \vec{B}$ drift can move in only a single direction.

Finally, we convert the $\Delta I/F$ of the spoke in each image into optical depth and integrate over the entire area in which the spoke appears for each image. The spoke's activity grows linearly with time and shows no sign of slowing before the spoke leaves the field of view, as shown in Fig. 8. We find that this spoke has a peak activity of around $64.6 \pm 2.9 \times 10^3$ km^2, which it obtained after ≈ 5850 seconds of growth. Fitting a line to the activity as a function of time gives a growth rate of 632 ± 33 km^2/min. Assuming a mean particle radius of 0.4 μm, the peak in the size distribution given by McGhee et al. (2005), this would imply that dust grains are being levitated above the B ring at an approximate rate of 2×10^{19} grains per second. Using the larger grain radius recently reported by D'Aversa et al. (2010) of 1.8 μm gives a rate of 10^{18} grains per second.

We calculate each spoke's peak activity by fitting a line to the activity as above and taking the maximum value of the fit, represented by the blue diamond in Fig. 8. For this spoke, the peak value we measure corresponds to the final image it is in before it moves out of the field of view, a common occurrence in this dataset. It is also common for a spoke to leave Saturn's shadow at its peak observed activity which then decrease in subsequent images. In such cases, we take the peak measured value as the maximum value of the spoke. Using this procedure, we find that most spokes have a peak activity level less than 60×10^3 km^2, as shown in Fig. 9, where we have plotted a histogram of spoke peak activity with 20×10^3 km^2 bins. There is a sharp decrease in the number of spokes beyond 60×10^3 km^2, with 103 of the measurable spokes falling below this activity and only 22 falling above, with the maximum spoke activity observed being 271×10^3 km^2 for an extremely large spoke which appeared in the September 19, 2008 observation.

As noted earlier, it is very common for an individual spoke's activity to change as it orbits Saturn. We find that linear fits to individual spoke activity levels work well for the majority of spokes, although a few spokes may be reaching their peak activity and then starting to fade out. Using the linear fits, we calculate the number of growing "active" spokes and fading spokes and present the results in Table 3. We use the error in the slopes of these fits to determine whether a spoke is increasing in activity. Spoke fits with slopes within one standard deviation of their respective errors count as unchanging, while those outside their error count as either increasing or decreasing. We find that the number of spokes with increasing activities is approximately twice the number with decreasing activities. This asymmetry is consistent with the observations being taken on the morning portion of the rings (local times), where the spokes have been observed to be more common and have the higher contrasts than at evening local times. Looking at the histogram of individual spoke growth rates, Fig. 10, we find that the distribution is skewed towards the positive, as expected. We shall further investigate the growth rates of spokes with regard to their corelation to magnetic longitude in Section 5.

Observation	# Spokes	Increasing	Decreasing	Unchanged
ISS_074RI_SPKLFMOV001_PRIME	12	3	6	3
ISS_081RI_SPKMVLFLP001_PRIME	18	9	5	4
ISS_085RI_SPKMVLFLP001_PRIME	23	13	7	3
ISS_086RI_SPKMVLFLP002_PRIME	15	10	3	2
ISS_088RI_SPKMVLFLP001_PRIME	35	23	11	1
ISS_094RI_SPKMVLFLP001_PRIME	11	2	7	2

Table 3: The number of spokes for which a Gaussian profile was sufficient for the measurement of the activity in multiple images, the number of spokes with an increasing activity, the number of spokes with decreasing activity, and the number of spokes which showed little or no change in activity.

While most of the spokes in these observations emerge from the planet's shadow on the rings in the first image they are visible, a fraction appear to form in between consecutive images. We shall refer to spokes which are growing radially as "forming" spokes. "Forming" spokes are typically "active" as well, in the previously reported sense that one edge is corotating while the other is undergoing Kepler shear (Grün et al., 1983). These spokes initially appear very faint and small both radially and azimuthally. As can be seen in Fig. 6, the radial extremes of the spoke have the lowest contrast. This is consistent with previous Voyager observations of forming spokes (Grün et al., 1983), though the consecutive images reported previously were separated by only 288 seconds. For our images, a typical separation is about 1000 seconds. We discuss several of these forming spokes in detail in the next section.

In the six southern observations, we find a total of 51 spokes which are clearly absent in one image and then appear in the next. The total duration of these observations is 3647 minutes, which implies a spoke formation rate of one every 72 minutes on this portion of the rings. Compared to the number of spokes that we observe leaving the shadow, > 200, this number is rather small which implies that most spokes on the morning portion of the rings are formed within the shadow region.

3.2. Spoke Particle Dynamics

The dynamics of small dust grains in planetary magnetospheres, such as those that comprise the spokes, is often complicated by such forces as radiation

pressure, Poynting-Robertson drag, and drag from collisions with the various plasma species and neutrals. However, these forces typically have effects over timescales of many years (Goldreich and Tremaine, 1982), while the spokes have lifetimes on the order of hours, as measured by the degree of shear of their edges (Smith et al., 1981; Grün et al., 1983). For such short timescales, all drag forces can be safely neglected, though collisions with ions and electrons will charge the dust grains, as will the photoelectric effect. The remaining forces that require consideration are gravity and the Lorentz force due to the magnetospheric electric and magnetic fields. The equation of motion for such a charged dust grain in a planetary magnetosphere is given by

$$\ddot{\mathbf{r}} = -\nabla\Phi_{\mathrm{G}} + \frac{q}{m}(\mathbf{E} + \frac{\dot{\mathbf{r}}}{c} \times \mathbf{B}) \tag{3}$$

where m and q are the grain's mass and charge, respectively, Φ_{G} is the gravitational potential, c is the speed of light, $\mathbf{B}$ is the planetary magnetic field at the dust grain's location, and $\mathbf{E}$ is the corotational electric field. For a plasma perfectly corotating with the planet, this electric field is given by

$$\mathbf{E} = -\frac{1}{c}(\mathbf{\Omega} \times \mathbf{r}) \times \mathbf{B} \tag{4}$$

where $\mathbf{\Omega}$ is the planet's rotational angular velocity and $\mathbf{\Omega} \times \mathbf{r}$ is the velocity of a corotating element of plasma at location $\mathbf{r}$.

Assuming that the spoke particles travel on circular orbits, the charge to mass ratio of a particle can be determined by measuring the deviation of its orbital velocity from Keplerian motion. Saturn's magnetic field is well approximated by a dipole aligned with the rotation axis with a small northward offset and which has a small octupole moment (Dougherty et al., 2005). We constrain the dust grains to orbit in the ring plane, neglecting the radial component of the magnetic field and the vertical component of the electric field, as these are both small and produce out of plane forces. For such a dust grain moving on a circular orbit, the charge to mass ratio can be found from the local gyrofrequency given by

$$\frac{qB}{mc} = -\frac{\omega^2 - \omega_K^2}{\omega - \Omega} \tag{5}$$

where ω is the grain's orbital angular velocity, $\Omega \approx 1.64 \times 10^{-4}$ s^{-1} is Saturn's angular rotation rate, which is uncertain to a level of 2%. B is the northward component of the magnetic field, given in the ringplane by

$$B = -g_{10}(R_S/r)^3 + \frac{3}{2}g_{30}(R_S/r)^5 \tag{6}$$

for an axisymmetric magnetic field such as Saturn's, which consists of a dipole with a nonzero quadrupole and octupole moments. (The quadrupole field is purely radial in the ring plane and contributes nothing to the out of plane field.) For Saturn's field, $g_{10} = 0.21084$ Gauss, $g_{30} = 0.02150$ Gauss, and $R_S = 60,268$ km (Dougherty et al., 2005), while r is the grain's distance from Saturn's center. The square of the orbital angular velocity for an uncharged dust grain, ω_K^2, is given by

$$\omega_K^2 = \frac{GM}{r^3}(1 + \frac{3}{2}J_2\frac{R_S^2}{r^2}) \tag{7}$$

where $GM = 3.793 \times 10^{22}$ cm^3/s^2 is the mass of Saturn, $J_2 = 1.6291 \times 10^{-2}$ is the planetary oblateness, and we have neglected higher harmonics of Saturn's gravity field (Jacobson et al., 2006).

For a spherical dust grain, the charge (in cgs units) is proportional to the electric potential as given by Gauss's Law:

$$q = r_{\rm g}\phi \quad , \tag{8}$$

where ϕ is the electric potential of the particle and $r_{\rm g}$ is the grain's radius. Since the charge on a particle, and therefore the Lorentz Force, is proportional to $r_{\rm g}$ while the mass is proportional to $r_{\rm g}^3$, smaller grains are affected more by the electric and magnetic fields than larger ones for a given electric potential. For negatively charged grains, the orbital velocity is always between the Keplerian orbital velocity and the corotational velocity.

3.3. Measuring Spoke Edges

In order to measure the deviation of a spoke from Keplerian motion, one needs images taken over a time spanning at least tens of minutes due to the closeness of the spokes to the corotation radius. We determine where the leading

and trailing edges of a spoke are by using the Gaussian fits to the spoke I/F by calculating the longitude of the peak and the width of the spoke. We take the longitude of the peak plus one half-width to be the position of the leading edge and the peak longitude minus one half width as the trailing edge. We calculate the variation in the edge locations as a function of time for comparison to the Keplerian and corotation rates at that radial location. We do this for each radial scan across the spoke to determine the shearing rates.

This measurement process is far more sensitive to the spoke fits than the measurement of a spoke's total optical depth. This is due to the orbital angular velocity of the dust grains, ω in Eq. 5, only ever deviating slightly from either the Kepler velocity, ω_K, or the planetary rotation rate, Ω, due to the spokes appearing near the corotation radius. As any measurement error will translate into a large error in the charge to mass ratio of the spoke particles, only the most robust and darkest spokes which are well-fit to Gaussians are considered for this motion analysis.

As in the case of faint spokes, spokes which appear in tight groups on the rings often have large uncertainties in the fits since they do not have enough (or often any) background B ring I/F between the spokes to allow for good fits using the Gaussian fitting technique. As such, these spokes make poor candidates for this measurement technique and are not considered. Table 4 provides a summary of the number of spokes in each observation which were measurable using this technique. The numbers are reduced from those in Table 3 since the total activity level of a spoke is much less sensitive to the individual fits, so fewer spokes could be used for the determination of spoke edge motion.

Once the angular motion of the spokes' edges has been determined, the corresponding charge mass ratio for the spoke particles can be calculated using Eq. 5. The result is a function of the distance from Saturn, as shown in Fig. 11.

Observation	# Spokes	Keplerian	Deviates	Transition
ISS_074RI_SPKLFMOV001_PRIME	7	1	5	1
ISS_081RI_SPKMVLFLP001_PRIME	8	4	1	3
ISS_085RI_SPKMVLFLP001_PRIME	12	4	7	1
ISS_086RI_SPKMVLFLP002_PRIME	7	1	5	1
ISS_088RI_SPKMVLFLP001_PRIME	12	4	5	3
ISS_094RI_SPKMVLFLP001_PRIME	3	1	1	1

Table 4: The number of spokes for which a Gaussian profile was sufficient for the measurement of the edges, the number of spokes that had edges which were observed to undergo Keplerian motion, the number of spokes which showed a deviation from Keplerian on at least one edge, and the number of spokes which transitioned from deviating from Keplerian to Keplerian.

3.4. Individual Spoke Motion

Our measurements of the spoke motion are more sensitive to the individual fits, and hence the signal noise level, compared to the overall activity measurements. Additionally, though the spokes may move 10° or more between images, the interesting quantity is the difference between the motion of an uncharged particle and the actual spoke motion. Since spokes appear near the corotation radius, the point in the rings where charged and uncharged particles orbit at the same rate, the deviations in spoke motion are typically small, even for a totally corotating spoke. This leads to some rather large error bars when calculating the charge to mass ratio of the spoke particles. We therefore restrict our analysis to spokes which have the best profiles in multiple images.

As an example of a spoke for which good measurements were achieved, we return to the active spoke highlighted earlier in Figs. 6 through 8, as an excellent example of a spoke which deviates from Keplerian motion. The data presented in Fig. 12 are the results of taking the differences in the fit parameters for the last four images the spoke appears in. Each panel in this figure is obtained from a pair of consecutive images, yielding three measurements. While the leading edge of the spoke moves in a Keplerian sense, the trailing edge deviates substantially, moving at a rate in between Keplerian and corotation, indicating negatively charged spoke particles. (Positively charge spoke particles would move faster than Keplerian for a spoke interior to the corotation radius, rather than slower than Keplerian, as this spoke's edge does.)

Figure 13 shows the results of converting the orbital motion into a charge to mass ratio (q/m) which yields a peak value of around -200 C/kg for the trailing edge between the fourth and fifth images in Fig. 6 (left panel), while the leading edge is appears to be uncharged for this spoke. Between the fifth and sixth images (middle panel), we calculate similar q/m, though there is one aberrant point at -250 C/kg. However, in the last two images in which the spoke appears (right panel), the motion is becoming nearly Keplerian and q/m becomes small. (The reason for the large values of q/m outside of $109,000$ km in the last panel is unknown as the spoke leaves the field of view immediately afterwards, though it is possibly due to another spoke beginning to form on top of this one.) Since the last measurement for this spoke shows a distinct reduction in q/m on the trailing edge of the spoke, we believe that this spoke was in the process of transitioning to Keplerian motion in the last images in which it was captured, a process which has been observed both in previous work by other authors based on Voyager data (Grün et al., 1992; Eplee and Smith, 1984), and here in our Cassini observations.

This type of behavior, with the leading edge of the spoke having a small measured q/m while the trailing edge has a much larger ratio, has been reported in spokes inside the corotation radius before by Grün et al. (1992). The spoke we report on here has a very large value for its trailing edge q/m, a factor of 4 higher than the largest previously reported. This may in fact be because the charging for this spoke is greater than previously measured, though it is possible that differences in the way the measurements were performed could also contribute.

If indeed this measurement is the actual charge-to-mass ratio of the particles on the trailing edge of the spoke and not, as has been speculated (Grün et al., 1992), the edge of a propagating spoke forming region, then the particles must be at a large negative potential. Assuming a grain radius of 0.4 μm and the density of ice, a potential of -1200 V is required to produce a q/m of -200 C/kg,

similar to the field emission voltage (Draine and Salpeter, 1979).[1] However, potentials of this size are unlikely unless the spokes are embedded in a dense and very energetic plasma, considerably hotter than the plasma predicted by the meteor impact model by Goertz and Morfill (1982). We conclude either that the non-Keplerian spoke-edge motions reflect the motion of particles charged by an extremely hot plasma, or the moving edge of a spoke-forming region.

4. Detailed Analysis of Individual Growing Spokes

We continue our examination of the spokes by analyzing in detail those which appear new and expand radially between images. A search of the southern movies revealed a total of 51 spokes which we are confident appear for the first time on the rings during our observations. Of these, 42 appeared on sections of the ring where there previously were no distinct spokes. The remaining 9 spokes appear in close proximity to another, older spoke as it fades out in the same region. Here we use the Gaussian fits to the spoke azimuthal profiles (found in section 2.1) to determine their radial expansion rates as well as the rates with which they shear azimuthally.

We measure these properties for as many new spokes as possible, though we must reject some due to various complicating factors. The first of these is brevity in the field of view. If a spoke appears near the leading edge of the frame, it will soon move out of the field of view leaving insufficient opportunity to determine its behavior. The second difficulty is with fitting the background B ring I/F. As the background is sometimes non-linear in the region around some spokes, and since the scale over which the background changes is comparable to the size of a large spoke, it is sometimes unclear if a change in the I/F is due to the spoke or to the background. We therefore reject spokes which are not well defined and in sections of the ring with non-linear backgrounds. Out

[1] Of course, the charge to mass ratio is proportional to the potential and inversely proportional to the square of the grain radius, so smaller grains do not require as large a potential for a given ratio. For a very small particle of 0.04 μm in radius, a potential of only -12 V is required.

of the original 51 spokes, we were able to obtain sufficiently good fits for 24 to measure radial and azimuthal rates. We also include 3 small spokes which came out of Saturn's shadow but which grow into large, easily fit spokes, and 1 spoke which grows a radial extension after leaving the shadow, for a total of 28.

For a given spoke, we have a set of fitted azimuthal profiles over a range of radii for each image the spoke appears in. We determine which of these fits to use by selecting those with widths larger than a particular value, determined by multiplying the sampling interval by a factor of 6. This is wider than the typical noise peak and is a good criterion for distinguishing spokes from the noise. We take the outermost and innermost fits which satisfy this width criterion as the radial extent of the spoke. (We do not use the amplitude of the fit for this determination as the spokes typically do not have a sharp cutoff in radius, and the fits at the very ends of the spoke typically have amplitudes near the noise level.)

To measure the change in the radial extent of the spokes, we take the terminii in 3 conscutive images, either inner or outer, use these data and the time of each image was taken to do a linear fit to the radii as a function of time, and take the slope of the fitted line to be the radial rate of change at the time of the middle image. We shall refer to these measurements as the inner and outer radial velocities of the spoke, though we do not mean to necessarily imply that the spoke particles themselves are moving radially.

In addition to the radial extent of the spokes, we also wish to measure the shear rate of both the leading and trailing spoke edges - ie, the rate at which two radially separated points on the edge separate in longitude – and determine the overall shape of the spokes. We take the edges of the spoke at each radius to be located at the Gaussian fit's peak location plus or minus one half width. We then fit a line to each edge and the spoke's center (defined by the peak location) using a procedure which minimizes the absolute value of the deviations of the data from the line. This type of fitting has the property of ignoring outliers more readily than a least squares fit. We use these linear fits to calculate the shear rate, which we define to be $d\Omega/dr$, with Ω the orbital rate. Additionally,

to characterize the shape of the spoke, we define the angle an edge's fitted line makes with respect to radial as the tilt angle for that edge. (A classic "active" spoke would then have one edge maintaining a tilt angle of 0°, corresponding to the corotating edge, while the other edge's tilt angle would increase due to Kepler shear.) This angle should not be confused with the shear angle, which is the separation in longitude of two points on the spoke's edge, and depends on the radial separation of the points.

We find that the initial image in which a spoke appears is usually unsuitable for tilt angle and shear measurements due to the faintness of the spoke compared to the noise in the background I/F, as well as the limited radial extent of the spoke. For this reason, reliable shear measurements for a new spoke usually begin in the second or third image.

We find that upon first appearance, all of the 24 new spokes are short, 58% are radial (with peak location tilt angles less than 15°), 50% lie inside of corotation, 29% lie outside corotation, and 21% cross corotation (taking corotation to be 112.3×10^3 km from Saturn), which is difficult to explain using an $\vec{E} \times \vec{B}$ drift.

We also find that out of the 28 spokes we can reliably measure, 21 exhibit normal shearing behavior, while 7 have more unusual behavior. Of these complex spokes, 4 appeared to be shearing at different rates in different parts of the spoke, including one where a radial extension appears to grow out of an old spoke. Two of these spokes appear to be sheared when they formed, contrary to the usual radial alignment of new spokes. Finally, one very peculiar spoke appears to shear backwards for a short time. We shall give examples of these spokes below. These odd behaviors may be due to a varying charge to mass ratio over the length of the spoke, as the spoke in Fig. 6 had, or perhaps a second spoke forming on top of an old one.

For our radial growth measurements, we find that a typical radially expanding spoke has radial velocities of ~ 0.5 km/s for both the inner and outer velocities. Spokes for which we obtain good fits from the initial appearance and for multiple consecutive images afterwards have radial velocities which fall off

gradually with time. In all of the measurable cases, excepting those that initially crossed corotation, one of the spoke radial termini moved *towards* corotation, in contradiction to the $\vec{E} \times \vec{B}$ drift prediction.

Below we describe 3 spokes which behave in a variety of ways reported previously from Voyager observations (Grün et al., 1983), 2 spokes which appear in close proximity to an older, fading spoke, and 3 spokes which exhibit behavior not reported on previously.

Classic Active: The first spoke we wish to examine is one which came out of the shadow at approximately two thirds its full radial extent, but which grew in radius and considerably in azimuth. This spoke is representative of a classic "active" spoke of which there are many examples. Figure 14 shows the scans taken of this spoke in 7 consecutive images in the September 26, 2008 observation, along with the locations of the edges as function of radius and longitude. The spoke emerges from the shadow in the first image and is initially ≈ 3600 km long, extending from 104.8×10^3 km to 108.4×10^3 km radially. The spoke grows radially throughout the observation, reaching a final inner radius of $\sim 104 \times 10^3$ km and outer radius of $\sim 109.6 \times 10^3$ km. The radial velocities of the inner and outer portions of the spoke as a function of time are plotted in Fig. 15. The initial growth of the spoke is ~ 200 m/s for the outer portion and ~ 400 m/s for the inner portion. These velocities are typical for a radially expanding spoke at the end of its expansion. The inward radial growth continues after outward growth has stopped, but interference from a second spoke prevents accurate measurements in the last two images, visible to the right of the spoke in Fig. 14.

This spoke's edges move in the classic "active" spoke manner. Figure 16 plots the tilt angles with respect to radial of the leading edge, trailing edge, and center of the spoke as a function of time. The trailing edge of the spoke is close to radial with a tilt angle of $\sim 10^\circ$ and remains at that angle for nearly the entire time the spoke is in the field of view, starting to shear in the last image. The leading edge is tilted by $\sim 30^\circ$ when the spoke leaves the shadow. It is initially shearing very slowly, but quickly approaches the Keplerian rate. Figure

16 shows the shear rates of the edges as well as the Keplerian rates predicted for each edge.

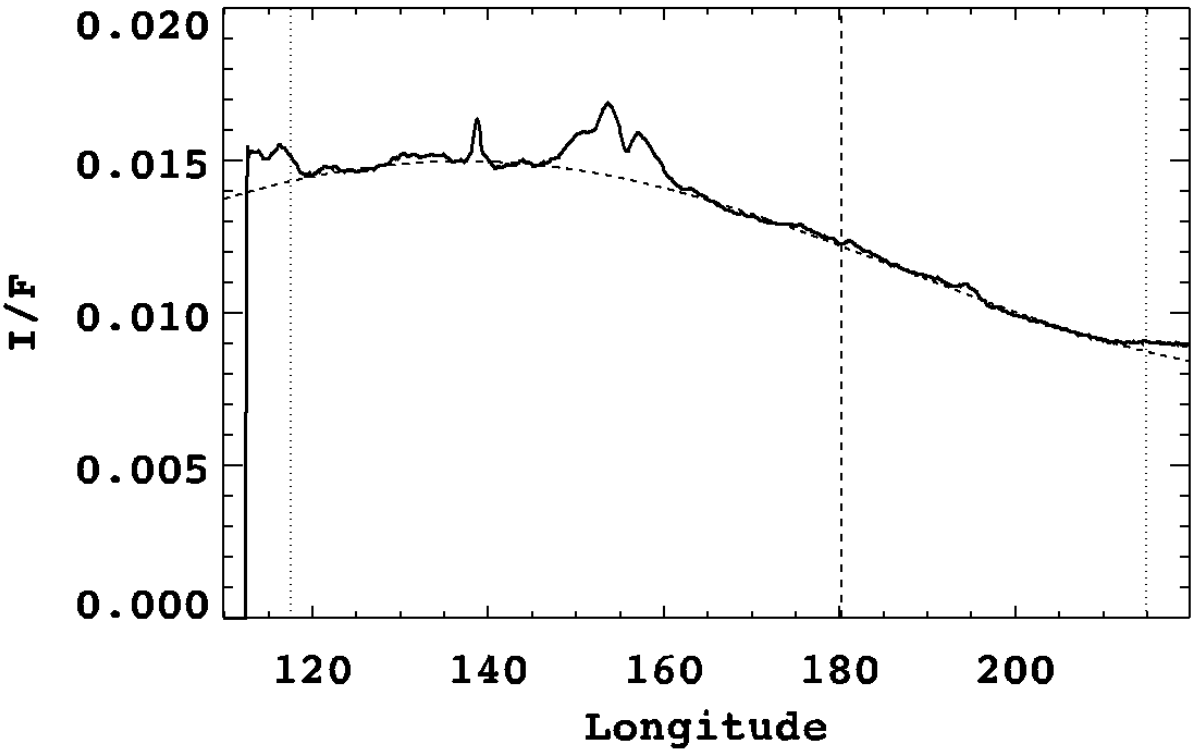

Figure 5: Global sinusoidal fit to the background B ring I/F in an azimuthal scan taken at 109,000 km from an image in the August 30, 2009 observation, the first of the periodicity oriented WAC movies of the northern side of the rings. The solid curve is the actual scan and shows a large spoke cluster visible between 150° and 160°, a narrow spoke near 140°, and another spoke entering the field of view near 115°. The dashed curve is the sinusoidal fit to the background, while the vertical dotted lines denote the fitting region. The sudden drop on the left is the edge of the image. Longitudes are right handed with the direction towards the Sun at 180°. Resolution for this image was 110 km per pixel.

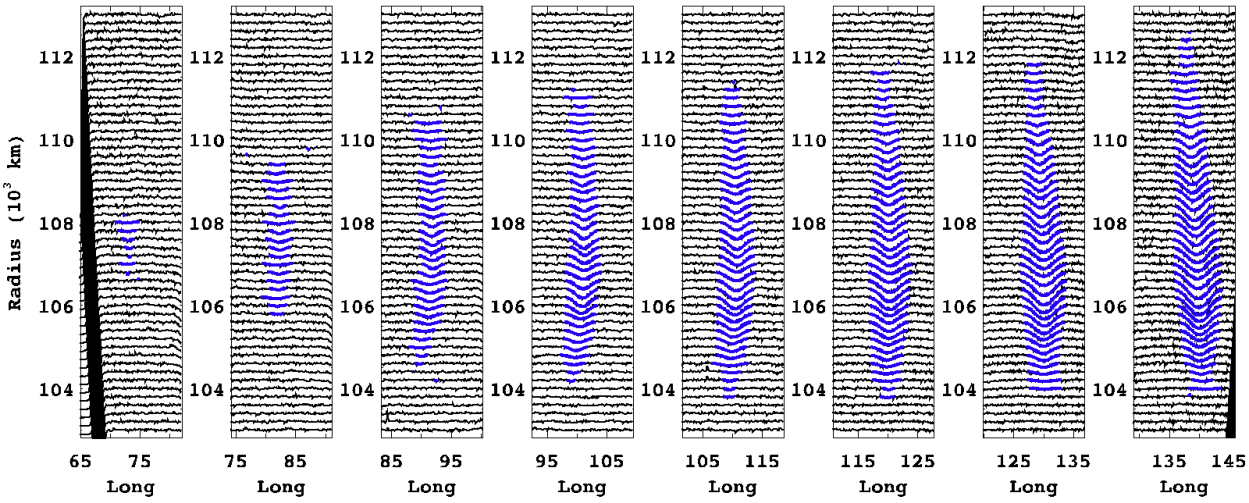

Figure 6: Scans from an active spoke in successive images from the August southern WAC movie placed at their respective radii and using the same normalization and color scheme as figure 4. Time increases from left to right, with the scans on the left from the first image the spoke clearly appears in. The other scans are of the same patch of B ring, corotated with the magnetic field to follow the spoke, with each subsequent image taken 975 seconds after the previous one. The spoke appears to grow both radially and azimuthally during this time, and also increases in contrast. Resolutions for these images range from (left) 58.4 km per pixel to (right) 59.7 km per pixel. The horizontal scale has been compressed compared to Fig 4.

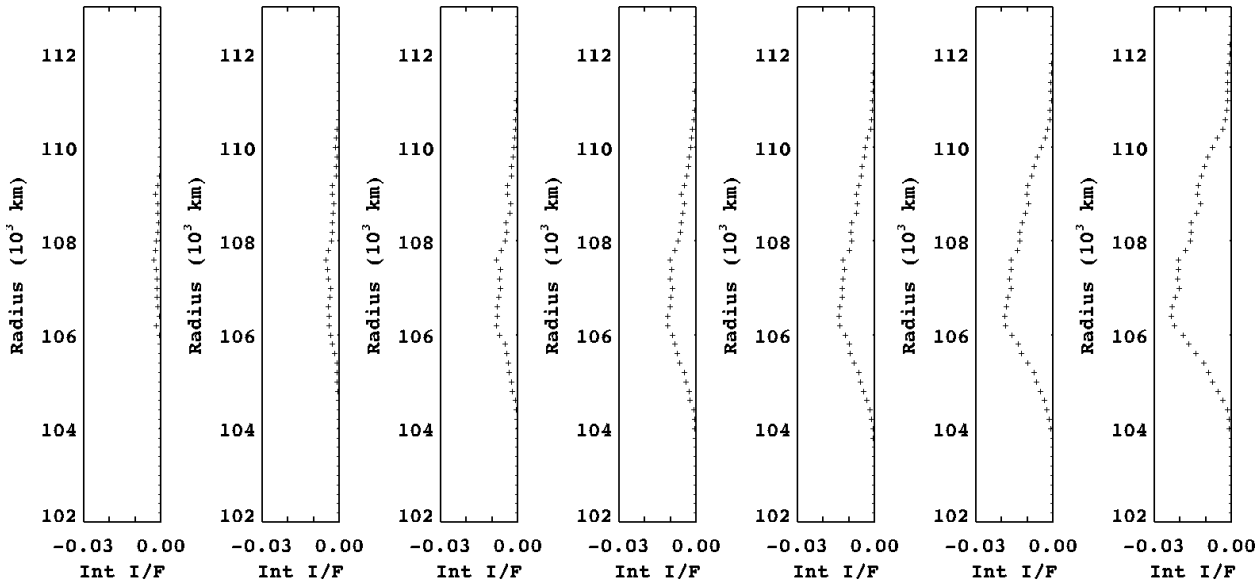

Figure 7: Area under the Gaussian portion of the fits as a function of radius for the active spoke in Fig. 6, again plotting successive images with intervals of 975 seconds and time increasing from left to right, and omitting the first image due to low signal. Radius is plotted on the y axis and negative values of the area denote negative $\Delta I/F$ for the spoke due to the low phase angle. The entire spoke increases in $|\Delta I/F|$ for the entire time.

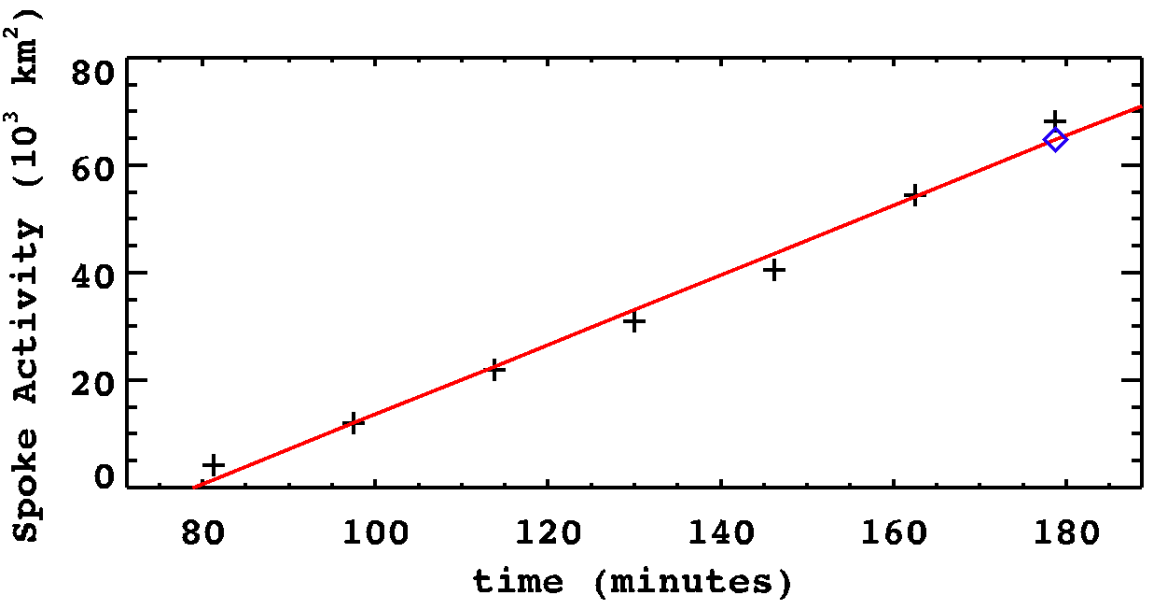

Figure 8: Spoke activity vs time for the active spoke in Fig. 6. Each cross represents the spoke's total activity for a single image, calculated by area-integrating the spoke optical depth. Time is measured from the start of the observation. The growth in activity is approximately linear, with the best fit (red line) indicating an increase of 632 ± 33 km^2/min and a maximum activity of $64.6 \pm 2.9 \times 10^3$ km^2 before the spokes leaves the field of view (blue diamond).

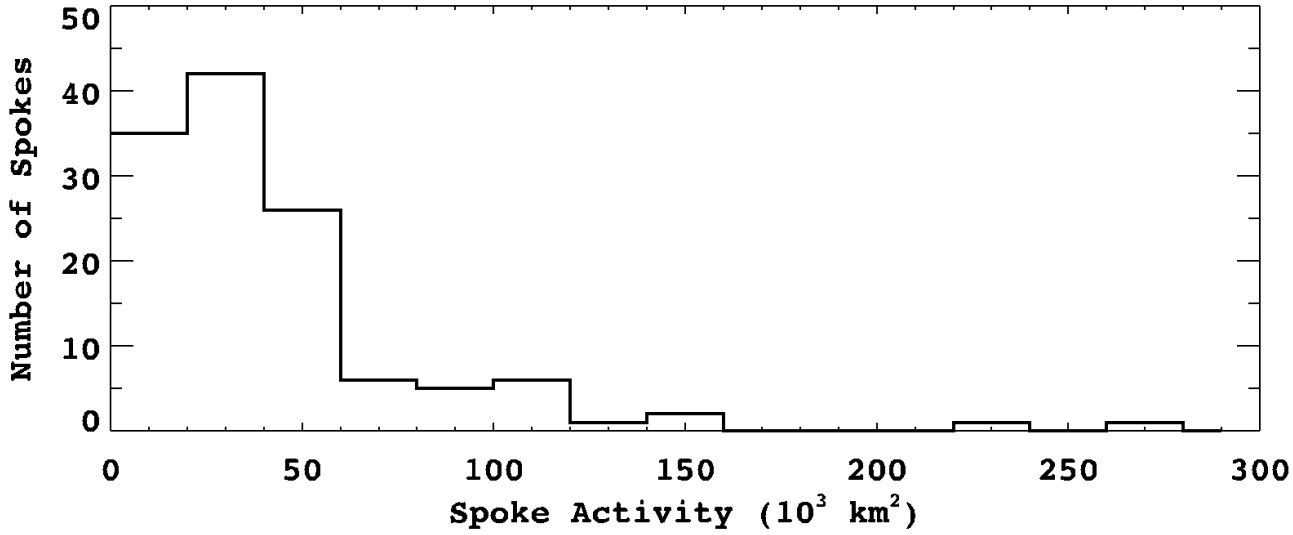

Figure 9: Histogram of peak spoke activity for all of the southern observations where individual spokes were measured by taking the maximum value of the linear fit to the activity. 82% of the measurable spokes have peak activities less than 60×10^3 km^2

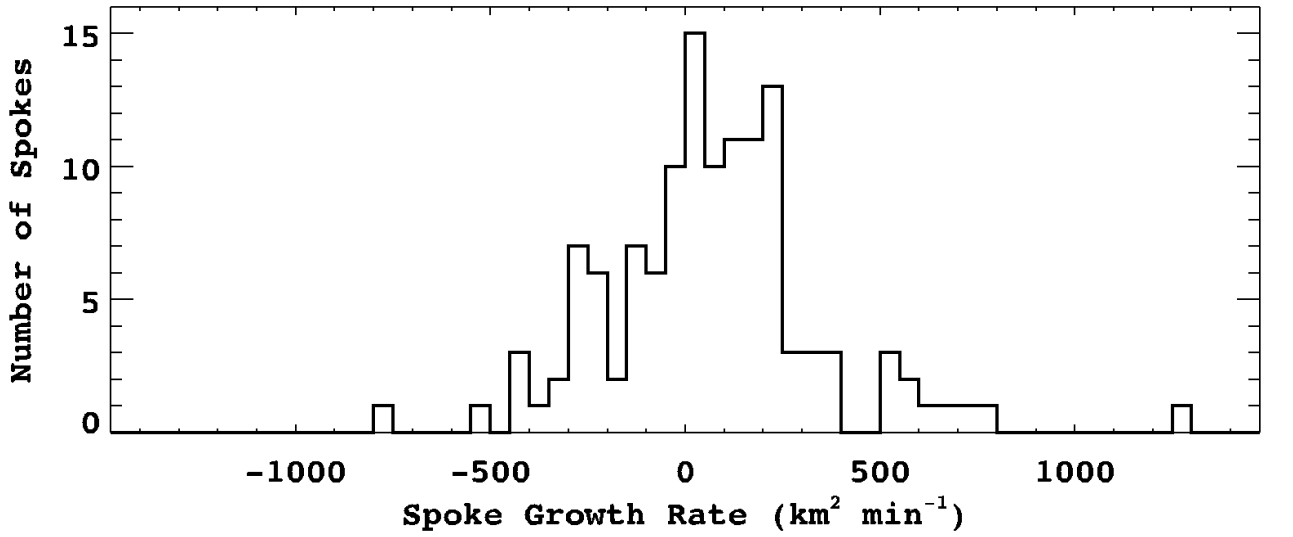

Figure 10: Histogram of spoke growth for all of the southern observations, where individual spokes were measured. Most spokes are growing instead of fading, consistent with the observations being taken on the morning portion of the ring, local time, where spokes have been observed to be most prominent and numerous.

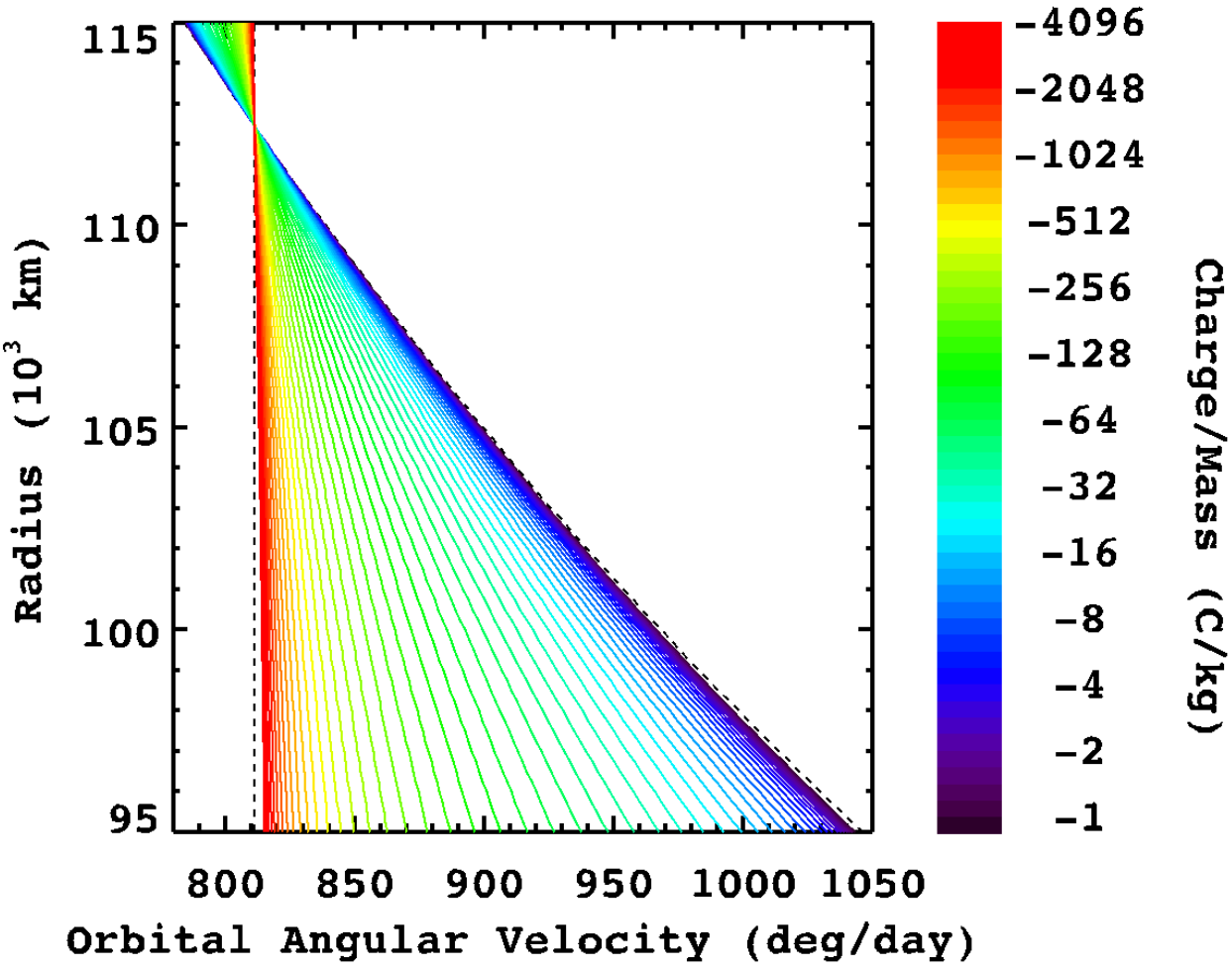

Figure 11: Angular velocity (x axis) of particles on circular orbits around Saturn with various charge to mass ratios over a range of radii (y axis). Particles range from a charge to mass ratio of -1 C/kg (purple) to -4096 C/kg (red) logarithmically, with each step changing by a factor of $2^{1/4}$. The vertical dashed line is the corotation angular velocity (assuming a period of 639 minutes), while the diagonal dashed line is the Keplerian mean motion.

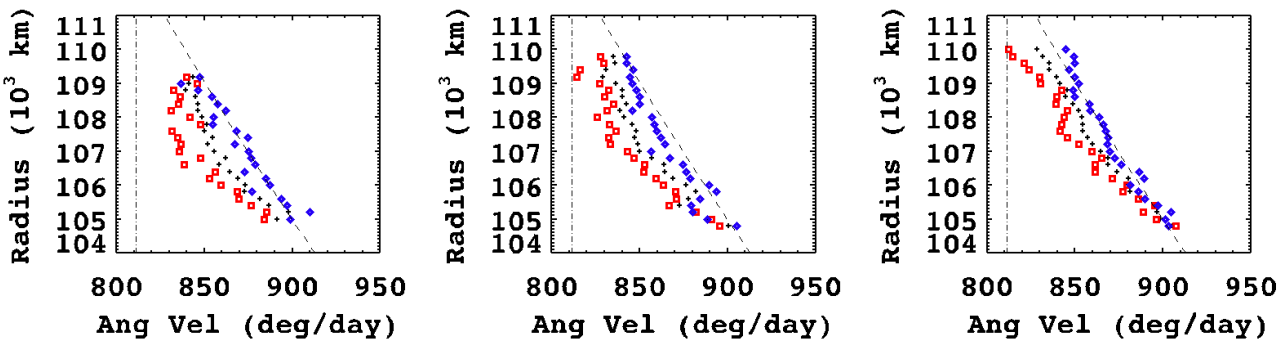

Figure 12: Motion of the edges and peaks of the Gaussian fits of an active spoke over a range of radii. The fits in four images were used to calculate the angular velocity of the leading (blue diamonds) and trailing (red squares) edges of the spoke fits, as well as the peaks (black crosses). The slanted dashed line represents Keplerian motion while the vertical dashed line is corotating with a period of 639 minutes. The leading edge of this spoke undergoes approximately Keplerian motion, while the trailing edge deviates substantially.

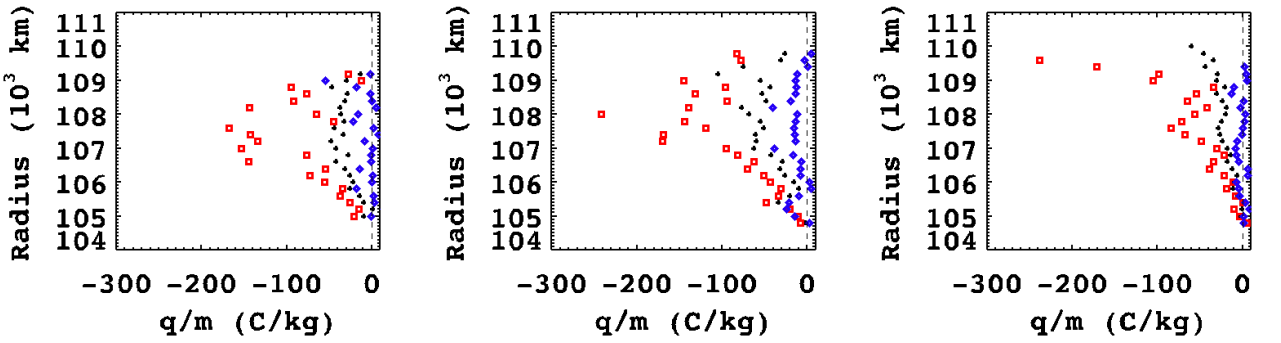

Figure 13: Charge to mass ratios of the particles comprising the spoke derived from the orbital angular velocities in Fig. 12. The trailing edge of the spoke gives charge to mass ratios as high as −200 C/kg, assuming motions are caused by magnetic acceleration of individual particles, while the leading edge is consistent with uncharged particles.

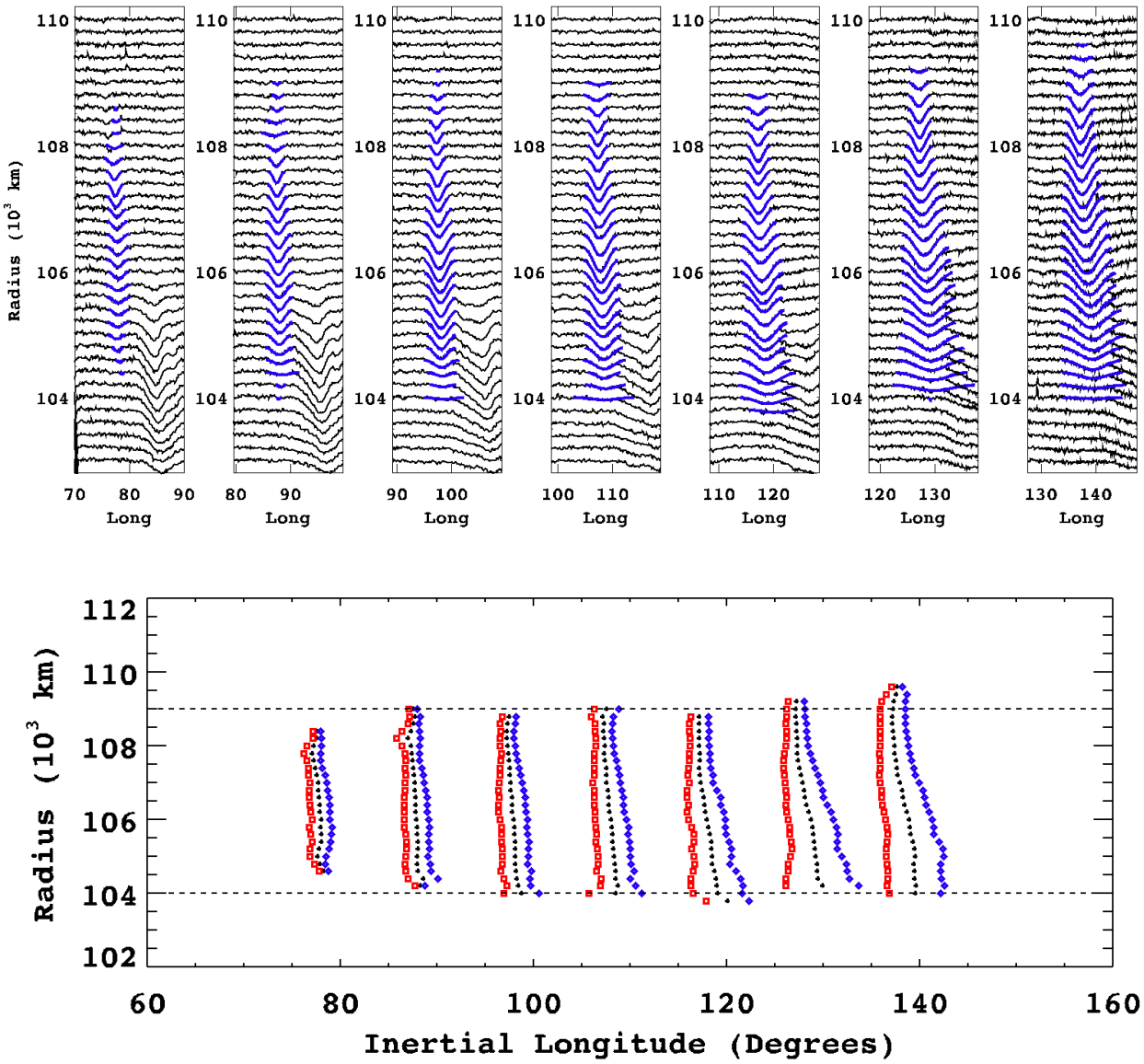

Figure 14: Azimuthal scans (top) and trailing (red boxes), peak (black crosses), and leading (blue diamond) edge locations based on the Gaussian fits (bottom) for a spoke appearing in 7 consecutive images from the September 26, 2008 observation which shows the classic "active" behavior for a spoke, where it grows azimuthally with time. The horizontal dashed lines denote the range of radii for the linear edge fits. A second spoke is visible to the right of this fitted spoke in the scans

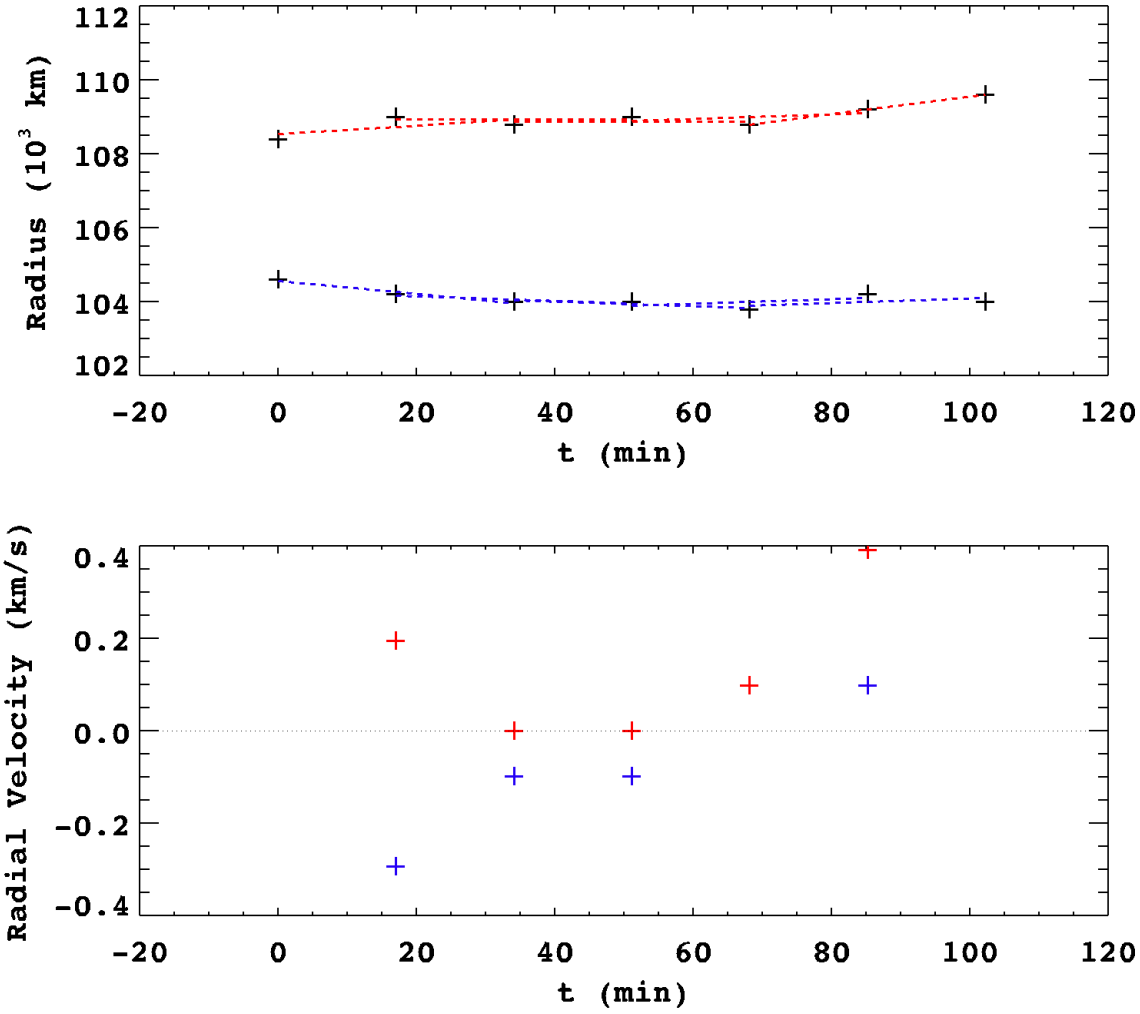

Figure 15: Radial extent derived from the Gaussian fits (top) and both inner (blue) and outer (red) radial velocities (bottom) as a function of time for the spoke in Fig. 14. The dashed lines are the fits to each set of 3 consecutive points used to calculate the velocities. This spoke comes out of Saturn's shadow at approximately two-thirds of its full extent and shows very little additional radial growth.

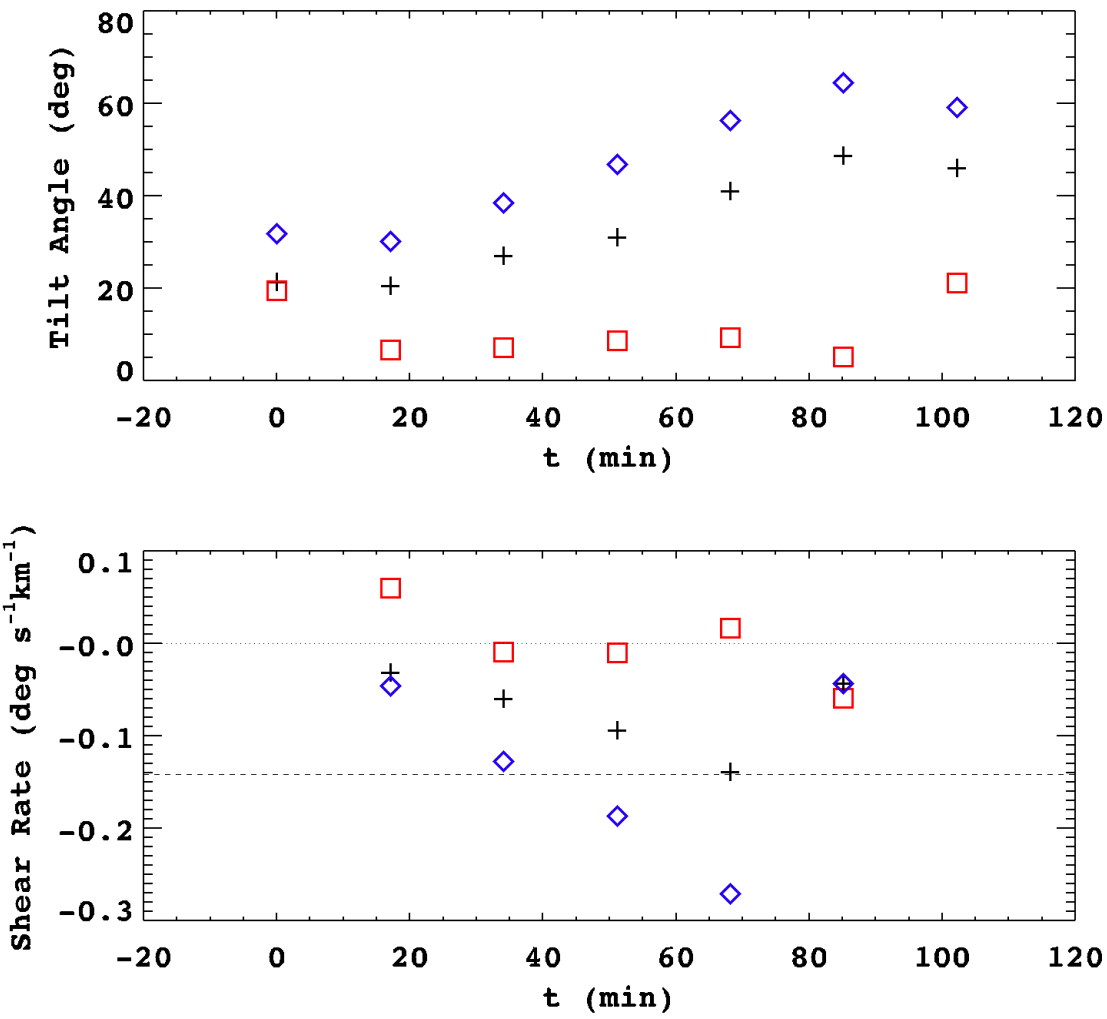

Figure 16: Tilt angles (top) and shear rates (bottom) for the spoke in Fig. 14. Blue diamonds mark the leading edge, black crosses the peak locations, and red squares the trailing edge. For most of the time observed, the spoke's trailing edge maintains a constant tilt angle of $\sim 10^{\circ}$ without shearing, while the leading edge is shearing out for all but the first measurement. Shear measurements after 60 minutes have a large uncertainty due to a second spoke interfering with the fits near the leading edge. The horizontal dashed line on the shear rate plot is the Keplerian rate calculated for the approximate center of the spoke (106.5×10^3 km), while the dotted line is zero shear, corresponding to corotation. The uncertainties of the last two sets of datapoints are large for this spoke due to the presence of a second spoke interfering with the edge fits.

Split Shear: The next interesting spoke is the growing spoke previously mentioned in section 3. It first appears as a small, faint spoke as it leaves the shadow. Figure 17 shows this spoke growing rapidly from its initial extent ($\sim$ 1000 km long) to approximately 8000 km in approximately one hour. Initially, both the inner and outer radial velocity of the spoke are ~ 1.2 km/s. The rate of expansion slows with time, as can be seen in Fig. 18. This is the fastest growing spoke we have been able to measure.

This spoke has a slightly unusual shape in that the inner portion appears to trail behind the outer portion for the first few images it appears in, though it rapidly catches up. We therefore split this spoke into an inner portion and an outer portion and fit the edges of each individually for the shear analysis. We choose 107×10^3 km as this is the radius that seems to separate the spoke's two different regions. The results of the analysis are insensitive to this choice. Fitting the edges of the spoke outside of this radius, we find another example of a classic "active" spoke, with the trailing edge remaining tilted at a small angle, $\sim 10^\circ$, as can be seen in Fig. 19. The leading edge is initially shearing more slowly than the Keplerian rate during the time the spoke is expanding the most radially, but it rapidly approaches Keplerian by the fourth image it appears in, after the expansion has slowed.

The inner portion of the spoke, on the other hand, is not behaving in the typical fashion. Once the fits are sufficient to measure the tilt, both edges shear at a decreasing rate, as seen in Fig. 20. These shear rates are faster than the expected rates for the measured edges, which are unusual in another regard: they are tilted in the opposite sense one would expect, narrowing away from the corotation radius instead of towards it. It is possible that these unusual aspects are due to either a second spoke forming on top of the first, or the charge to mass ratios of the particles varying along the spoke's length, as was measured in the previous section.

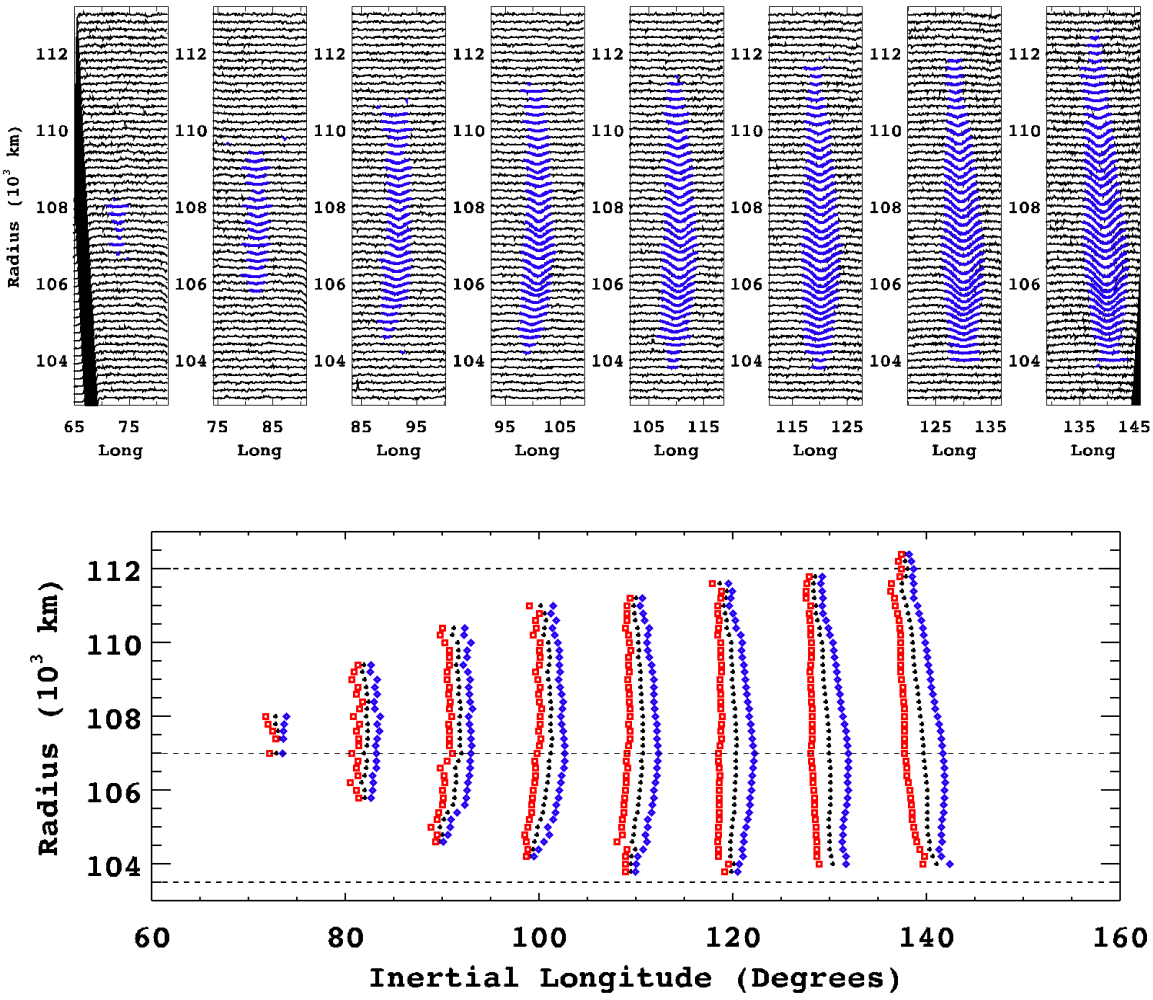

Figure 17: Azimuthal scans (top) and trailing (red boxes), peak (black crosses), and leading (blue diamond) edge locations based on the Gaussian fits (bottom) for a spoke appearing in 8 consecutive images for a rapidly growing spoke from the August, 2008 observation. The horizontal dashed lines mark the two regions used for the inner and outer portions of the spoke for shear analysis (Figs. 19 and 20).

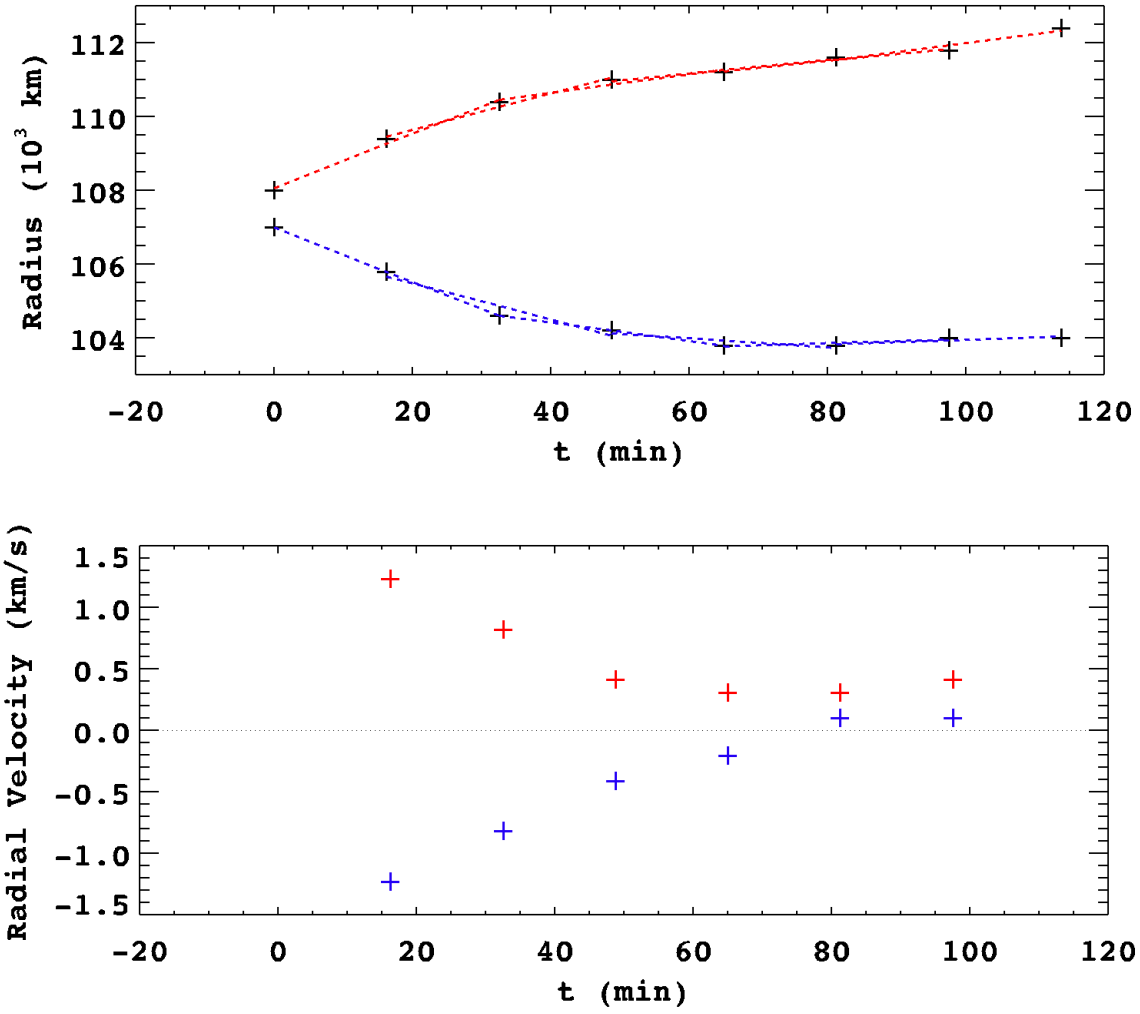

Figure 18: Radial extent derived from the Gaussian fits (top) and both inner (blue) and outer (red) radial velocities (bottom) as a function of time for the spoke in Fig. 17. The dashed lines are the fits to each set of 3 consecutive points used to calculate the velocities. This spoke comes out of Saturn's shadow a mere 10^3 km long and grows rapidly, at an initial rate over 1 km/s both inwards and outwards. The radial growth slowly diminishes with time.

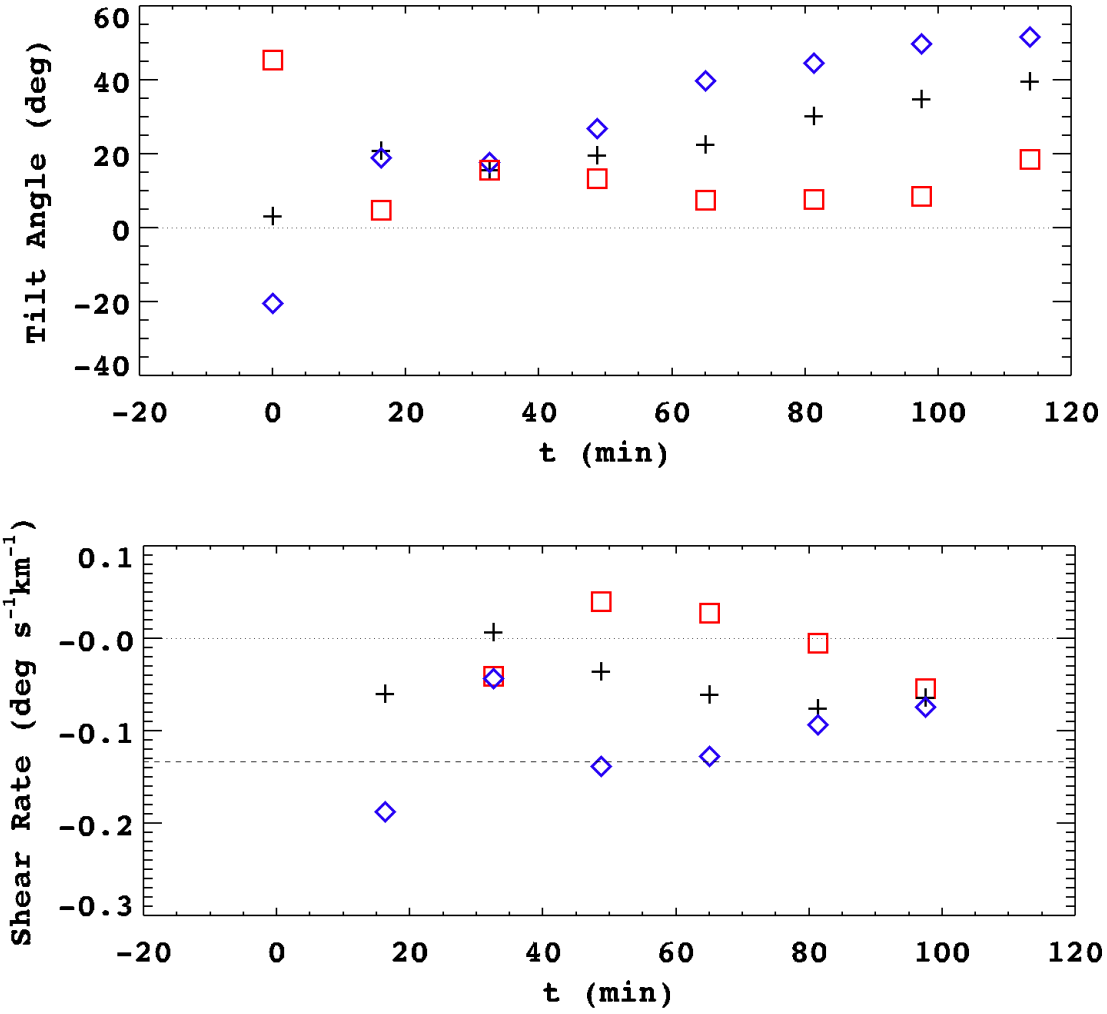

Figure 19: Tilt angles (top) and shear rates (bottom) for the outer portion of the spoke in Fig. 17. Blue diamonds mark the leading edge, black crosses the peak locations, and red squares the trailing edge. The horizontal dashed line on the shear rate plot is the Keplerian rate calculated for the approximate center of the outer portion (109.5×10^3 km), while the dotted line is zero shear, corresponding to corotation. This part of the spoke behaves like a classic "active" spoke once the fits become reliable, with the spoke's trailing edge maintaining a constant tilt angle of $\sim 10^\circ$ while the leading edge shears out. The first set of datapoints has a large uncertainty due to the small number of edge points in the linear fit. The last set also has a large uncertainty due to the proximity of the image's edge to the spoke limiting the amount of background available for the azimuthal fits.

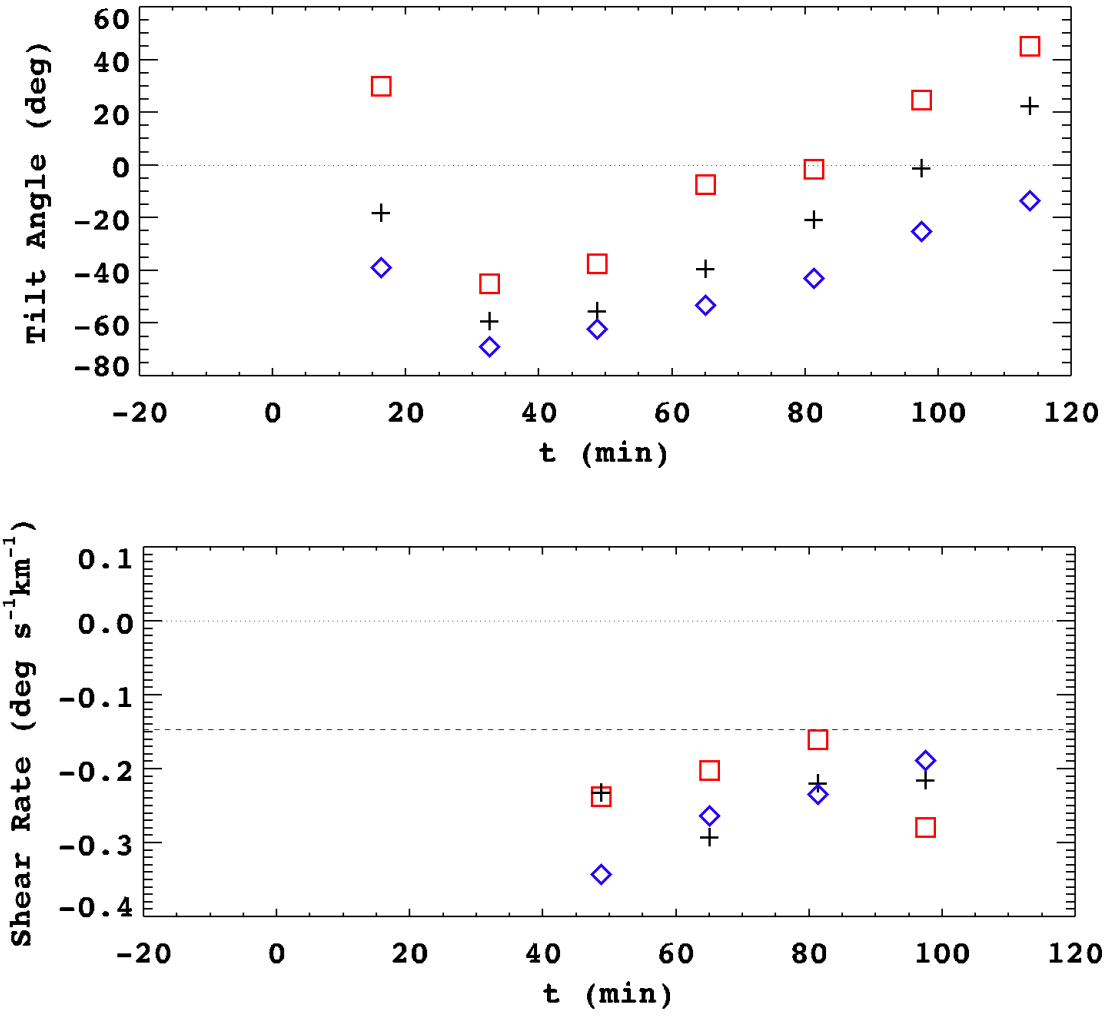

Figure 20: Tilt angles (top) and shear (bottom) for the inner portion of the spoke in Fig. 17. Blue diamonds mark the leading edge, black crosses the peak locations, and red squares the trailing edge. The horizontal dashed line on the shear rate plot is the Keplerian rate calculated for the approximate center of the inner portion (105.25×10^3 km), while the dotted line is zero shear, corresponding to corotation. Both the leading and trailing edges for this part of the spoke start off at a tilt angle of $\sim -65°$ and shear out at a rate greater than Keplerian. The first two sets of datapoints have large uncertainties due to the small number of edge points in the linear fit. The last set also has a large uncertainty due to the proximity of the image's edge to the spoke limiting the amount of background available for the azimuthal fits.

Crossing Corotation: Some growing spokes have leading and trailing edges which shear at nearly the same rate during the growth phase and hence remain relatively narrow, such as the one shown in Fig. 21 from the August 2008 observation, which forms near the corotation radius. The spoke appears in 8 consecutive images, and is initially $\sim$ 800 km in extent radially, from 111.8×10^3 km to 112.6×10^3 km. The spoke initially grows at approximately 0.5 km/s inwards and 0.7 km/s outwards, again slowing with time, as can be seen in Fig. 22. The spoke ranges from a radius of $\sim 110.5 \times 10^3$ km to $\sim 114.5 \times 10^3$ km, crossing the corotation radius at $\sim 112.3 \times 10^3$ km. We measure the tilt of the edges in the first reliable image at 10° for both the trailing and leading edges. Both the edges shear out at rates which are less than the Keplerian rate. Figure 23 shows the tilt angles and shear rates for this spoke's edges.

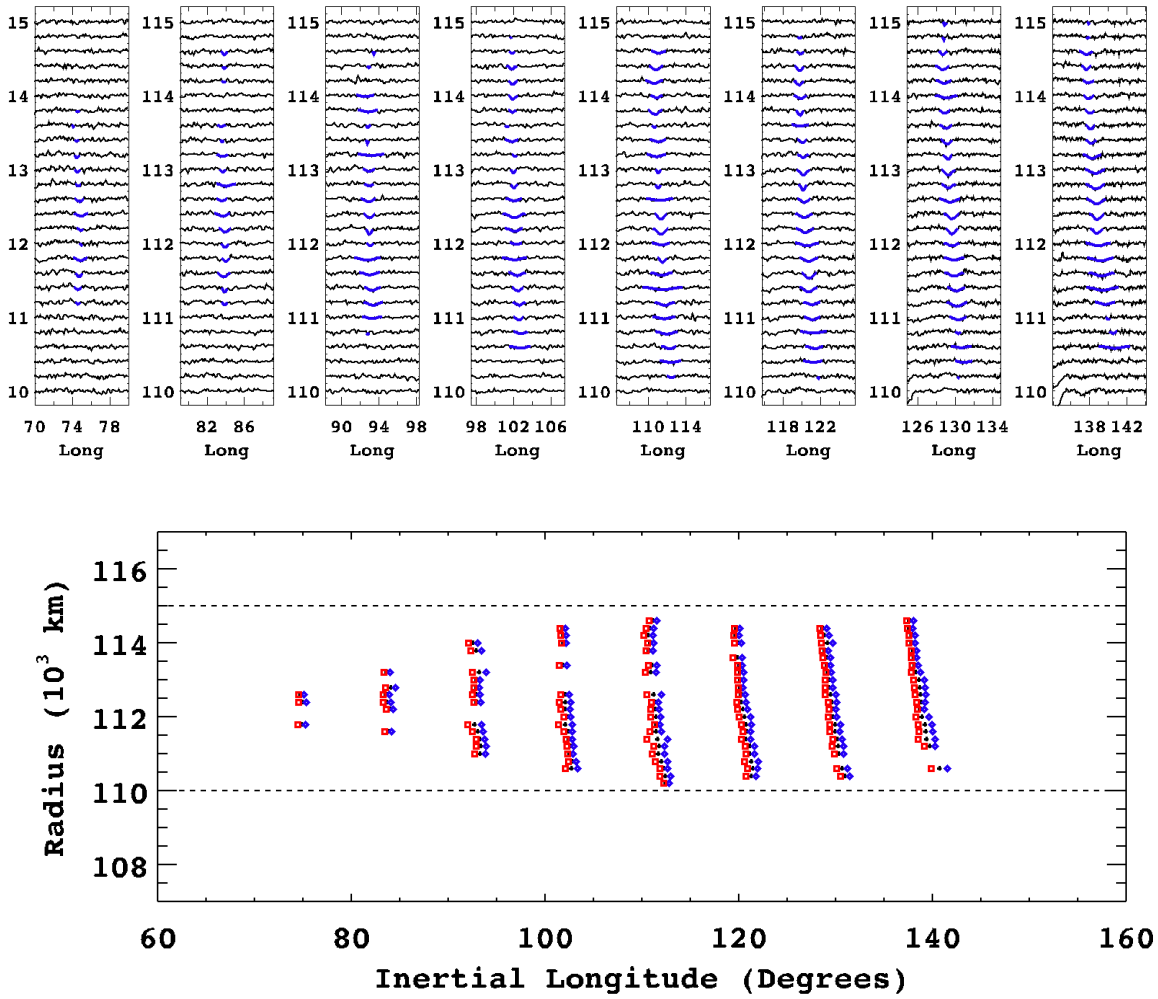

Figure 21: Azimuthal scans (top) and trailing (red boxes), peak (black crosses), and leading (blue diamond) edge locations based on the Gaussian fits (bottom) for a narrow growing spoke which crosses the corotation radius appearing in 8 consecutive images from the August 2008 Observation. The horizontal dashed lines denote the range of radii for the linear edge fits.

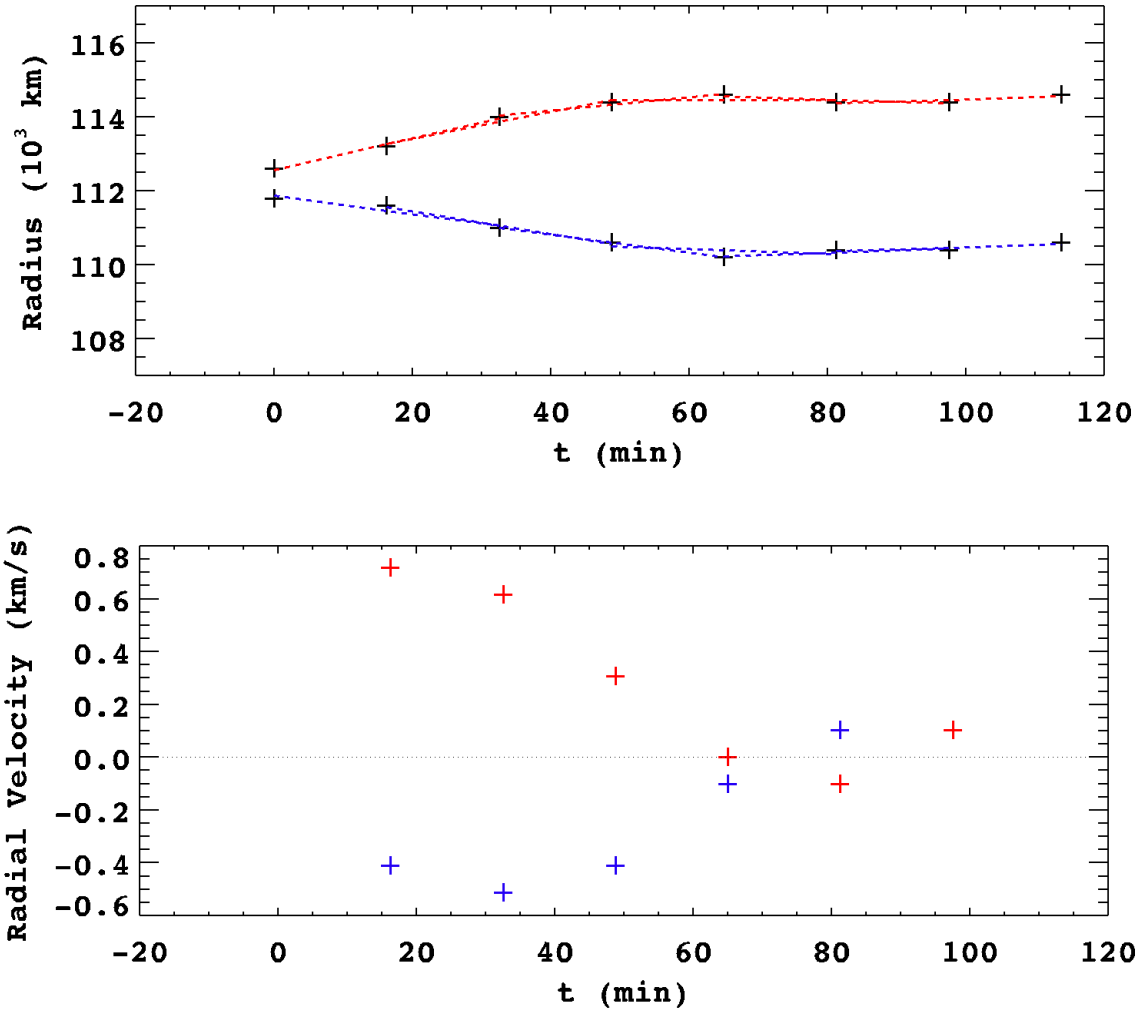

Figure 22: Radial extent derived from the Gaussian fits (top) and both inner (blue) and outer (red) radial velocities (bottom) as a function of time for the spoke in Fig. 21. The dashed lines overlaid on the radial extent are the fits to each set of 3 consecutive points used to calculate the velocities. This spoke grows at a rate of ~ 0.6 km/s outwards and ~ 0.5 km/s inwards, with radial growth diminishing with time.

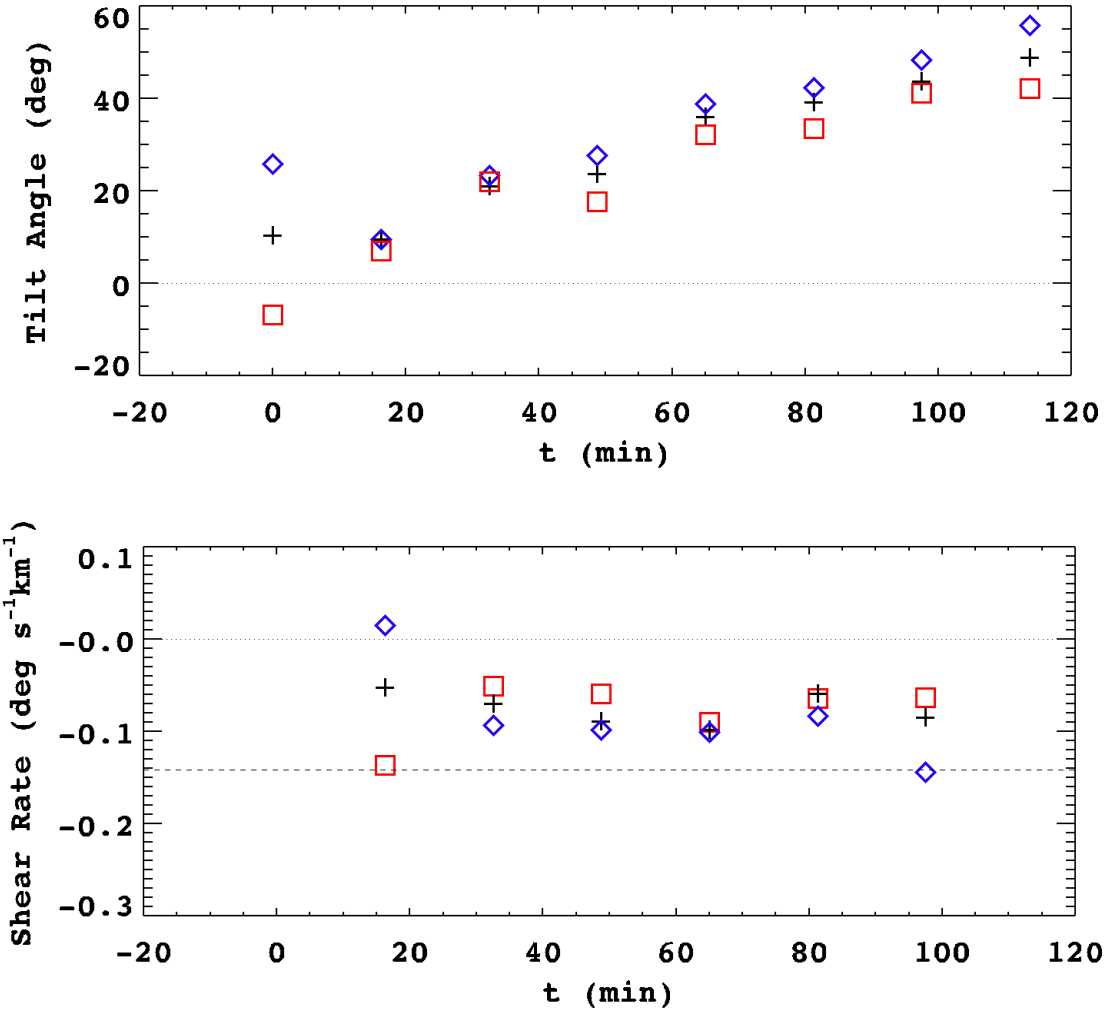

Figure 23: Tilt angles (top) and shear rates (bottom) for the spoke in Fig. 21. Blue diamonds mark the leading edge, black crosses the peak locations, and red squares the trailing edge. The dashed line on the shear rate plot is the Keplerian rate calculated for the approximate center of the spoke (112.5×10^3 km), while the dotted line is zero shear, corresponding to corotation. For this spoke, both the leading and trailing edges start nearly radial and shear out at approximately the same constant rate, which is less than the Keplerian rate. The first set of datapoints has a large uncertainty due to the small number of edge points in the linear fit.

Radial Extension: Just as in Voyager observations, Cassini has observed spokes which appear to be sheared into the classic spokes wedge shape, but have a radial extension coming out of the outermost part. In our next example, we observe the growth of the radial part of one of these spokes. Figure 24 shows the profiles and the edge locations for this spoke. The inner portion of the spoke, the large wedge shaped part, initially has leading and trailing edges which are tilted at 50° and 30°, respectively, and are not shearing. After the third image the spoke appears in, some 40 minutes after its first detection, the edges do begin to shear and have reached the Keplerian rate by the 6th image, as shown in Fig. 26.

Once the new radial extension of this spoke appears, it expands rapidly outwards at an initial rate of $\sim$ 0.8 km/s which slows with time, as seen in Fig. 25. Once the extension grows to the point that the edges are measurable, the extension is clearly radial, as can be seen from the tilt angle of the peak locations in Fig. 27. The leading and trailing edges of the extension have tilt angles of opposite sign but approximately the same magnitude, which decreases as the extension grows, so that the extension forms a radially aligned isosceles triangle.

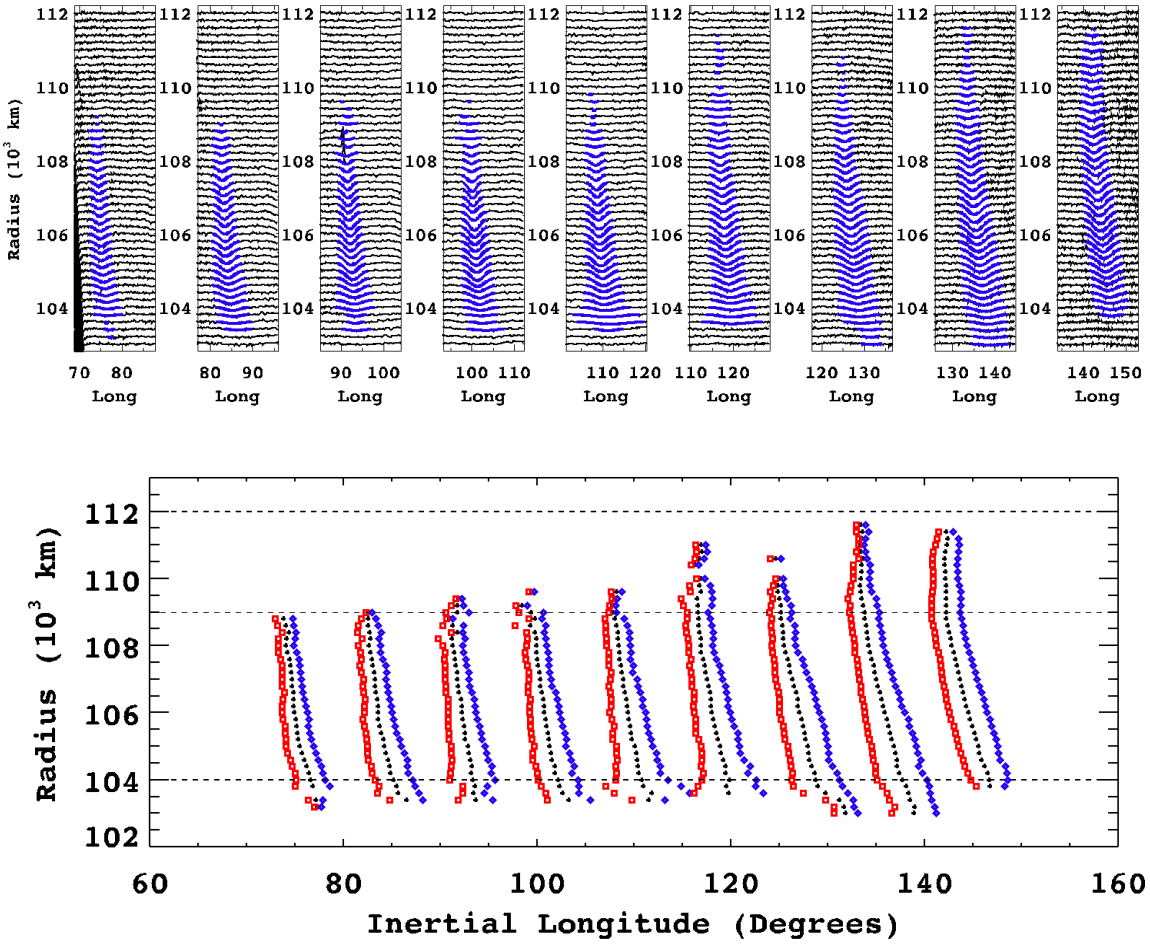

Figure 24: Azimuthal scans (top) and trailing (red boxes), peak (black crosses), and leading (blue diamond) edge locations based on the Gaussian fits (bottom) for a wedge-shaped spoke producing a radial outgrowth appearing in the October 2008 observation. Plot shows scans and edges from 9 consecutive images. The horizontal dashed lines denote the range of radii for the linear edge fits for the growing outer portion of the spoke (109×10^3 km to 112×10^3 km) and the inner portion (104×10^3 km to 109×10^3 km).

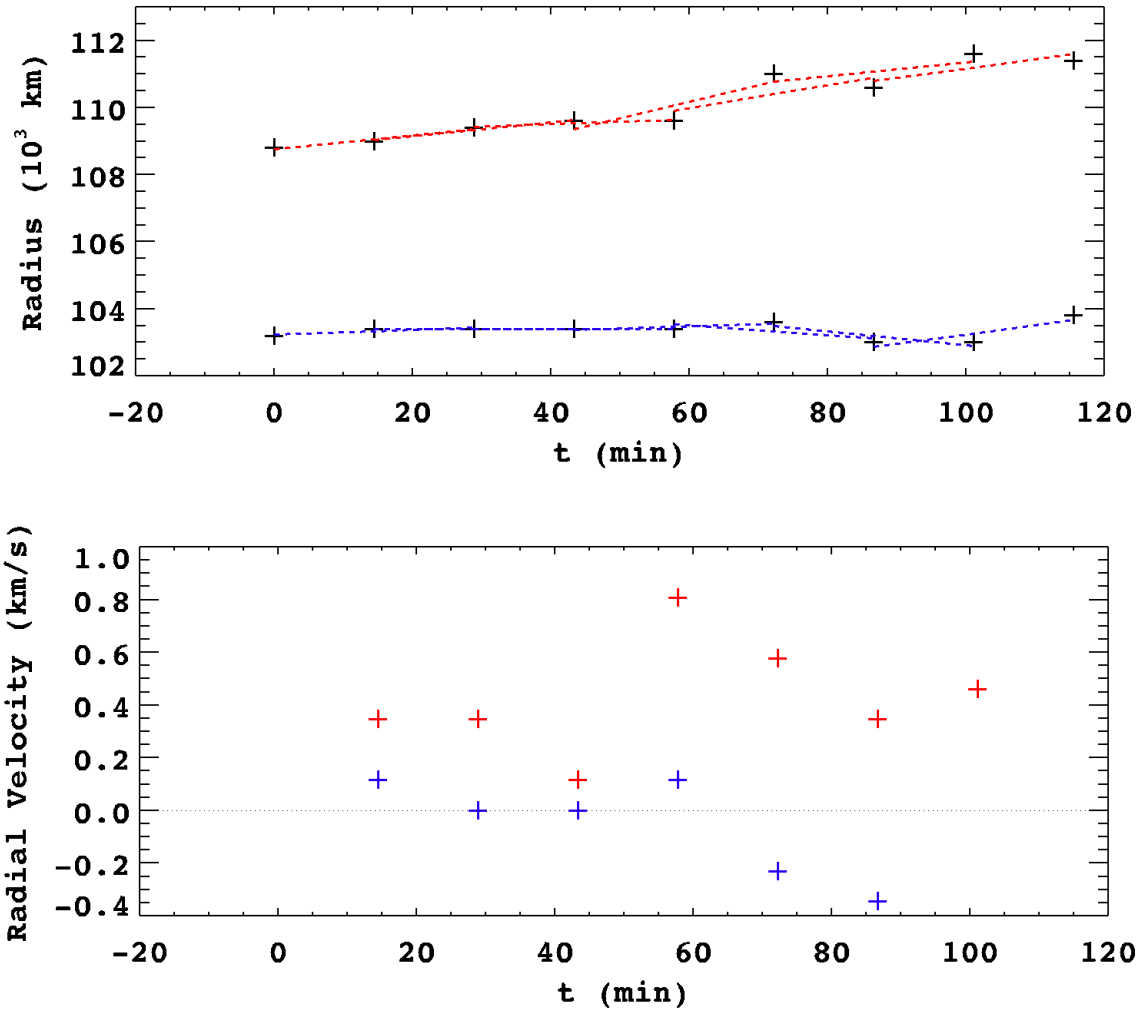

Figure 25: Radial extent derived from the Gaussian fits (top) and both inner (blue) and outer (red) radial velocities (bottom) as a function of time for the spoke in Fig. 24. The dashed lines overlaid on the radial extent are the fits to each set of 3 consecutive points used to calculate the velocities. The radial extension grows outwards starting at ~ 0.8 km/s and approximately at 58 minutes and then decreases with time. The inner, wedge-shaped portion of the spoke shows little radial growth inward.

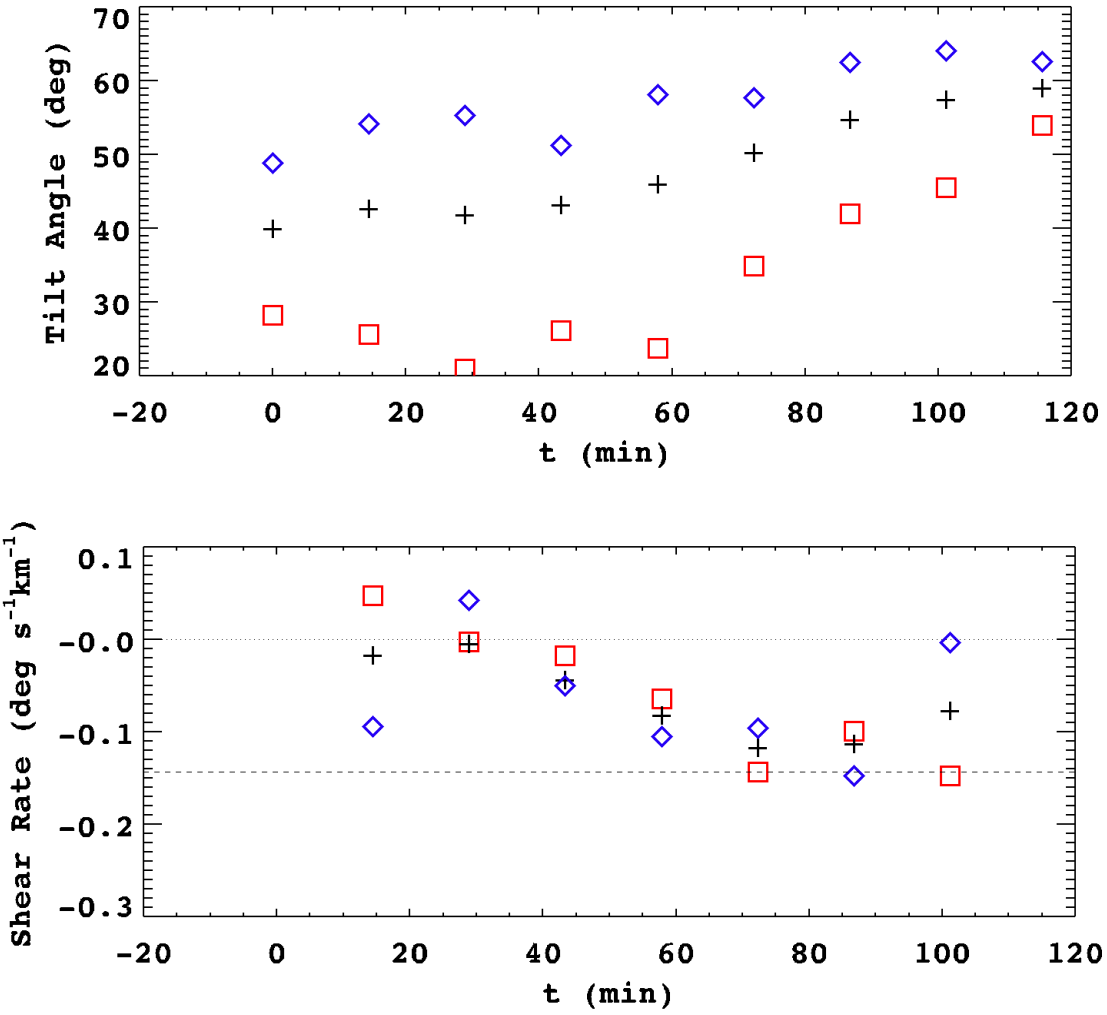

Figure 26: Tilt angles (top) and shear rates (bottom) for the inner portion of the spoke in Fig. 24. Blue diamonds mark the leading edge, black crosses the peak locations, and red squares the trailing edge. The dashed line on the shear rate plot is the Keplerian rate calculated for the approximate center of the spoke (106.5×10^3 km), while the dotted line is zero shear, corresponding to corotation. This spoke is initially tilted $\sim 50°$ from radial on the leading edge and $\sim 30°$ on the trailing edge. Both edges are initially not shearing but transition to Kepler shear during the observation. The first and last sets of datapoints have large uncertainties due to large errors in the background fits caused by Saturn's shadow and the edge of the image, respectively.

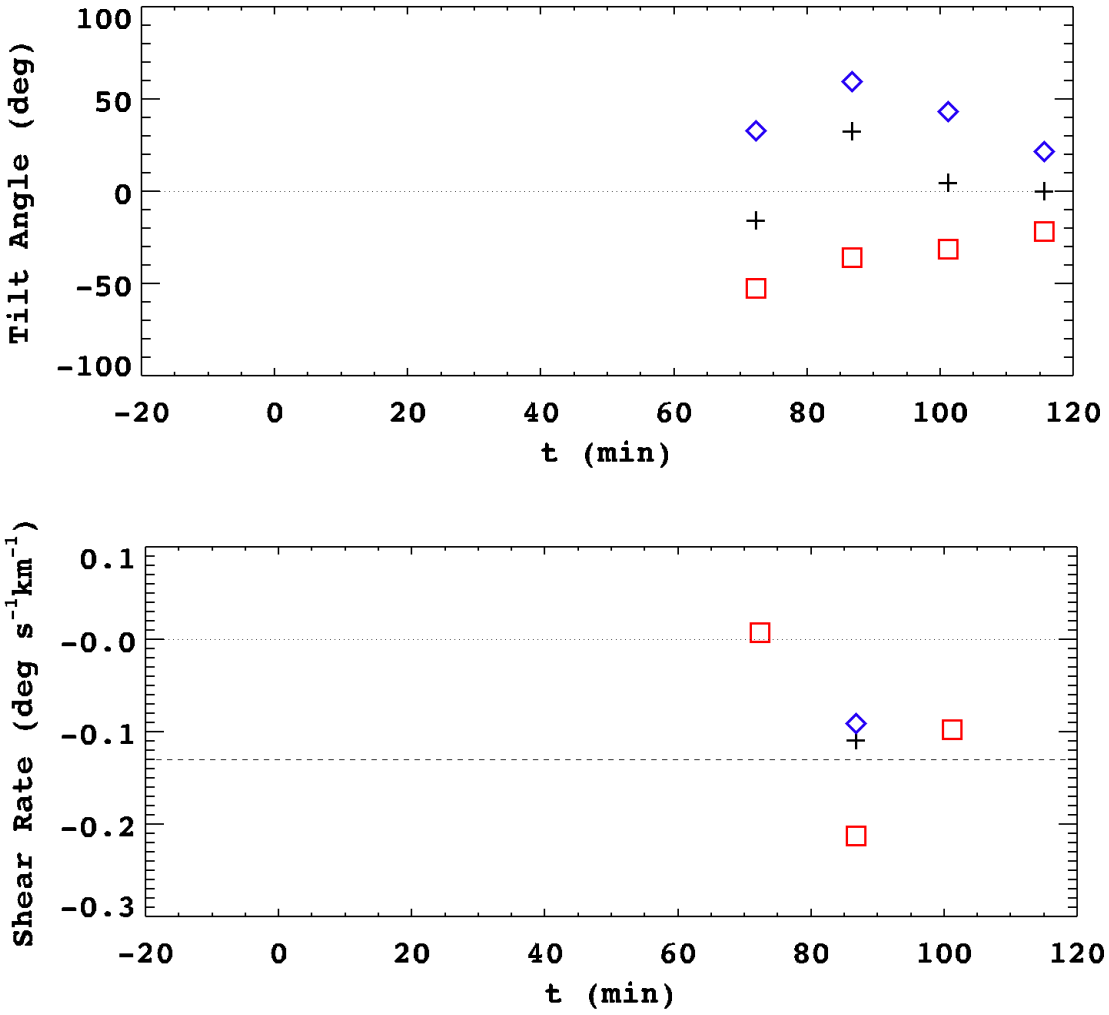

Figure 27: Tilt angles (top) and shear rates (bottom) for the outer radial extension of the spoke in Fig. 24. Blue diamonds mark the leading edge, black crosses the peak locations, and red squares the trailing edge. The dashed line on the shear rate plot is the Keplerian rate calculated for the. approximate center of the extension (110.5×10^3 km), while the dotted line is zero shear, corresponding to corotation. The shear rates are too noisy to be of any use for this extension, as it only appears clearly in the last 4 images. However, the shear angles of these images show that the extension is in fact radial, as can be seen from the tilt angle of the peak locations. The extension is widest where it contacts the original spoke, causing the edge tilt angles to be nonzero.

There also are two examples in our set of 28 of an old spoke fading away followed by a new spoke forming near the old spoke. In the first example, the old spoke's trailing edge is tilted at a $\sim 55^\circ$ angle to radial and is shearing very slowly. The new spoke appears within 5° of the old one and is radial to within 10° once it becomes measurable, as expected. (Additionally, a second spoke also appears next to this new one, again shifted towards trailing.) The inward radial growth is not measurable for this spoke due to interference with another spoke farther inwards, however, the outward growth is again ~ 0.5 km/s. This spoke is also an example of one which crosses the corotation radius, extending from $\sim 112 \times 10^3$ km to $\sim 115.6 \times 10^3$ km in radius.

In the second example, the original spokes's trailing edge is tilted at $\sim 60^\circ$ to radial while the leading edge appears to exhibit the same shearing pattern as the spoke in Fig. 18, with the outer portion sheared normally, and the inner portion sheared in the opposite sense to normal Kepler shear. This inner portion is nearly radial in the first image it appears in and quickly shears as the spoke fades. The new spoke which appears is also complex, consisting of an outer part and an inner part, where the inner part is more narrow and shears more slowly than the outer part. This new spoke is between two more forming spokes, causing edge measurements to be unreliable. However, the maximum radial growth for this new spoke is again ~ 0.5 km/s.

To summarize, when examined in detail, we observe many spokes which behave in the manner reported from Voyager observations. We have, however, observed spokes which deviate from the typical behavior of being radially aligned when they form and having a constant shear along their length. A small number of spokes were observed to be already sheared when they appeared on the rings, while some spokes appear to have regions which are sheared in the opposite sense that is expected. We have also observed the outward growth of a radial extension from a sheared, wedge-shaped spoke. Typical radial growth rates are of order 1 km/sec and slowly decrease with time.

5. Determination of Spoke Activity Periodicity

5.1. Data Reduction

For purposes of determining the periodicity and phase of the spoke activity, we use two sets of observations: the southern-side lit-face ones already analyzed for individual spoke activity and dynamics, as well as additional observations taken of the lit-face northern side of the rings after equinox.

Northern observations: The northern observations, taken from August 30, 2009 to September 13, 2009, consist of a series of 13 observing periods totaling approximately 169 hours, or nearly 16 full (but not consecutive) Saturn rotations, over 2 weeks. (Northern vernal equinox occurred on August 11, 2009.) These observations were taken during a single Cassini orbit, as the spacecraft moved away from Saturn, passed through apoapse, and then started moving inwards again. The large apoapse of this orbit meant that the geometry of these observations changed little during this period, which provided a rare opportunity to perform observations similar to the Voyager approach movies, i.e. many observations in the same geometry over an extended period of time.

Our northern observations contain both NAC and WAC movies, sample images of which are shown in Fig. 2. The phase angle at the start of these observations was 78.4° and increased slowly to 118.9° at the end, while the ring plane opening angle to the spacecraft started at 11.6° and ended at 6.1°. The opening angle of the ring to the Sun varied between 0.3° at the start to 0.5° at the end, due to the two week timeframe over which these observations were taken.

One unfortunate aspect of the proximity of the northern images to equinox is the large amount of Saturn shine on the rings relative to the direct solar illumination. The typical variation in the B ring I/F for one of our scans is a factor of two over the 100° of longitude covered in a WAC. However, the extremely low solar elevation angle causes the light ray path length through the spokes to become very long so that even a spoke with a small normal optical depth will have a large effective, or slant, optical depth due to the geometry, greatly enhancing their contrasts.

We find that using the particle size distribution derived from Hubble data in `rt3` produces model results which do not match our northern observations. The code predicts that the spokes will, in most cases, have a negative contrast (dark against the background B ring) for the geometries observed, while the actual spokes appear bright. Substituting other size distributions within the error bars quoted by McGhee et al. (2005) into `rt3` did not produce results consistent with the observations. The most straightforward way to account for this discrepancy is to assume that the spoke particles have "irregular" (i.e., non-spherical) shapes, as such particles have phase functions which scatter far more light than Mie scatterers at the intermediate phase angles we observe in the northern observations. Doyle et al. (1989) had previously considered the effects of irregular particles in Voyager data, comparing the phase function of spherical particles with those of "cube-like" and "plate-like" particles, using the semi-empirical theory of Pollack and Cuzzi (1980) for the irregular particles. However, they did not use the irregular particle phase functions in their modeling, on the grounds that the spherical and irregular particle phase functions were similar at the largest phase angles sampled by Voyager (see their figure 19), and a lack of Voyager spoke observations at intermediate phase. At such phase angles, particularly near phase angles of 70 degrees, the irregular particles scatter about 5 times more light than do the spherical particles. This result holds for other particle shapes, such as oblate spheroids (Throop et al., 2004). For small phase angles, numerical values of the phase function for spherical and irregular particles obtained by Doyle et al. (1989) are similar for the phase angle range of the early southern movies, so our previous modeling of those images is unaffected by the particles' shapes.

The actual phase function of the spoke particles determined from these Cassini observations will be addressed in a future paper. For now, we note that our photometric measurements are consistent with the spoke particles being irregularly shaped and lacking a means to convert $\Delta I/F$ to optical depth perform an analysis using the integral of the $\Delta I/F$ of the spokes (instead of the optical depth) as a substitute for the actual activity. This is possible due to the

nearly constant viewing geometry during the northern observations, and shall be justified momentarily.

To perform our global measurements of the northern activity, we chose a portion of the ring 40° across longitudinally and 8000 km long radially. This longitudinal range was limited by the amount of ring visible in the NAC images, while the radial range covered the ring region where the spokes are most prominent, from 104,000 to 112,000 km. Due to the motion of the spacecraft, it was necessary to shift the assigned longitude of the observed patch for some observations to prevent portions of it from leaving the field of view of the NAC. The total shift between the initial and final observational sequence was 18°, with the initial position of the patch's center being 10° away from the sub-solar longitude, measured from west to east, and shifting eastward over the course of the entire set of observational sequences or movies. However, the patch remained fixed during each movie. For each image, the change in I/F from the background was first found by fitting the background as described in section 2.1 to each azimuthal scan and then subtracted out of the profiles. The resulting I/F profiles were then area-integrated over the selected region to give the spoke activity at the time the image was taken.

Figure 28 shows the activity as a function of time over the course of all 13 northern movies. The phase changes from 78.4° at the beginning of the first observation to 118.9° at the end of the final observation, while the switch from WAC to NAC images occurs between the sixth and seventh observation, as denoted by the change in symbol. Despite these changes, there is no obvious trend in the spoke I/F. Instead, there is a fairly constant background I/F with an occasional sharp increase caused by a large spoke or group of spokes passing through the field of view. The lack of any trend leads us to believe that the real I/F to optical depth conversion factor for this range of geometries is roughly constant or, at the least, varying very slowly. This slow variation may add power to the spectrum we calculate, but only at very long periods and is thus justification for using the I/F directly for our calculations.

Southern observations: To derive the activity for the southern observations,

we first take our individual spoke fits obtained in section 2.1 and convert the spoke $\Delta I/F$ into optical depth using the procedure in section 2.2. We then calculate the contribution from individual spokes by integrating the optical depth to determine their activity. We then use the optical depth profiles of the spokes to calculate their centroids. This provides us with the activity and location of every spoke in every image. Then, in each image, we define a patch of ring 40° wide to be consistent with the northern observations. This patch is located 105° west of the sub-solar longitude, at 5:00 am local time for all of the observations. For each image, we total the activity for all the spokes with centroids falling in this patch. This produces a time series of spoke activity for the southern observations. Figure 29 shows the spoke activity over time for the southern movies.

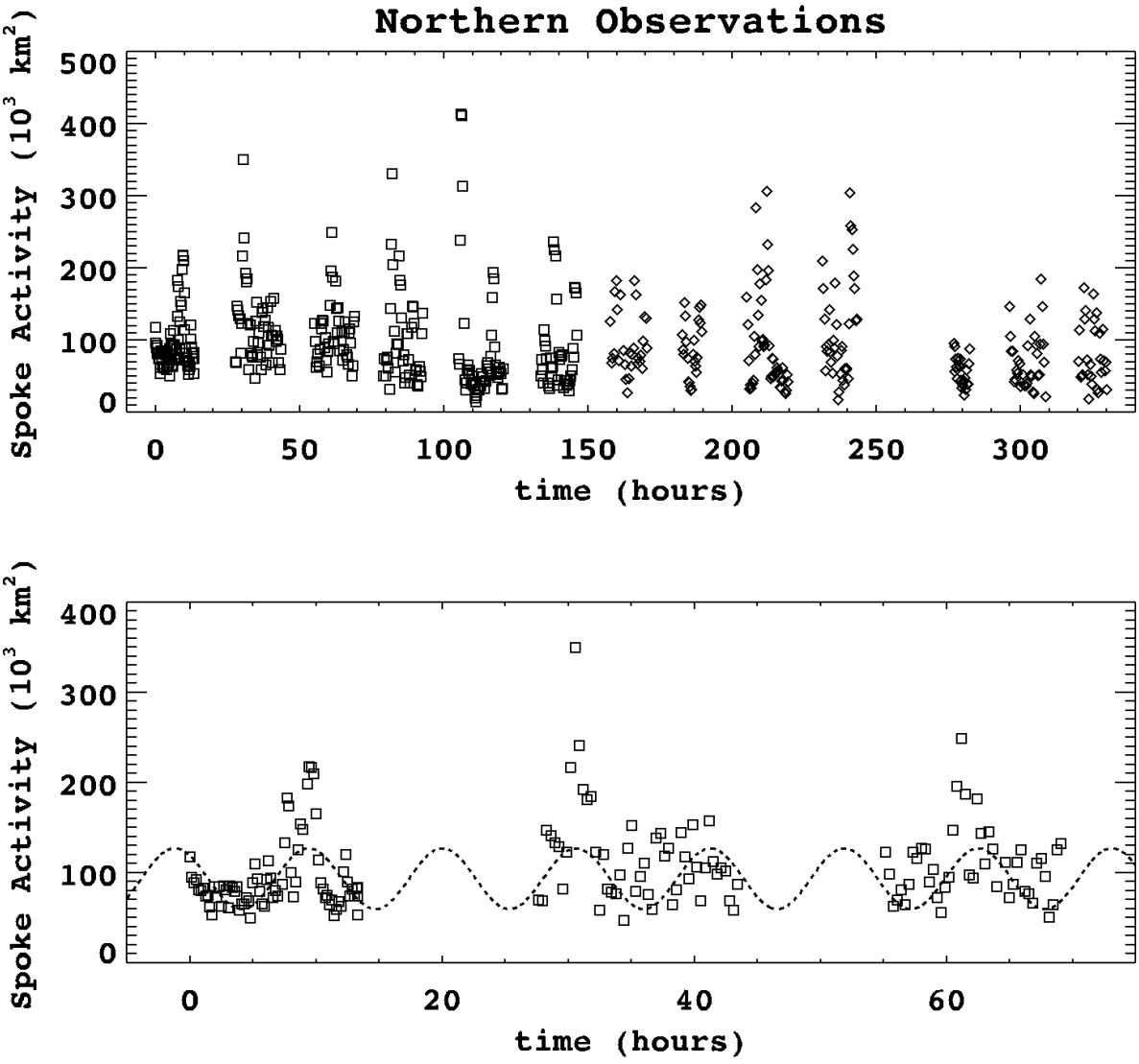

Figure 28: Data sets for the northern observations. (top) Combined data set from all the spoke periodicity movies taken on the northern side of the rings after equinox showing the spoke activity summed within the ring patch over the course of 14 days. Each datapoint was calculated by integrating the difference in I/F between the spokes and background in a ring patch 40° wide and from 104,000 km to 112,000 km radially in a single image. Images taken in the WAC (squares) and NAC (diamonds) are both present. (bottom) The first three observations and the best sinusoidal fit to the entire northern data set (with a 637.06 minute period) overplotted.

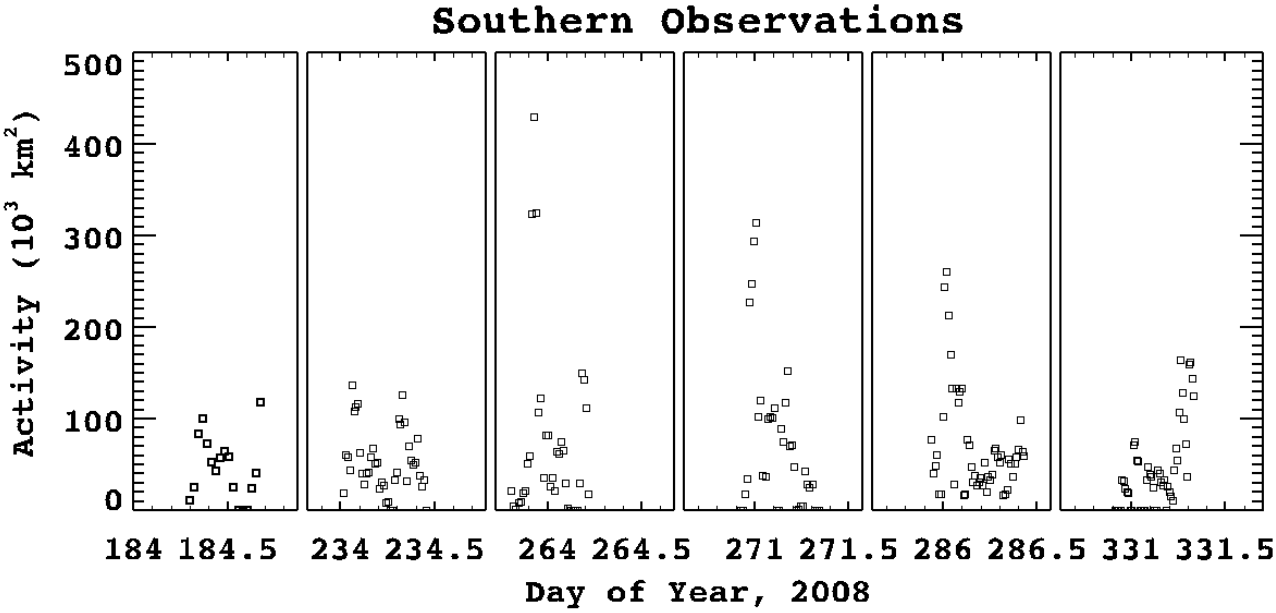

Figure 29: Data set from the spoke periodicity movies taken on the southern side of the rings prior to equinox showing the spoke activity summed within the ring patch. Each datapoint was calculated by integrating the difference optical depth of all the spokes falling within a ring patch 40° wide and 8000 km in radial extent in a single image.

Combining northern and southern observations: As the northern activities are an integral over the $\Delta I/F$ of the spokes and the southern ones are an integral of the actual optical depth of the spoke particles, the data sets need to be combined with care. To do so, we split the observations into three groups. The early southern observations were left as a group, but the later northern observations were split into two groups, one for those taken using the WAC and a separate group for the NAC observations. For each of these groups, we calculated the mean value of the activity and its standard deviation. We then subtracted out the respective means from each northern set and normalized the data so that each northern set had the same standard deviation as the southern observations. The mean value of the southern observations was then added back into each northern set. In performing this procedure, we are implicitly assuming that the spoke activity in each set of data is varying to the same degree and about the same mean, despite the separation in time of the north and south observations as well as the different location of the ring patch. We justify this assumption by noting that even if there is a change in the mean activity level between our north and south observations, such a change would only introduce an extremely long period variation and would not affect the power spectrum around periods near one Saturn rotation. Additionally, differences in activity due to the changing ring patch location on the rings are expected, as the spokes are known to be most prominent on the morning portion of the rings, local time. Our normalization corrects for any such differences.

In addition to the corrections for the activity, we also adjust the time tag of the observations in order to account for the differences in the longitudes, relative to the Sun, of the different sets at the time they were observed. We adjust the timing of the later northern observations by subtracting the time it would take the spokes to go from the patch used in the early observations, at 75 degrees from midnight measured in the orbital direction, to the location of the patch in the later observations, at 190 degrees. We assume the spokes orbit at the Keplerian rate for an object at a distance of $107,000$ km for this adjustment. This time adjustment amounts to 190 minutes.

It should be noted that the periods for both the northern and southern SKR did vary over the duration of our observations, with a slight variation during the southern spoke observations ($\sim$ 1 min) and a larger one between the southern and northern spoke observation ($\sim$ 5 min). However, these shifts are very small during the southern observations and are on the order of a few minutes between the northern and southern spoke observations. Compared to the separation in the periods, $\sim$ 12 mins, and the width of our peak, they are negligible. Figure 30 shows the rotation rates and periods of the two SLS4 components, derived from the sub-solar longitude zero crossings provided by the RPWS team at http://www-pw.physics.uiowa.edu/sls4/

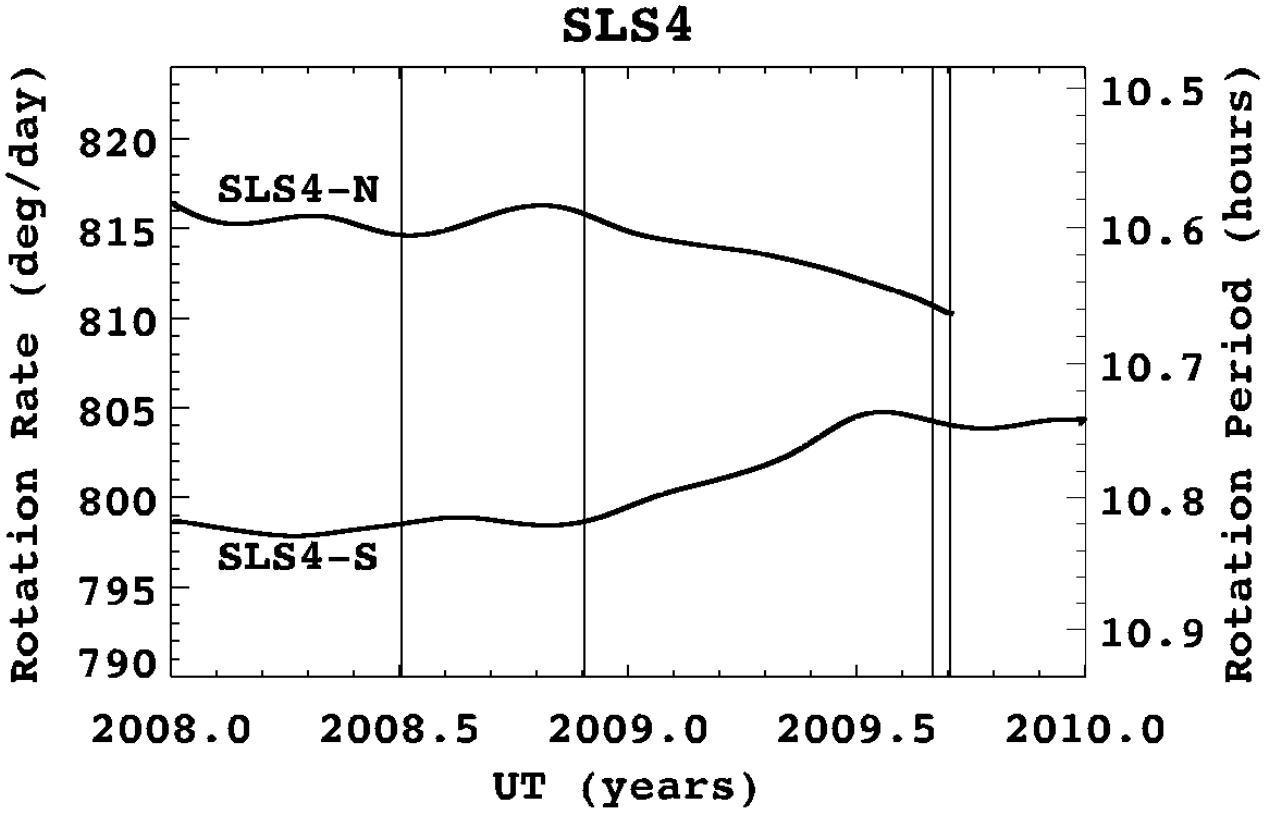

Figure 30: Rotation rates and periods for the two components of SLS4 during the two sets of spoke observations. The vertical lines mark the extent of the southern (July to November of 2008) and northern (August 30 to September 13 of 2009) observations.

5.2. Computing Power Spectrum

We calculate the power spectrum of the spoke activity using the same technique previously employed on the Voyager data by Porco and Danielson (1984) as it is well suited for unequally spaced datasets (Ferraz-Mello, 1981). To ensure that our spectra are sampled finely enough, we compute the spectral power at frequency intervals equal to one fifth of the smallest possible frequency detectable over the timespan of the dataset. This guarantees that all of the features in the spectra will be adequately sampled.

Northern data. We first calculate the power spectrum for just the later northern observations. These are well suited to this kind of analysis due to their very close spacing and very good sampling rate, covering nearly 16 full (but not consecutive) Saturn rotations over a period of two weeks, or a time spanning ≈ 31 rotations. These data have gaps in the coverage, primarily due to the spacecraft data downlinks to Earth, which are approximately one Saturn rotation long. (Unfortunately, the earlier southern observations, covering a mere 6 rotations over a timespan of ≈ 330 rotations, were too sparse to perform a comparable analysis on them alone.) Figure 31 shows the power spectrum for the northern observations for periods between 250 and 4000 minutes. A distinct peak can be seen at 637.1 minutes with a half-width of 9.2 minutes, which we identify as the period of the spoke activity. In addition to the peak, there is power in the spectrum in two wings, located around 450 minutes and 1100 minutes. This power is due to the average sampling rate of the dataset and remains present when the actual data are replaced with a pure sinusoid at the appropriate frequency. There is also some power near 324 minutes, which is approximately one half the period of our peak.

Southern data. Turning now to the 6 southern observations, calculating the power spectrum of these data produces many peaks due to the large gaps between the observations, making a determination of the real period impossible. As there are many false peaks in the spectrum, the power spectral method is ill-suited to analyze the southern data. We therefore employ another method in Section 5.3 to search for periodicities in this data set.

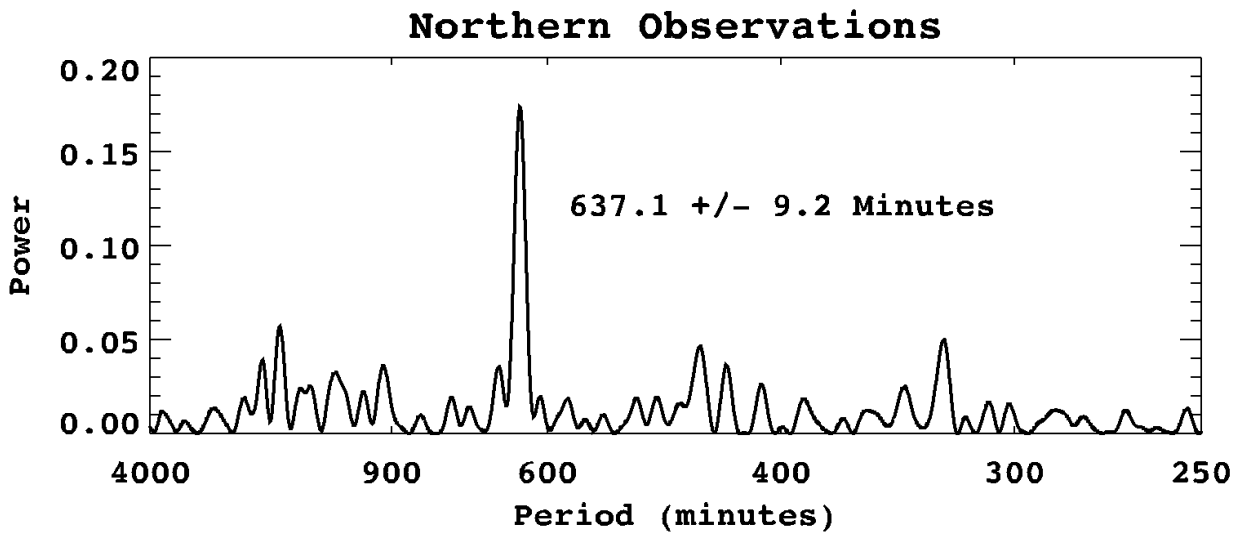

Figure 31: Power spectrum derived from the northern-side observation data (Fig. 28) taken shortly after equinox, starting on August 30, 2009 and ending on September 13, 2009. The peak is located at 637.1 minutes and has a half width at half maximum of 9.2 minutes.

Combining northern and southern data: As the northern data only span a period of approximately 2 weeks, the resolution of the northern power spectrum is limited to $\approx$ 9 minutes. To attempt an improvement on this, under the assumption that the southern data may be variable with the same period as the north, we perform our power spectrum analysis on the entire dataset, including both the northern and the southern observations. We exclude the first two southern movies, which showed no sign of any peak in spoke activity, in order to increase the signal to noise. The results are presented in Fig. 32. The general features of the northern spectrum are preserved, including the large amount of power located near 637 minutes, with some high frequency structure imposed upon it.

Figure 33 zooms in on the area around the large peak located near 637 minutes in Fig. 32. The broad peak present in power spectrum from the northern observations develops two forms of high frequency structures on it. The first is a rapid oscillation with a width of $\approx$ 0.8 minutes. The second is a longer

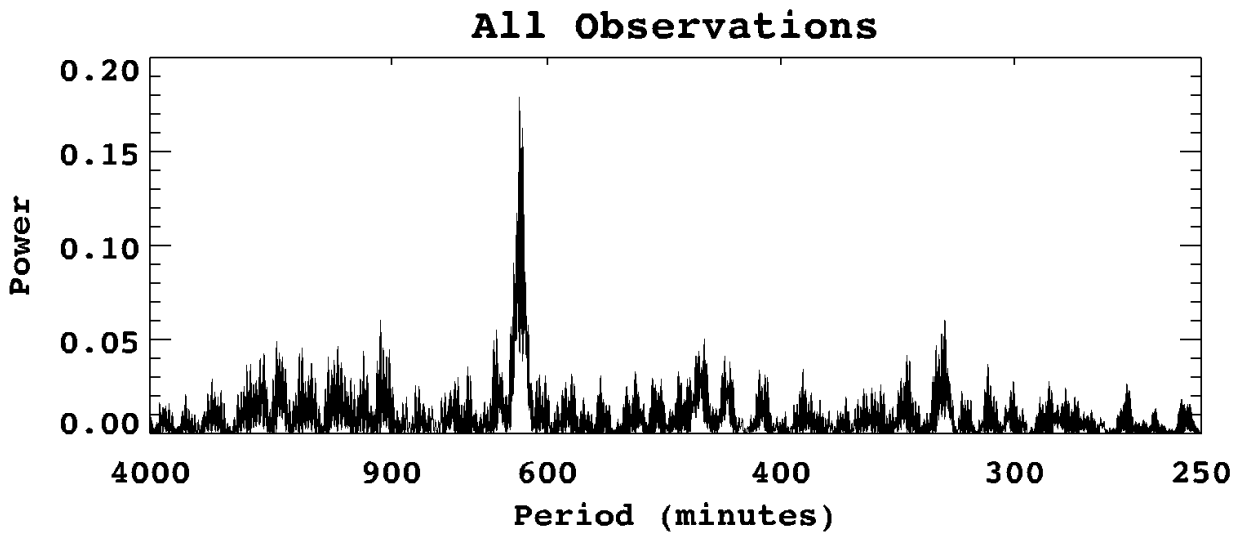

Figure 32: Power spectrum of all the combined data from the four southern observations which showed enhancements in spoke activity as well as the northern observations near equinox. A clear peak exists at 637 ± 9 minutes.

period pattern ≈ 4.4 minutes wide. These structures are consistent with the frequency shift one would expect if additional cycles are added to the dataset. The first, shorter interval is what we find for the period shift if one added an extra rotation to the entire dataset, which now spans a total of 8616 hours. The 4.4 minute pattern corresponds to adding an additional rotation to the southern observations alone, which lasted 1611 hours.

From this spectrum, we find that there are two plausible periods for the spoke activity: ≈ 634 minutes and ≈ 638 minutes, corresponding to the averages value of the two groups of narrow peaks with the most power. Both of these periods are shorter than the period of the SKR as reported from RPWS data early in the Cassini mission, which varied from 645.4 minutes as of January 1, 2004 to 650.2 minutes on August 10, 2007 (Kurth et al., 2008), denoted by vertical dark blue lines in Fig. 33; it has recently been determined that this source with the longer period is located in the southern hemisphere. However, there is an additional SKR source in the northern hemisphere with a period of approximately 637

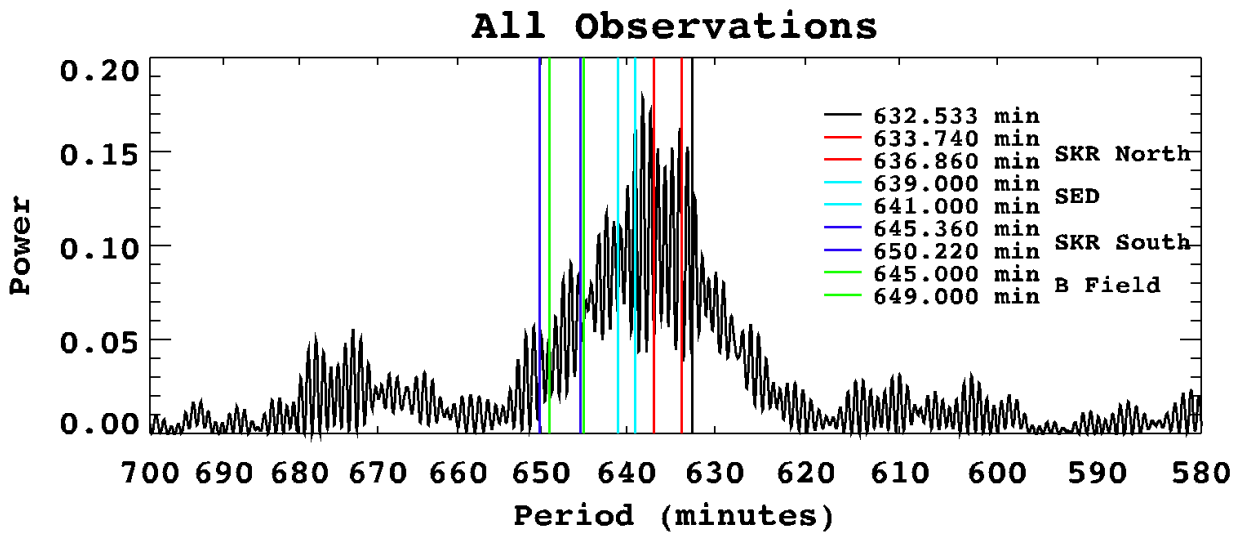

Figure 33: Power spectrum identical to that in Fig. 32, but zoomed in around the main peak at ≈ 637 minutes. Vertical lines indicate the measured ranges of various periods of interest: (red) northern SKR source, (light blue) SED period, (dark blue) southern SKR source, (green) magnetic field oscillations, (black) recent estimate of the internal rotation rate of the planet by Anderson and Schubert (2007).

minutes as of May, 2009 (Gurnett et al., 2009a), which varied between the vertical red lines in the figure. The northern SKR period had an average value of 637 minutes from day 358, 2008 to day 167, 2009, while the southern period had an average value of 647.2 minutes (Gurnett et al., 2009b). (Our northern data were acquired a few months later, starting on day 242, 2009, while the last observation in our southern data set occured on day 330, 2008.) This new northern period is well within one half-width of our northern spectrum's peak (Fig. 31) and within the peak centered at 638 minutes in the combined spectrum (Fig. 32). While the possibility of power at the southern SKR period cannot be completely ruled out due to the width of the peak, the peak falls almost exactly on the northern SKR period, implying that any contribution from the southern period is likely minimal.

It's also interesting to note that during the observational timespan of the southern spokes (mid to late 2008), the northern SKR source was more active

than the southern one (Gurnett et al., 2009a). Finally, our longer period is slightly shorter than the original SKR period reported from Voyager observations of 639 minutes 24 seconds (Desch and Kaiser, 1981).

The Cassini era SED period, measured by RPWS to be $\sim$ 640 minutes (Fischer et al., 2007), falls within the peak in the northern power spectrum. However, we find it unlikely that there is an actual connection between spoke activity and the SEDs, as we have observed spokes during both active SED periods and times when there were no SEDs (Fischer et al., 2011). Additionally, the spokes are located on magnetic field lines which map to latitudes well above that where the storms producing SEDs are located ($\sim 39^\circ$ planetocentric latitude for the innermost region containing spokes compared to $\sim 35^\circ$ for the storms).

Finally, fluctuations in the magnetic field have periods similar to that of the southern SKR period (Andrews et al., 2008; Provan et al., 2009). The period of these fluctuations was 649 ± 0.5 minutes during the southern observations. During the northern observations, the period was 645 ± 0.5 minutes Andrews (2010). This second period barely falls within the peak of the northern power spectrum.

5.3. Determination of Preferred Magnetic Sector for Spoke Activity

In section 5.2, we performed a power spectral analysis on the time series produced by our spoke activity measurements for the northern and southern sides of the rings - both separately and then in combination - to search for any periodic variations in the appearance of spokes on the rings. We saw that the earlier southern-side data were too poorly sampled over the observing interval of ≈ 146 days to yield any periodic signatures with significant power, but the later well-sampled northern-side data produced a pronounced peak near 637 min.

As Voyager-era spoke activity was found to be coincident with (what was then believed to be) the magnetic field longitude of the Voyager-observed SKR-active sector (Porco and Danielson, 1984), it is of interest to determine whether or not the same correspondence holds true in the Cassini era. This issue is

more complicated now than for Voyager, due to the two distinct SKR sources with different periods and possibly different levels of SKR activity (Kurth et al., 2007; Gurnett et al., 2009a). Here we use the latest coordinate system provided by Gurnett et al. (2011) based on the SKR which provides two separate coordinates, SLS4-N and SLS4-S, which are based on the northern and southern SKR emissions, respectively.

If, as in the Voyager era, the spoke creation/modification process is in some way connected to the SKR process or arises from the same sector in the magnetic field, we would expect to find the spoke-active sector coincident with the SKR-active sector: i.e. the spoke-active sector should fall near 100 deg in one or both of the SLS4 coordinate systems.

Northern Data. We use the same data that is shown in Fig. 28 except that instead of producing a time series, we use the time and location of the center of the ring patch to determine the SLS4-N (or SLS4-S) longitude for each data point, as outlined in section 2. We collect the data into 20 degree wide longitude bins and calculate the average activity by taking the total activity in each bin dy dividing by the number of images which fall into each specific bin.

Figure 34 shows the data from individual images plotted in SLS4-N, as well as average activity per 20° bin. We find that there is a substantial variation in the activity in the binned results, although the peak is not located at 100° as expected. Instead we find that the peak of spoke activity is located at $\approx 210°$ in these coordinates, where we have defined the peak as the location of the maximum of the $m = 1$ component of the Fourier Transform of the averaged activity, which we have overplotted the mean activity in Fig. 34. The amplitude of the $m = 1$ component is approximately 33% of the average value, due to the pronounced asymmetry in the activity.

SLS4-S does not organize the data into as narrow a range of longitudes as SLS4-N does, as can be seen from Fig. 35. However, there is still a pronounced variation in the spoke activity, with a peak at $\approx 185°$ and the amplitude of the $m = 1$ term dropping marginally to 28% the average value. The reason for this difference is that while SLS4-N and SLS4-S are nearly in phase at the beginning

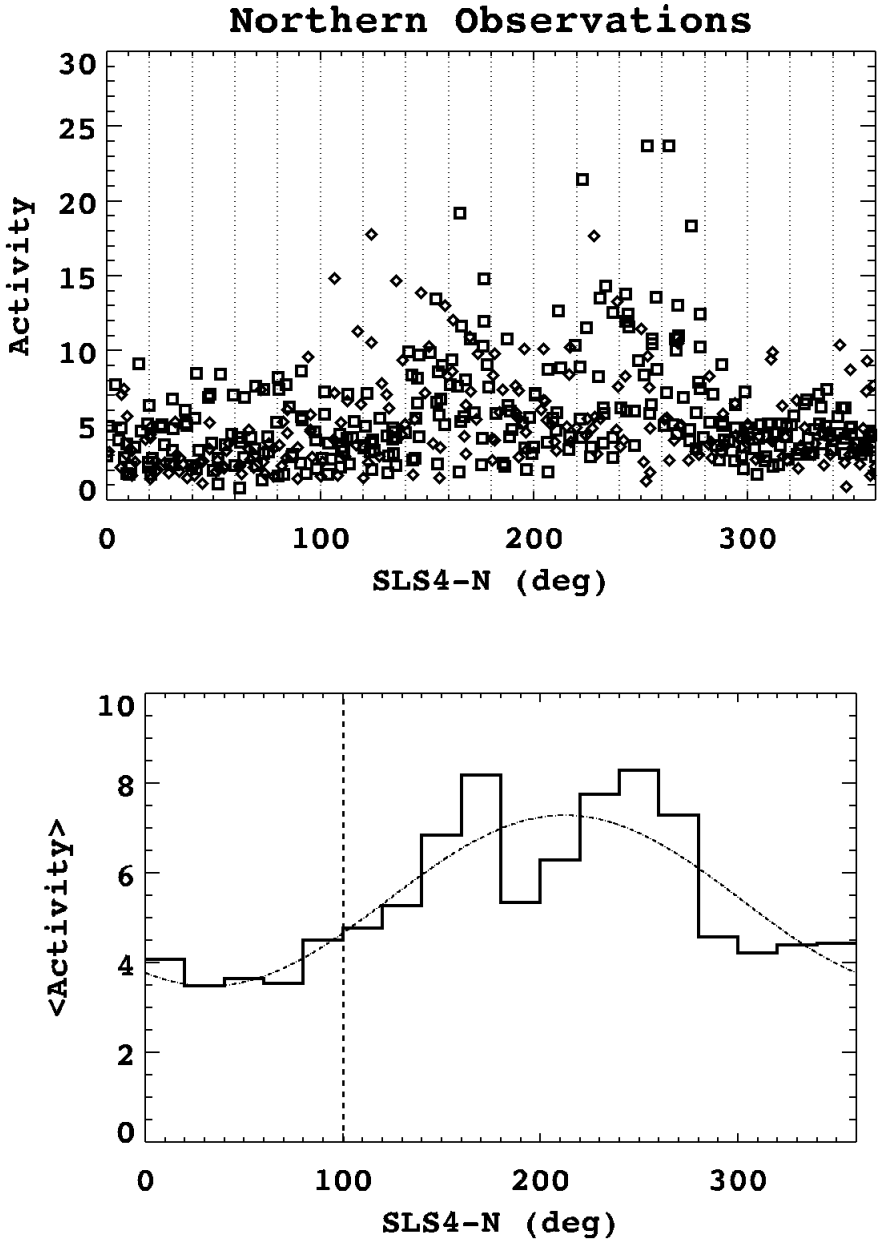

Figure 34: Spoke activity plotted as a function of SLS4-N. Boxes indicate data from WAC images while diamonds are from NAC images. Vertical dotted lines indicate the boundaries of the bins used to calculate the average activity (bottom). The dashed vertical line is the longitude of peak SKR activity for the northern source, while the dot-dashed line is the $m = 1$ component of the Fourier Transform.

of the observations, the difference being $< 10°$, this increases to $90°$ over the observations due to the slightly different periods.

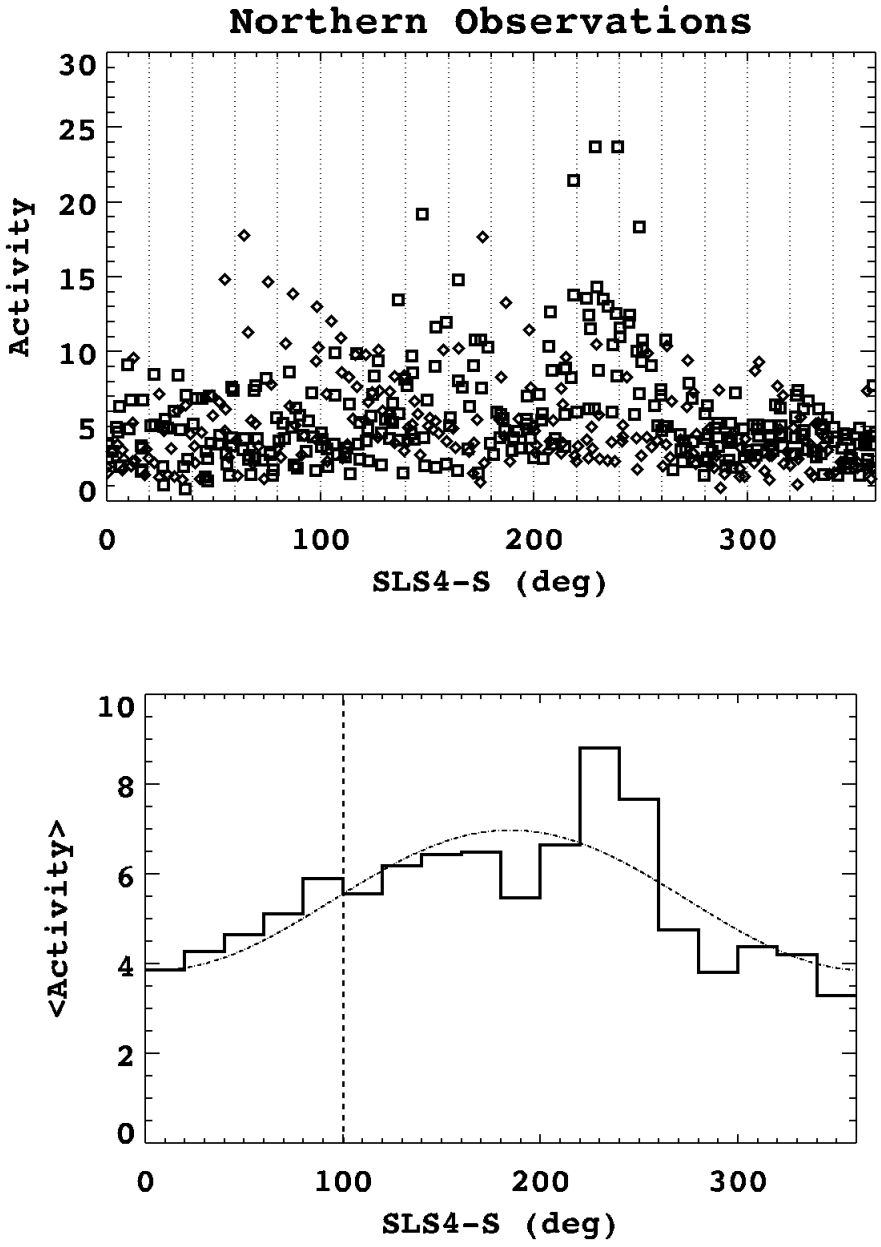

Figure 35: Post-equinox spoke activity plotted as a function of SLS4-S. Boxes indicate data from WAC images while diamonds are from NAC images. Vertical dotted lines indicate the boundaries of the bins used to calculate the average activity (bottom). The dashed vertical line is the longitude of peak SKR activity for the southern source, while the dot-dashed line is the $m = 1$ component of the Fourier Transform.

Southern Data. We use the data from Fig. 29 and follow the same procedure to plot the (admittedly sparse) spoke activity data for the pre-equinox, southern observations in the SLS4 coordinate systems and find once again that the activity has enhancements in both SLS4-S and SLS4-N. Figures 36 and 37 show the activity plotted versus SLS4-N and SLS4-S, respectively. The enhancements of the spoke activity both appear near 200° in their respective coordinate systems, with the peaks of the $m = 1$ patterns falling at 217° and 203° respectively. Again, SLS-4N has a more pronounced enhancement than SLS4-S, with the $m = 1$ component of the activity plotted in SLS4-N being $\approx 30\%$ of the constant offset, but only $\approx 13\%$ in SLS4-S.

Unlike the northern observations, the southern observations are spread out over such a long period of time that the phase difference between the two coordinate systems varies greatly from observation to observation, from as little as 15° to as much as 137°, and cannot be used to explain why the peak activity locations are similar.

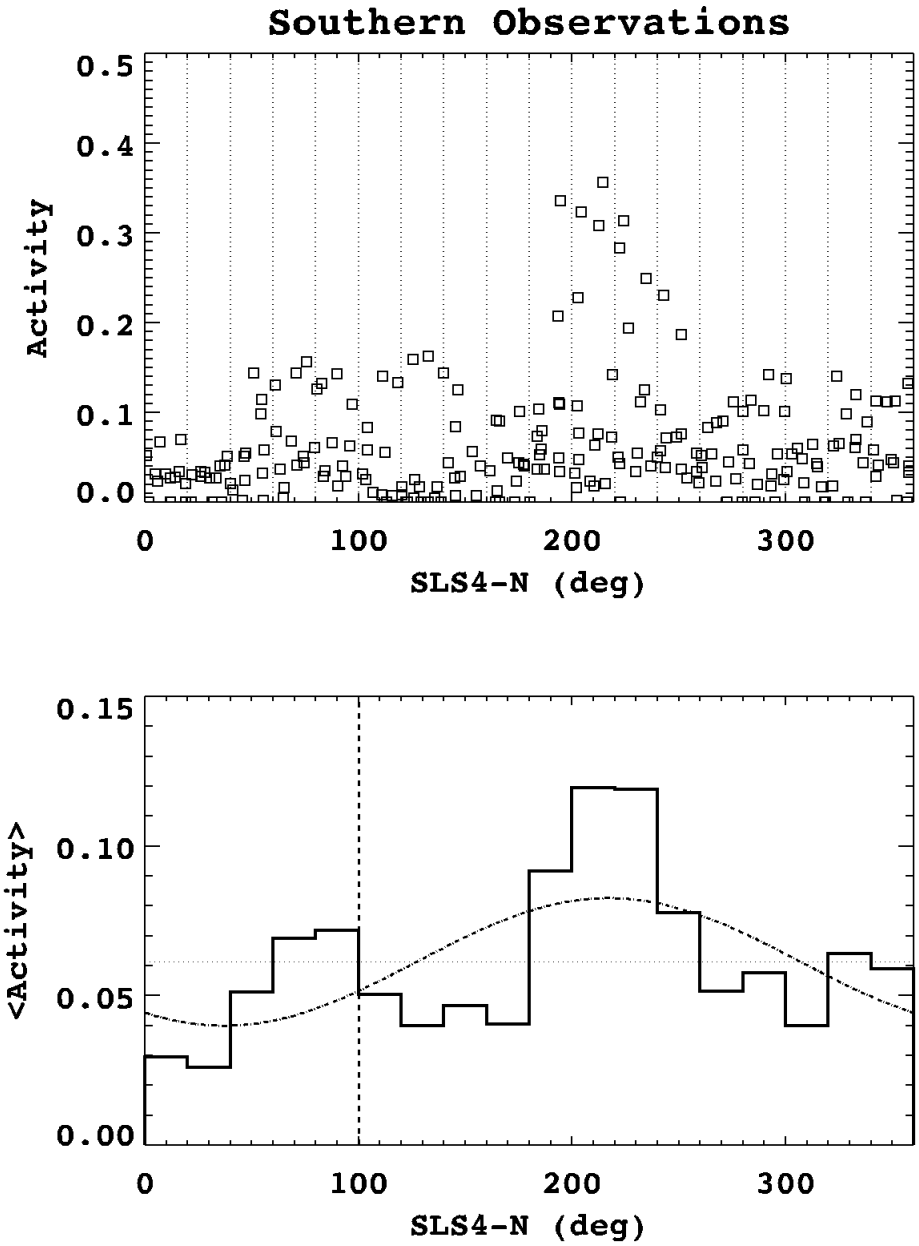

Figure 36: Pre-equinox spoke activity plotted as a function of SLS4-N. All data are from WAC images. Vertical dotted lines indicate the boundaries of the bins used to calculate the average activity (bottom). The dashed vertical line is the longitude of peak SKR activity for the northern source, while the dot-dashed line is the $m = 1$ component of the Fourier Transform.

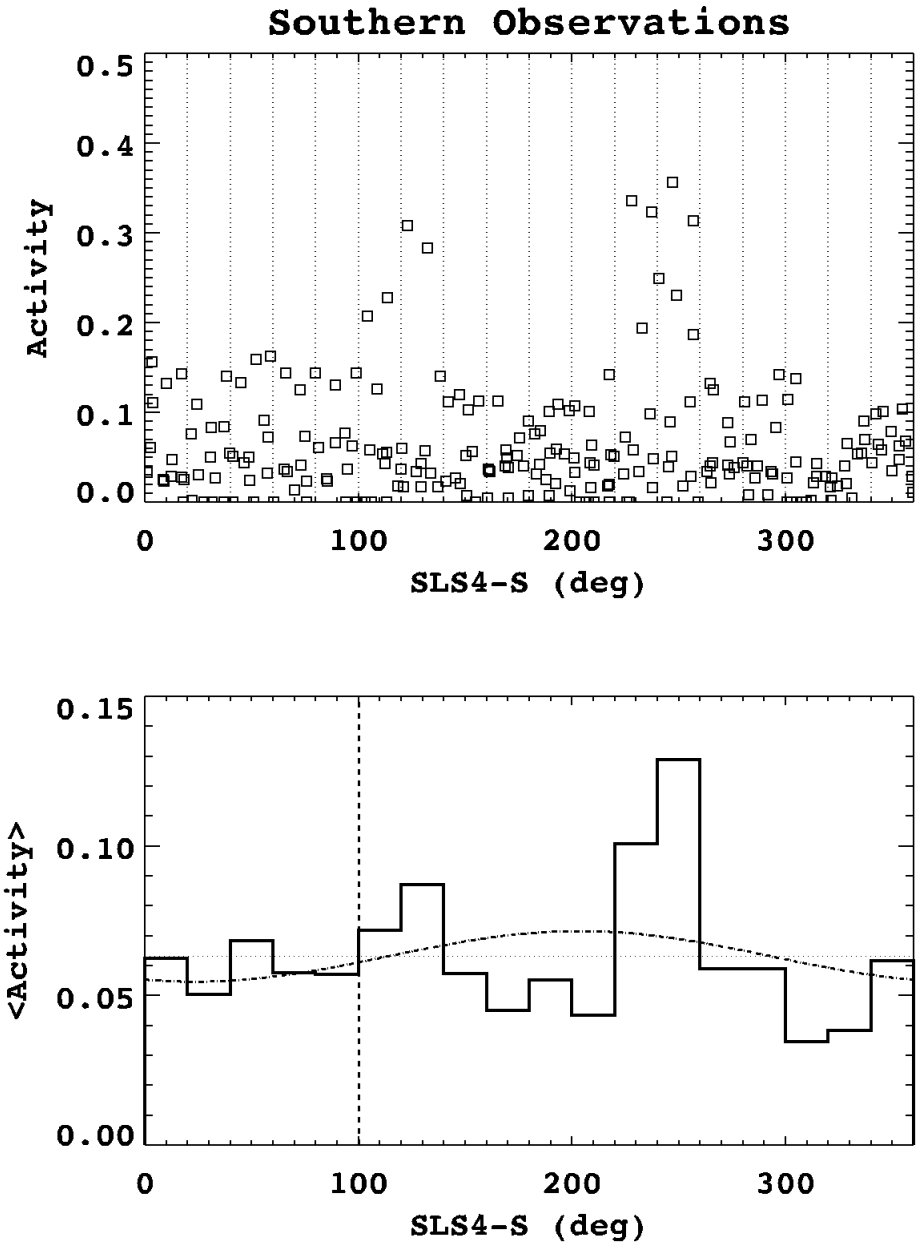

Figure 37: Pre-equinox spoke activity plotted as a function of SLS4-S. All data are from WAC images. Vertical dotted lines indicate the boundaries of the bins used to calculate the average activity (bottom). The dashed vertical line is the longitude of peak SKR activity for the southern source, while the dot-dashed line is the $m = 1$ component of the Fourier Transform.

Plotting the activity as a function of magnetic longitude produced an enhancement near 200° in both the SLS4-N and SLS4-S coordinate systems. This enhancement is similar to, but phase shifted from, the enhancement observed for the activity in Voyager data plotted against the original SLS coordinate system, where it was located at 100°, the SKR active sector.

As a final check to determine whether there were periods which organized the data better than SLS-4, we conducted a search whereby we generated a series of coordinate systems with constant periods in the range of our power spectrum peak. We found that no constant period in this range did a significantly better job organizing the data than was accomplished using SLS-4. Additionally, as the southern observations were taken over a long timespan, we also generated coordinate systems which varied linearly with time. Again, none of these coordinate systems performed significantly better than SLS-4.

Spoke Growth. In addition to direct spoke activity measurements, we were able to determine the rate of growth (rate of change in total activity with respect to time) of some spokes in the southern observations, as was mentioned in Section 2. Here we use the spoke growth rates as an alternative to the activity and determine whether or not there is a prefered magnetic longitude for spoke growth and if it is the same as that for the overall activity, 200°.

To evaluate the degree to which the spoke growth is organized, and how significant this organization is, we first create a histogram of spoke growth for spokes with positive growth rates as a function of SLS4-N and calculate the $m = 1$ components of its Fourier Transform, taking the peak location to be the mean longitude. We then calculate the standard deviation of the longitude in two ways. The first uses the square of the spoke growth as a weighting function and is given by

$$\sigma_\lambda = \left[\frac{\Sigma_{i=1}^{N} GR_i^2 (\lambda_i - \langle\lambda\rangle)^2}{\Sigma_{i=1}^{N} GR_i^2} \right]^{1/2} \quad , \tag{9}$$

where the summation is over all of the positive growth spokes, including the 28 spokes newly appearing spokes from section 4, $\langle\lambda\rangle$ is the mean longitude, and GR_i is the measured growth rate of the ith spoke. The second method simply

uses the unweighted data, setting the SA_i to 1 in the above equation. In both cases, we use the cyclic nature of the longitude to make the difference $\lambda_i - \langle\lambda\rangle$ lie in the the range from $-180°$ to $180°$ for all spokes to avoid artificially high values of σ_λ caused by $\langle\lambda\rangle$ being near $0°$ or $360°$.

For our southern observations, we found that $\langle\lambda\rangle = 205.5°$, which is very close to the $203°$ we were expecting based on the activity measurements. Using the weighted data, we found that $\sigma_\lambda = 76.0°$, while for the unweighted data, $\sigma_\lambda = 90.7°$. To determine if this is a statistically significant clustering, we conducted trials where a random angle from $0°$ to $360°$ was added to each longitude in the dataset, wrapping the data as needed to keep the longitudes in the range from $0°$ to $360°$. For each trial we performed the above calculations again, calculating a new histogram and $\langle\lambda\rangle$, and the two σ_λ values. We found that using the weighted σ_λ, the trials would produce a lower value, and hence more clustered group of growing spokes, 6.8% of the time. For the unweighted σ_λ, more clustering was observed only 4.2% of the time. We therefore conclude that this clustering of growing spokes is significant at the 95% level.

6. Conclusions and Discussion

In this paper, we have i) found that the typical solitary spoke has azimuthal profiles which are well fit by Gaussians; ii) shown that most spokes are either increasing or decreasing in activity as they orbit Saturn, with a small number of forming spokes appearing between consecutive images; iii) measured the presumed charge to mass ratio of the spoke particles, assuming the advancing spoke edges are due to individual particle motions (as was previously done for Voyager observations), and found the values too high for this interpretation to be reasonable, unless the spokes are embedded in a very hot plasma; iv) measured the radial growth of forming spokes and found that the growth rates at each terminus is typically ≈ 0.5 km/s and no more than 1 km/s; v) found that spoke activity on the northern side of the rings is variable with a period coincident with that of SLS4-N, the northern SKR, and that the southern side spoke activity also varies with this period though there is a possibility of the southern SKR period being present; vi) found that the location of the greatest spoke activity for the spoke observations, both northern and southern, was located at 200° in both coordinate systems at the time of these observations, 100° out of phase with the peak SKR emission longitudes (Gurnett et al., 2011); and vii) found that growing spokes observed on the southern side of the rings also preferentially cluster around 200° in SLS4-N. We address each of these points below.

For the majority of spokes, azimuthal profiles taken through them are well fit by Gaussians. This is especially true of solitary spokes, but many spoke clusters can also be well fit by multiple Gaussians. Even for most active spokes, Gaussians adequately fit the profiles during the growth of the spoke, where the width and amplitude of the fits increase from image to image at every radius. Also, the entire spoke increases in optical depth, with the center increasing faster than the edges, as well as area coverage. Any model of spoke formation must account for these typical characteristics of a growing spoke.

By area-integrating the optical depth of the spokes in the southern movies,

we determine that activity levels of individual spokes is typically increasing or decreasing as it orbits Saturn. Relatively few spokes' activities remain constant throughout an observation. This indicates that dust grains are being added to or subtracted from the spokes throughout much of their lifetimes. As our observations were of the morning portion of the rings, local time, more spokes were observed to increase in activity than decrease. Typically, a spoke's activity would either increase or decrease monotonically for the entire time it was visible, a period of ≈ 2 hours for these observations. This indicates that spoke formation is a slow, continuous process. While we have seen 51 instances of a spoke appearing in an image where there was none previously, the new spokes are always quite faint and just beginning to emerge from the noise of the observation.

By utilizing the Gaussian form of the typical spoke's azimuthal profile, we have been able to track the edges of the most prominent spokes which appear in multiple images. Many of these spokes have edges which exhibit motion deviating from Keplerian. Assuming that the dust grains comprising the spoke are on circular orbits, we calculate their charge to mass ratio and find that the electric potential must be large and negative for a typical spoke particle, 0.4 μm in radius (McGhee et al., 2005), to exhibit the degree of deviation we observe. Such large potentials are difficult to produce on dust grains unless the spokes are embedded in a very hot plasma. As there is no evidence for such a hot plasma, we interpret the spoke edge motions as not as being the result of individual particle motions, but as the motion of the spoke forming region, which extends the entire length of the spoke. It is still possible that the deviating edge consists of the smallest grains comprising the spoke, with the larger grains moving on the Keplerian edge. These particles, however, must be very small, on the order of tens of nanometers in radius to bring the electric potential down to a reasonable level. As smaller particles require longer to charge, we find this unlikely.

The Gaussian fits have also provided a means to measure the radial growth of the spokes as a function of time. We find that forming spoke will grow radially both inwards and outwards at speeds of less than 1 km/s, typically 0.5 km/s. This growth is fastest when the spoke is beginning to form and

slows with time as the spoke reaches its full extent. Spokes which are growing radially are often active spokes in the sense that one edge is corotating with the magnetic field while the other is undergoing Kepler shear. However, we see a wide variety in spoke behaviors, including spokes which remain narrow with both edges corotating while they form as well as spokes which appear to have two regions which shear differently.

We have used Cassini spoke observations to calculate the power spectrum of spoke activity observed on the northern side of the rings and found a period of 637.1 ± 9.2 minutes. While the error on the period is rather large due to the short timespan of the observations, this period is very close to the northern SKR period as recently reported by RPWS (639.5 to 639.8 minutes). It is also very close to the SKR period reported during the Voyager flybys (Kaiser et al., 1984).

Though there appears to be no indication of a peak at the period of the southern SKR in in our power spectrum of the northern spoke activity, the southern SKR period organizes the northern data reasonably well; this may be the result of the coordinate systems being nearly in phase at the time of the observations. The southern observations were too sparsely sampled to produce a useful power spectrum.

In addition to the SKR, there are several other phenomena of interest with periods near our peak. The Cassini era SED period, ≈ 640 minutes (Fischer et al., 2007), falls within the peak using the northern data alone; both of the periods singled out in the combined spectrum are shorter than the SED period. Voyager observations seemed to indicate a possible link between SEDs and spoke activity (Porco and Danielson, 1984). However, some of our Cassini observations of spokes occur at times when there are no SEDs being produced. Specifically, during the southern observations, 3 of our 4 observations with good signal occur during an extended period (> 1000 days long) during which no SED activity was detected. Of the two observations with no prominent spokes, the July and August observations of 2008, the first occurred during a period of SED activity, while the second occurred during a period of no SED activity (Fischer et al.,

2011). Moreover, the storm that has been demonstrated to produce the Cassini-era SEDs is located at 35° south planetocentric latitude (Dyudina et al., 2007). Mapped along Saturn's magnetic field lines (Dougherty et al., 2005), this storm is connected to a region in Saturn's rings at ≈87,000 km, well interior to, and therefore completely missing, the spoke region. This leads us to conclude that any connection between the spokes and SEDs is very likely non-existent.

Also, in addition to the SKR and SED measurements, Cassini has also measured fluctuations of the magnetic field which have periods similar to that of the southern SKR period (Andrews et al., 2008; Provan et al., 2009). For the times of our observations, the period was 649 ± 0.5 minutes during the southern observations and 645 ± 0.5 minutes during the northern observations (Andrews, 2010). The first period falls close to one of the many peaks we see in the southern power spectrum, while the second period is barely within one half width of the peak in our northern power spectrum.

We used the latest coordinate system based on the SKR in order to plot spoke activity as a function of magnetic longitude and find that there is an enhancement similar to the one found in Voyager data, but phase shifted with respect to the SKR sources. This enhancement occurs in both the northern and southern observations and in both the northern and southern SKR-based coordinates (Gurnett et al., 2011), SLS4-N and SLS4-S, respectively, near 200°, though it is less pronounced in SLS4-S. While it may be coincidental that the peak activity is the same in both coordinate systems during the northern observations, since they are nearly in phase during the time they were taken, this is not possible for the southern observations, since they were taken over a long period of time with many different phases between the two coordinate systems. It would therefore appear that the southern spoke activity picks up both the northern and southern SKR periods.

Finally, we also examined the growth of spokes in the southern observations as a function of SLS4-N and found that spokes with increasing activity occur preferentially around 200°, the same longitude where activity is greatest.

Acknowledgements

We acknowledge E. Baker and B. Knowles for designing the observations used in this work. We thank Matt Hedman for an initial review of this manuscript, as well as the two anonymous reviewers who provided valuable comments which helped improve this paper. The authors were supported by both NASA and the Cassini project.

References

Anderson, J. D. and Schubert, G. (2007). Saturn's gravitational field, internal rotation, and interior structure. *Science*, 317:1384–1387.

Andrews, D., Bunce, E., Cowley, S., Dougherty, M., Provan, G., and Southwood, D. (2008). Planetary period oscillation in Saturn's magnetosphere: Phase relation of equatorial magnetic field oscillations andd Saturn kilometric radiation modulation. *Journal of Geophysical Research*, 113:A09205.

Andrews, D. J. (2010). private communication.

D'Aversa, E., Bellucci, G., Nicholson, P. D., Hedman, M. M., Brown, R. H., Showalter, M. R., Altieri, F., Carrozzo, F. G., Filacchione, G., and Tosi, F. (2010). The spectrum of a Saturn ring spoke from Cassini/VIMS. *Geophysical Research Letters*, 37.

Desch, M. D. and Kaiser, M. L. (1981). Voyager measurement of the rotation period of Saturn's magnetic field. *Geophysical Research Letters*, 8:253–256.

Dougherty, M., Achilleos, N., Andre, N., Arridge, C., Balogh, A., Bertucci, C., Burton, M., Cowley, S., Erdos, G., Gaimpieri, G., Glassmeier, K., Khurana, K., Leisner, J., Neubauer, F., Russel, C., Smith, E., Southwood, D., and Tsurutani, B. (2005). Cassini magnetometer observations during Saturn orbit insertion. *Science*, 307:1266–1270.

Doyle, L. R., Dones, L., and Cuzzi, J. N. (1989). Radiative transfer modeling of Saturn's outer B ring. *Icarus*, 80:104–135.

Doyle, L. R. and Grün, E. (1990). Radiative Transfer Modelling Constraints on the Size of Spoke Particles in Saturn's Rings. *Icarus*, 85:168–190.

Draine, B. T. and Salpeter, E. E. (1979). On the physics of dust grains in hot gas. *Astrophysical Journal*, 231:77–94.

Dyudina, U. A., Ingersoll, A. P., Ewald, S. P., Porco, C. C., Fischer, G., Kurth, W., Desch, M., Del Genio, A., Barbara, J., and Ferrier, J. (2007). Lightning

storms on Saturn observed by Cassini ISS and RPWS during 2004 2006. *Icarus*, 190:545–555.

Eplee, R. and Smith, B. (1984). Spokes in saturn's rings: Dynamical and reflectane properties. *Icarus*, 59:188–198.

Evans, K. F. and Stephens, G. L. (1991). A new polarized atmospheric radiative transfer model. *J. Quant. Spectrosc. Radiat. Transfer*, 46:413–423.

Farmer, A. J. and Goldreich, P. (2005). Spoke formation under moving plasma clouds. *Icarus*, 179:535–538.

Farrell, W. M., Desch, M. D., Kaiser, M. L., Kurth, W. S., and Gurnett, D. A. (2006). Changing electrical nature of Saturn's rings: Implications for spoke formation. *Geophysical Research Letters*, 33:7203.

Ferraz-Mello, S. (1981). Estimation of periods from unequally spaced observations. *Astronomical Journal*, 86:619–624.

Fischer, G., Gurnett, D. A., Kurth, W. S., Zarka, P., Moore, L., and Dyudina, U. A. (2011). Peak electron densities in Saturn's ionosphere derived from the low-frequency cutoff of Saturn lightning. *Journal of Geophysical Research*. submitted.

Fischer, G., Kurth, W. S., Dyudina, U. A., Kaiser, M. L., Lecacheux, A., Ingersoll, A. P., and Gurnett, D. A. (2007). Analysis of a giant lightning storm on Saturn. *Icarus*, 190:528–544.

Goertz, C. K. and Morfill, G. (1982). A Model for the Formation of Spokes in Saturn's Ring. *Icarus*, 53:219–229.

Goertz, C. K. and Morfill, G. (1983). Plasma clouds in Saturn's rings. *Icarus*, 55:111–123.

Goldreich, P. and Tremaine, S. (1982). The dynamics of planetary rings. *AR&A*, 20:249–283.

Gombosi, T. and Ingersoll, A. (2010). Saturn: Atmospher, Ionosphere, and Magnetosphere.

Grün, E., Goertz, C. K., Morfill, G. E., and Havnes, O. (1992). Statistics of Saturn's spokes. *Icarus*, 99:191–201.

Grün, E., Morfill, G. E., Terrile, R. J., Johnson, T. V., and Schwehm, G. (1983). The evolution of spokes in Saturn's B ring. *Icarus*, 54:227–252.

Gurnett, D. A., Groene, J. B., Averkamp, T. F., Kurth, W. S., Ye, S.-Y., and Fischer, G. (2011). An SLS4 Longitude System Based on a Tracking Filter Analysis of the Rotational Modulation of Saturn Kilometric Radiation. *Planetary, Solar and Heliospheric Radio Emissions (PRE VII)*, pages 51–64.

Gurnett, D. A., Lecacheux, A., Kurth, W. S., Persoon, A. M., Groene, J. B., Lamy, L., Zarka, P., and Carbary, J. F. (2009a). Discovery of a north-south asymmetry in Saturn's radio rotation period. *Geophysical Research Letters*, 36:L16102.

Gurnett, D. A., Persoon, A. M., Groene, J. B., Kopf, A. J., Hospodarsky, G. B., and Kurth, W. S. (2009b). A north-south difference in the rotation rate of auroral hiss at Saturn: Comparison to Saturn's kilometric radio emission. *Geophysical Research Letters*, 36:L21108.

Horányi, M., Morfill, G. E., and Cravens, T. E. (2010). Spokes in Saturn's B ring: Could lightning be the cause? *IEEE Transactions on Plasma Science*, 38.

Jacobson, R. A., Antreasian, P. G., Bordi, J. J., Criddle, K. E., Ionasescu, R., Jones, J. B., Mackenzie, R. A., Meek, M. C., Parcher, D., Pelletier, F. J., Owen, W. M., Roth, D. C., Roundhill, I. M., and Stauch, J. R. (2006). The Gravity Field of the Saturnian System from Satellite Observations and Spacecraft Tracking Data. *Astronomical Journal*, 132:2520–2526.

Jones, G. H., Krupp, N., Krüger, H., Roussos, E., Ip, W.-H., Mitchell, D. G., Krimigis, S. M., Woch, J., Lagg, A., Fränz, M., Dougherty, M. K., Arridge,

C. S., and McAndrews, H. J. (2006). Formation of Saturn's ring spokes by lightning-induced electron beams. *Geophys. Res. Lett.*, 33.

Kaiser, M. L., Desch, M. D., Kurth, W. S., Lecacheux, A., Genova, F., Pedersen, B. M., and Evans, D. R. (1984). *Saturn*, chapter Saturn as a radio source, pages 378–415. University of Arizon Press.

Kurth, W. S., Averkamp, T. F., Gurnett, D. A., Groene, J. B., and Lecacheux, A. (2008). An update to a Saturnian longitude system based on kilometric radio emissions. *Journal Geophys. Res.*, 113:A05222.

Kurth, W. S., Lecacheux, A., Averkamp, T. F., Groene, J. B., and Gurnett, D. A. (2007). A Saturnian longitude system based on a variable kilometric radiation period. *Geophys. Res. Lett.*, 34.

McGhee, C. A., French, R. G., Dones, L., Cuzzi, J. N., Salo, H. J., and Danos, R. (2005). Hst observations of spokes in Saturn's B ring. *Icarus*, 173:508–521.

Mitchell, C. J., Horányi, M., Havnes, O., and Porco, C. C. (2006). Saturn's spokes: Lost and found. *Science*, 311:1587–1589.

Pollack, J. B. and Cuzzi, J. N. (1980). Scattering by nonspherical particles of size comparable to a wavelength: A new semi-empiracl theory and its application to tropospheric aerosols. *Journal of the Atmospheric Sciences*, 37:868–881.

Porco, C. and Danielson, G. E. (1982). The periodic variation of spokes in Saturn's rings. *Astron. Journal*, 87:826–833.

Porco, C. C. and Danielson, G. E. (1984). The kinematics of spokes. In Greenberg, R. and Brahic, A., editors, *IAU Colloq. 75: Planetary Rings*, pages 219–222.

Porco, C. C., West, R. A., Squyres, S., McEwen, A., Thomas, P., Murray, C. D., Del Genio, A., Ingersoll, A. P., Johnson, T. V., Neukum, G., Veverka, J., Dones, L., Brahic, A., Burns, J. A., Haemmerle, V., Knowles, B., Dawson, D., Roatsch, T., Beurle, K., and Owen, W. (2004). Cassini imaging science:

Instrument characteristics and anticipated scientific investigations at saturn. *Space Science Reviews*, 115:363–497.

Provan, G., Cowley, S., and Nichols, J. (2009). Phase relation of oscillations near the planetary period of Saturn's auroral oval and the equatorial magnetospheric magnetic field. *Journal of Geophysical REsearch*, 114:A04205.

Smith, B. A., Soderblom, L., Batson, R., Bridges, P., Inge, J., Masursky, H., Shoemaker, E., Beebe, R., Boyce, J., Briggs, G., Bunker, A., Collins, S. A., Hansen, C. J., Johnson, T. V., Mitchell, J. L., Terrile, R. J., Cook, A. F., Cuzzi, J., Pollack, J. B., Danielson, G. E., Ingersoll, A. P., Davies, M. E., Hunt, G. E., Morrison, D., Owen, T., Sagan, C., Veverka, J., Strom, R., and Suomi, V. E. (1982). A New Look at the Saturn System: The Voyager 2 Images. *Science*, 215:504–537.

Smith, B. A., Soderblom, L., Beebe, R. F., Boyce, J. M., Briggs, G., Bunker, A., Collins, S. A., Hansen, C., Johnson, T. V., Mitchell, J. L., Terrile, R. J., Carr, M. H., Cook, A. F., Cuzzi, J. N., Pollack, J. B., Danielson, G. E., Ingersoll, A. P., Davies, M. E., Hunt, G. E., Masursky, H., Shoemaker, E. M., Morrison, D., Owen, T., Sagan, C., Veverka, J., Strom, R., and Suomi, V. E. (1981). Encounter with Saturn - Voyager 1 imaging science results. *Science*, 212:163–191.

Spitale, J. N. and Porco, C. C. (2009). Time variability in the outer edge of Saturn's A-Ring revealed by Cassini imaging. *The Astronomical Journal*, 138:1520–1528.

Spitale, J. N. and Porco, C. C. (2010). Detection of free unstable modes and massive bodies in Saturn's outer B ring. *The Astronomical Journal*. submitted.

Throop, H. B., Porco, C. C., West, R. A., Burns, J. A., Showalter, M. R., and Nicholson, P. D. (2004). The jovian rings: new results derived from Cassini, Galileo, Voyager, and Earth-based observation. *Icarus*, 172:59–77.

West, R. A., Knowles, B., Birath, E., Charnoz, S., Di Nini, D., Hedman, M., Helfenstein, P., McEwen, A., Perry, J., Porco, C., Salmon, J., Throop, H., and Wilson, D. (2010). In-flight calibration of the Cassini imaging science subsystem cameras. *Planetary and Space Science*. in press.